Modeling and Measurement of Frost Characteristics on Heat Exchanger Surfaces

A Thesis

Submitted to the

College of Graduate Studies and Research

in Partial Fulfillment of the Requirements

for the Degree of

Doctor of Philosophy

in the Department of Mechanical Engineering

University of Saskatchewan

Saskatoon

By

Hong CHEN

Spring 2000

PERMISSION TO USE

The author grants permission to the University of Saskatchewan Libraries to make this thesis available for inspection. Copying of this thesis, in whole or in part, for scholarly purposes may be granted by my superior (Robert W. Besant), the Head of the Department of Mechanical Engineering, or the Dean of the College of Engineering. It is understood that any copying or publication or use of this thesis or parts thereof for financial gain shall not be allowed without my written permission. It is also understood that due recognition to me and the University of Saskatchewan must be granted in any scholarly use which may be made of any material in this thesis.

Requests for permission to copy or to make other use of the material in this thesis in whole or in part should be addressed to:

Head, Department of Mechanical Engineering

University of Saskatchewan

57 Campus Drive

Saskatoon, SK

S7N 5A9

ABSTRACT

Frost growing on heat exchanger fins is a common problem for refrigeration and air-conditioning equipment. Frost growth on heat exchanger fins causes the performance of heat exchangers to decline mostly because frost accumulation blocks the air flow paths and an increase of the air flow pressure drop. Often the air flow rate with frost growth and heat rate decrease.

A test facility was developed to characterize frost growing on heat exchanger flat plates and finned surfaces where the cold surfaces and air supply conditions were similar to those experienced in freezers. Several new measurement techniques were used to measure frost height and mass accumulation and heat flux.

A numerical model for predicting frost growth on flat plates and plate-fin exchangers was developed. The model treats the frost as a transient, one-dimensional porous media and includes transient two-dimensional heat conduction in the fins.

The numerical model was validated using experimental data for frost height, frost density, air pressure drop across the fins and heat rate through the cold base. The agreement between the experimental data and simulation results were within the uncertainty bounds for most of the data.

It is found that for a *constant* air-flow rate through the heat exchanger over a four hour test period, the blockage of air-flow resulting from the frost growth increases the pressure drop across the heat exchanger by up to a factor of 10, while heat transfer rate decreases by only 21%.

ACKNOWLEDGEMENTS

I would like to express my sincere thanks and appreciation to my supervisor, Professor Robert W. Besant. Thank you for your support, guidance and expertise throughout this work. Thanks also to Leena Thomas, my research partner for the frost height on fin studies, for your time and truly interesting discussions, research related and not. Thanks are due to YanHui Mao for the experimental test facility design and the data collection and analysis for flat plates with frost. Also thanks to Mr. Dave Deutscher for his help with the experimental studies.

Finical assistance from the NSERC and ASHRAE during my Ph.D. program is also acknowledged and appreciated.

TABLE OF CONTENTS

LIST OF TABLES

LIST OF FIGURES

Nomenclature

A	General variable in Equation (6.9) for average value calculation
A	Heat exchanger total heat transfer area on one side, m^2
a	Offset in Equation (6.2)
a	k_a/k_i
A_{base}	Un-finned base surface area, m^2
A_c	Exchanger minimum free-flow area, varies with frost height, m^2
A_f	Fin surface area, m^2
B	Frost porosity, $(\rho_i-\rho_f)/(\rho_i-\rho_a)$
b	Slope in Equation (6.2)
B_1	0.1726(T/273.16)
B_2	0.751
B_3	B_2+0.3
B_c	Proportion of the frost volume representing ice spheres and ice planes
C	Empirical coefficient to account for the reduction of entrance and exit pressure losses, Equation (4.39)
c_a	Specific heat of dry air, J/kg·K
C_f	Friction coefficient or Fanning friction factor, $C_f=2\tau_s/(\rho_{air}V^2)$
c_{fin}	Specific heat of fin, J/kg·K
c_i	Specific heat of ice, J/kg·K
c_p	Specific heat of frost, J/kg·K
c_v	Specific heat of vapor, J/kg·K
D_{AB}	Binary diffusion coefficient for water vapor in air at the film temperature, m^2/s
D_{eff}	Effective vapor diffusion coefficient within the frost layer, m/s
$D_{eff,s}$	Effective vapor diffusion coefficient on the air-frost interface, m/s
D_h	Hydraulic diameter, m
f	Moody(or Darcy) friction factor
h_f	Convective heat transfer coefficient, W/m^2K
h_{fin}	Fin height, 0.04m
h_{mf}	Convective mass transfer coefficient, m/s
h_{sg}	Enthalpy of sublimation, J/kg
k^+	Dimensionless roughness number
k'	Average roughness height of frost, m
k_a	Thermal conductivity of air, W/mK
k_b	Thermal conductivity of air bubbles, W/mK
k_c	Thermal conductivity of ice cylinders, W/mK
k_i	Thermal conductivity of ice, W/mK
k_l	Low limit of thermal conductivity, W/mK
k_p	Thermal conductivity of ice planes, W/mK
k_s	Thermal conductivity of ice spheres, W/mK
k_u	Upper limit of thermal conductivity, W/mK
k_{air}	Thermal conductivity of air, W/mK
K_c	Contraction loss coefficient for flow at heat exchanger entrance
K_e	Expansion loss coefficient for air flow at heat exchanger exit
k_{eff}	Effective thermal conductivity of frost, W/mK

k_{fin}	Thermal conductivity of fin, W/mK
k_{ice}	Thermal conductivity of ice, W/mK
l_{fin}	Fin length, 0.1m
$\dot{m}$	Phase change rate, kg/m^3s
m_f	Frost mass accumulation on each fin piece, kg
m''_f	Frost mass concentration, kg/m^2
n	Number of samples
n	Number of fins
Nu_D	Nusselt number for full developed flow
Nu_x	Local Nusselt Number
p_a	Dry air pressure, Pa
Pr	Prandtl number
p_{ref}	Reference Pressure, Pa
p_t	Total gas phase pressure, Pa
p_v	Vapor pressure, Pa
q_{base}	Heat rate through un-finned base, W
q_{fin}	Heat rate through one fin, W
q_{total}	Total heat rate through the base, W
Q	Volume flow rate, m^3/s
R_a	Air gas constant, J/kg·K
Re_D	Inlet Reynolds number based on the hydraulic diameter
R_v	Vapor gas constant, J/kg·K
S	Heat source term in Equation (4.24), W/m^3
SEE	Standard error of estimate
SES	Standard error of simulation
Sh_x	Local Sherwood number, $h_{mf}*D_h/(D_{AB})$
t	Time, s
T	Temperature, K
T_0	Air flow temperature, K
T_a	Airflow temperature, K
T_b	Cold base temperature, K
T_c	Cold plate temperature, K
t_{fin}	Fin spacing, m
T_{in}	Airflow temperature at the entrance of the finned section, K
T_{out}	Airflow temperature at the exit of the finned section, K
T_{ref}	Reference Temperature, K
V	Air velocity in finned section, m/s
V*	Friction velocity, m/s
V_0	Airflow velocity, K
V_{in}	Airflow velocity before entering finned section, m/s
W	Humidity ratio, kg/kga
W_0	Air flow humidity ratio, kg/kga
W_{fs}	Humidity ratio at frost surface, kg/kg
W_{in}	Inlet airflow humidity ratio, kg/kga
W_{out}	Air flow humidity ratio at the exit of the finned section, kg/kga
x	coordinate axis, m

x_k x position for k^{th} sample
y coordinate axis, m
z coordinate axis, m

Greek Symbols

β Bias between simulation and data
ε_0 Initial condition of volume fraction of ice on fin surface
ε_a Volume fraction of air within frost, $\varepsilon_a = 1-\varepsilon_\beta$
ε_β Volume fraction of ice within the frost layer, $\varepsilon_\beta=\rho_f/\rho_i$
δ Designates a measurement error when used as a prefix
δ_f Frost thickness, m
$\bar{\delta}_f$ Average frost height, m
δ_{fin} Fin thickness, 0.3mm
$\delta_{f\text{-}avg}$ Average frost thickness on fin, m
$\delta_{f\text{-}base}$ Average frost thickness on un-finned base, m
μ Dynamic viscosity of air, Pa· s
ρ_a Density of air, kg/m^3
ρ_f Frost density, kg/m^3
$\bar{\rho}_f$ Average frost density, kg/m^3
ρ_{fin} Fin density, kg/m^3
ρ_i Density of ice, kg/m^3
ρ_v Density of vapor, kg/m^3
τ_s Surface shear stress, Pa
τ_w Wall shear stress, Pa
ν Kinematic viscosity of air, m^2/s
ΔP Pressure drop across fins, Pa
ΔT Air flow temperature change across fins, K
ΔW Air flow humidity ratio change across fins, kg/kg
Θ_c $1-B_c$

CHAPTER 1

INTRODUCTION

1.1 Introduction

When moist air passes over a surface at temperatures below the dew temperature of the air, some of its vapor content will be condensed on the surface. If the surface temperature is below the 0°C, vapor will be deposited first as water droplets which subsequently freeze and, if the temperature is less than about -5°C, a porous structure of ice crystals forms. This layer of ice crystals is known as frost.

Frost growth on heat exchanger surfaces including fins is a common problem for cold air refrigeration systems, air conditioning equipment and air-to-air heat recovery systems for ventilation air during cold weather. Among these various systems, frost growth on refrigeration heat exchangers is the problem of greatest importance. Frost growth on heat exchanger surfaces affects the thermal performance of heat exchangers in several ways; these are:

1. Frost growth on heat exchanger surfaces increases the thermal resistance between the fin and airflow and decreases the cooling capacity of heat exchangers used in refrigeration and air conditioning systems. For a given airflow rate and temperature difference between the airflow and a finned surface, frost growth of a finite thickness decreases the rate of heat

transfer because the effective thermal conductivity of frost is finite and a temperature difference will occur across the frost layer.

2. Frost growth on heat exchanger surfaces reduces the airflow through the heat exchangers and increases the air pressure drop through heat exchangers. Eventually, after many hours of frost growth, the airflow path can become nearly or completely blocked.

3. In order to continue satisfactory performance of heat exchangers that accumulate frost, periodic or cyclic defrosting is required to remove the frost accumulation. Generally, during a defrost cycle, the cooling system will be shut down and heat is supplied to the heat exchanger to raise its temperature well above freezing. Niederer (1976) indicated that only 15% to 20% of the heat supplied for defrosting was actually carried out by the condensate. The rest of the heat input for defrosting increased the temperature of the heat exchanger and it was lost to the surrounding environment. When water is evaporated during defrost cycle it often ends up back on the heat exchanger surface during the next frost growth period.

As a result of the frost accumulation, refrigeration systems currently used in the industry are often oversized by about 50% compared to the case where no frost is grown while the average energy input is 25% greater than the same system with no frost accumulation.

Designers of refrigeration heat exchangers need to know the rate of frost accumulation and how this frost growth is related to the airflow blockage or pressure drop and the reduction in the heat rate. Studies of frost growth on finned-tube heat exchangers have shown that there are large temporal and spatial variations in the frost growth which depend on the design of the heat exchanger and its operating conditions (Ogawa et al., 1993). The frost height and mass accumulation of frost per unit area are the most important characteristics of a frost layer because they are directly related to the airflow blockage, heat rate reduction, and heat required to defrost heat exchangers.

Frost is comprised of air trapped in a porous matrix of ice crystals with typical crystal size from 30 to 300 μm and a range of porosities from 0.3 to 0.9 and with humid air inside the pores. During frost growth, heat is transferred from humid airflow adjacent to the frost-air interface by convection where it is conducted through the frost layer to a cold heat exchanger surface. Water vapor is transferred from the airflow to the frost-air interface by convection, i.e. turbulent or molecular diffusion where it diffuses by molecular diffusion through the frost layer towards the cold heat exchanger surface. Vapor ablimation (i.e., the reverse of sublimation), or the phase change from vapor to the ice crystals, occurs both at the air-frost interface and within the frost layer. Frost accumulation is always accompanied by the release of the latent heat of sublimation. Frost growth, therefore, always involves the coupling of heat and mass transfer processes throughout the frost layer.

The frosting process is a complicated phenomenon involving simultaneous heat and mass transfer with phase change and a moving boundary under unsteady state conditions. To date, accurate prediction of the frost growth on heat exchangers has not been very satisfactory despite of 50 years of research. It is the objective of this study to develop a numerical model to predict the characteristics of the frost growth on heat exchangers and the effects of frost growth on the performance of the heat exchangers.

1.2 Previous Work of Frost growth on Heat Exchangers

Over a period of more than 50 years, nearly 150 studies have been published on frost growth on heat exchanger surfaces. Many of these papers were summarized by O'Neal and Tree (1985) and Padki et al. (1989) so only a brief overview will be given for work before 1989.

1.2.1 Previous Work on Experimental Study

Stoecker (1957, 1960) was one of the first to investigate frost formation on coil heat exchangers in refrigeration systems using aluminum flat plate fins on 5/8 inch coolant copper tubes arranged in line. Based on his experimental results, he recommended the wide spacing of fins and over-sizing the coil heat exchanger since this would allow higher coolant temperature and longer duration before defrosting is necessary.

Wagner (1963) conducted experiments on finned tube heat exchangers with frost growth. He concluded that holding the other operating conditions steady that: 1)

increasing the airflow velocity increased the frosting rate and the overall heat transfer coefficient between the air and the coolant; 2) increasing inlet air humidity ratio increased the overall heat transfer coefficient and the frosting rate; and 3) the airflow pressure drop across the heat exchanger was the most critical parameter for change under frosting conditions.

More recently several experimental studies have been done to investigate the heat exchanger performance under frosting conditions. Gates et al. (1973), Rite and Crawford (1991), Kondepudi and O'Neal (1989) and Senshu et al. (1990) investigated the heat transfer and pressure loss in typical refrigeration heat exchangers under frosting conditions. Ogawa et al. (1993) investigated geometric modifications of fins within tube and fin heat exchangers to improve their performance under frosting conditions. They found that an extended leading edge on the fins on the upstream side of heat exchangers helped to reduce frost blockage.

In their fundamental studies of frost growth on cold plate surfaces Hayashi et al. (1977) and Tokura et al. (1983) showed that before frost starts to form on a clear flat surface water droplets form at nucleation points (i.e. microscopic scratches and surface imperfections). At some time when the surface temperature is many degrees below freezing these water droplets suddenly freeze while these frozen droplet expand creating an imperfection at the last point on the droplet surface to freeze. This imperfection in the frozen droplet then becomes a nucleation site for a frost crystal to grow normal to the

surface. Latter this single crystal starts to for dendritic branches like tree branches which form a canopy we call frost.

O'Neal and Tree (1984) examined frost formation in parallel plate geometry under forced convection conditions. They found that above some critical Reynolds number, frost growth is independent of Reynolds number. Below that critical Reynolds number, frost growth increases with increasing Reynolds number. They found that the critical Reynolds number was 15900 for a range of Reynolds number from 4400 to 32400 for airflow between parallel flat plate. This observation is not in agreement with other reported data (e.g. Abdel-wahed et al. 1984). The latter took their data for a range of Reynolds number from 3000 to 140000 for air flowing over a horizontal plate.

Frost height is one of the most important characteristics of frost growth on heat exchanger fins but it is the most difficult parameter to measure accurately because any direct contact with an instrument causes the frost interface to change. Cremers and Mehra (1982) conducted an experimental study on frost growth under free convection conditions on small vertical cylinders. They used a travelling microscope to focus on the frost-air interface. If the frost-air interface was very irregular, they noted that it resulted in a greater uncertainty than when the surface was smooth. In spite of this observation, they did not specify their height measurement uncertainty. These frost height data may therefore be used only for qualitative comparisons to indicate how certain operating conditions influence frost growth.

Using new techniques to measure frost height and mass concentration, Mao et al. (1992, 1993) presented correlations for frost growth characteristics on a cold flat plate when air at room temperature passes over in forced convection. Frost height was measured over the length of the flow path using a travelling laser beam directed parallel to the frosted surface and adjusted in height so that 50% of the beam was blocked by the frost. For smooth frost, this non-contact method allowed frost height uncertainties as low as 0.04mm and permitted several measurements per minute. To account for the difference between the air and plate temperature from the freezing point of water, they correlated all their frost property data, such as frost height, density and heat flux, as functions of five independent dimensionless variables, namely: time, distance from the leading edge, air speed or Reynolds number, air humidity ratio and a temperature difference ratio.

Rite and Crawford (1991) weighed the mass of frost accumulation for a heat exchanger. Mao et al. (1992) used a disk removal method to obtain the local distribution of frost mass concentration on a flat surface with a one-dimensional frost growth pattern. It was shown in Mao et al. (1992) that for frost thickness greater than 1 mm and less than 4 mm, the uncertainty in the mass concentration was less than 4%.

1.2.2 Previous Work on Theoretical/Numerical Modeling

There have been many empirical and semi-empirical attempts to model frost growth. These are summarized in Padki et al. (1989). Parish and Sepsy (1972) presented a simple numerical model of frost formation under forced convection whereby the average frost properties were predicted. Padki et al. (1989) presented another simple

method for modeling the average properties of frost in different geometries. Both of these models assumed that the frost properties inside the frost layer are constant in time.

Tao et al. (1993a) presented a physical model with coupled heat and moisture diffusion within the frost layer modeled as a porous media. They compared their simulation results to the correlations by Mao et al. (1992) for frost growth on a flat plate supplied by humid room air. In Tao's model both spatial and temporal variations of the frost density and temperature as well as frost height and heat flux are predicted.

Although the agreement between their simulations and correlations was fairly good, Tao introduced a modified effective diffusion coefficient for water vapor within the frost layer and assumed some boundary conditions that were not based on physical data. More recently, Le Gall et al. (1997) slightly modified this model by Tao by eliminating one equation and the need for two boundary conditions. They used a slightly different effective diffusion coefficient for water vapor in the air in the porous frost layer. Le Gall also compared their simulations with the data of Mao et al. (1992) showing reasonable agreement using their modified diffusion coefficient. Lee et al. (1997) presented yet another model for frost growth where the heat and mass transfer processes were de-coupled and the frost properties do not change with time inside the frost layer. Their simulations showed reasonable agreement with their very limited experimental database.

1.2.3 Summary of the Previous Work

To date, most of the previous studies were not concerned with developing precise models for frost growth on surfaces; rather, they were aimed at developing simple models for frost growth and measuring the performance of typical heat exchangers when frost growth occurred. Based on their data, these researchers made recommendations for operating conditions that will alter frost growth on heat pumps and domestic refrigerators. Descriptions were provided for their test facility instrumentation along with sensor errors but no uncertainty analysis was presented. No general correlations were presented which would allow the designer to extrapolate their data to slightly different heat exchanger geometries or operating conditions. For example, none of these studies include data for very cold operating conditions such as are typical of commercial freezers. Consequently, these papers are best suited to suggest trends for frost growth as a result of changes in a few operating parameters.

Despite decades of experimental frost growth research, no comprehensive means of predicting frost growth for new operating conditions in typical heat exchangers is available for anything but flat plates. Often there are seven or more independent operating and design variables for heat exchangers with frost growth (i.e. time, length of path through the heat exchanger, cold surface temperature, air supply temperature and humidity, air supply turbulence and speed, and heat exchanger surface geometry), making the acquisition of a sufficiently comprehensive data set for frost growth on heat exchangers a daunting task. Correlating such frost data with seven or more independent variables would be very difficult and, since the uncertainty in some of the variables is

typically large for refrigerator operating conditions (i.e. humidity, temperature difference, etc.), the reliability of any such correlations would be poor. An alternative means of presenting frost characteristics on heat exchanger surfaces is through an accurate physical/numerical model. This is the approach taken in this thesis because numerical simulation extrapolations of experimental data includes the essential physics of frost growth. Numerical models are important because they can simulate a wider range of operating conditions and account for time variable operating conditions that are common in practice but often impractical in experimental research. Once validated, numerical models can be useful for the design and optimization of operating conditions of heat exchangers.

1.3 Research Objectives

The main purpose of this research is to develop a model to characterize frost growth on heat exchanger surfaces that are operating under typical refrigeration and freezer conditions. This research fills a need for accurate frost data for surface temperatures as low as –40°C, air supply temperatures as low as -25°C and relative humidities up to nearly 100%. Such operating conditions are common in food freezing refrigeration systems. To develop an accurate model, frost data are to be measured both for flat plate surfaces and finned surfaces on which the temperature will vary substantially from point to point. Previous studies of frost growth on heat exchangers were confined to much warmer surface and air temperatures; so, this thesis will present new data and a new model. In past research studies, finned surfaces were avoided for

fundamental frost growth studies because they give rise to two- and three-dimensional frost growth patterns for which it is very difficult to measure the frost height distribution.

The object of the experimental research is to devise and calibrate the instrumentation required to characterize frost on heat exchanger flat surfaces and fins and to measure the heat rate. These experiments will include the measurement of frost height, airflow pressure drop, and mass concentration on a finned heat exchanger surfaces. The main purpose of these data is to validate the model over a wide range of operating conditions that are typical of food freezing heat exchangers.

In spite of large number of studies on frost growth problem, existing frost growth models have been restricted to flat plates. No models exist to predict frost growth on the finned surfaces of heat exchangers. It is the object of this research study to develop and validate a numerical model for frost characteristics on heat exchanger fins. Subsequently, this model can be used to simulate a wider range of operating conditions.

1.4 Overview of the Thesis

The presentation of this research work begins in Chapter 2 with the description of test facility, instrumentation and measurement techniques. The numerical model of frost growth on flat plate surfaces is described in Chapter 3 and is validated using experimental data in Chapter 4. The numerical model of frost growth on heat exchanger fin surfaces is described in Chapter 5 and is validated in Chapter 6. The summary and conclusions of this research study are presented in Chapter 7. The appendices present the model

simplification, experimental data, model validation, sensitivity results and the source code of computer program for the numerical model.

CHAPTER 2
EXPERIMENT APPARATUS AND MEASUREMENT

2.1 Introduction

The frost height and mass accumulation of frost per unit area are the most important characteristics of a frost layer because they are directly related to the airflow blockage, heat rate reduction, and the heat energy required to defrost heat exchangers. The object of this research is to devise and calibrate the instrumentation required to characterize frost on heat exchanger fins and to measure the heat rate. This includes the measurement of frost height, airflow pressure drop, and mass concentration on a finned heat exchanger surface.

In the past, frost height was measured using manual and mechanical techniques. These techniques were invariably slow and were only suitable for smooth frosted surfaces with height variations in one direction. Thousands of measurements are required to characterize the uneven frost growing on a heat exchanger fin due to surface temperature variations. A frost height measurement technique using a laser beam was developed by Besant et al. (1990) with an uncertainty of $\pm$ 0.03 mm when the supply air was at room temperature. This technique was adapted to freezer operating conditions by Mao et al. (1999) with an uncertainty of $\pm$ 0.04 mm for smooth frost and about an order of magnitude larger for rough frost.

In this study, a new fully-automated laser scanning system is described. This system measured both the transmitted and scattered laser light signals from a frosted

surface. The local frost thickness was calculated using the light signal data and the position of laser beam with respect to the solid surface.

Previous research on frost growth used various means to weigh the mass of frost accumulation for large heat exchanger surfaces or even the entire heat exchanger to give the total mass accumulation of frost (Rite and Crawford 1991). Mao et al. (1992) used a disk removal method to obtain the local distribution of frost mass concentration on a flat surface with a one-dimensional frost growth pattern which was supplied with air at room temperature. For a frost thickness greater than 1 mm and less than 4 mm, the uncertainty in the mass concentration was less than 4%. Mao et al. (1999) used this same method for measuring frost accumulation on a flat plate subject to freezer operating conditions. This technique of removing and weighing components of the surface was extended to frosted fins in this study.

Some researchers used a heat flux meter to measure the heat flux through a surface with a uniform layer of frost (O' Neal and Tree, 1984). Mao et al. (1991) extended this method to include a one-dimensional variation in frost characteristics and the corresponding heat flux. The uncertainty in the measured heat flux was typically less than 6% when air supply was at room conditions and for freezer operating conditions (Mao et. al., 1999). In this study, the heat flux meter scheme was modified to the measurement of total heat rate through a finned surface.

The total heat rate of the fin assembly was measured using a calibrated heat flux meter as part of the base assembly in the test loop. The uncertainty in the heat rate measurement was estimated to be ± 6 W for the total surface area (Mao et al., 1999)

2.2 Test Loop

The test loop for the experiments of frost growth on the flat plate and frost growth on heat exchanger fins is same while the test sections are different.

The airflow test loop schematic, shown in Figure 2.1, includes a vacuum system to induce the desired airflow. A well-insulated ducting system, test section and orifice plate to measure the airflow rate are shown in Figure 2.2. Air supply from the cold environmental chamber was cooled to about -40°C, mixed with air from the second, somewhat warmer, chamber at about 0°C giving a high relative humidity airflow, which passes over test section. The main difference between this test loop and the one reported by Mao et al. (1991) is the mixing of very cold air with moderately cold air before the supply inlet and the large amount of insulation (RSI≈3.5 Km^2/W) used on the supply air duct to minimize heat gains. The temperature and dew point of the supply air were measured to a high accuracy by a platinum RTD temperature sensor and a calibrated chilled mirror. The airflow rate was measured downstream using a standard orifice meter.

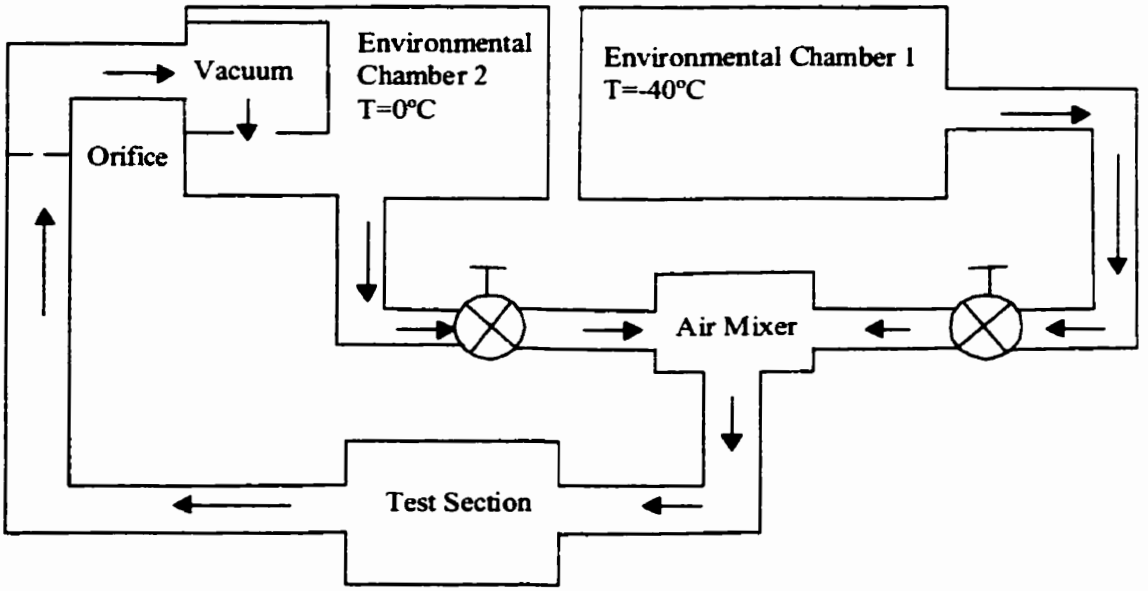

Figure 2.1 Schematic of the frost growth test loop

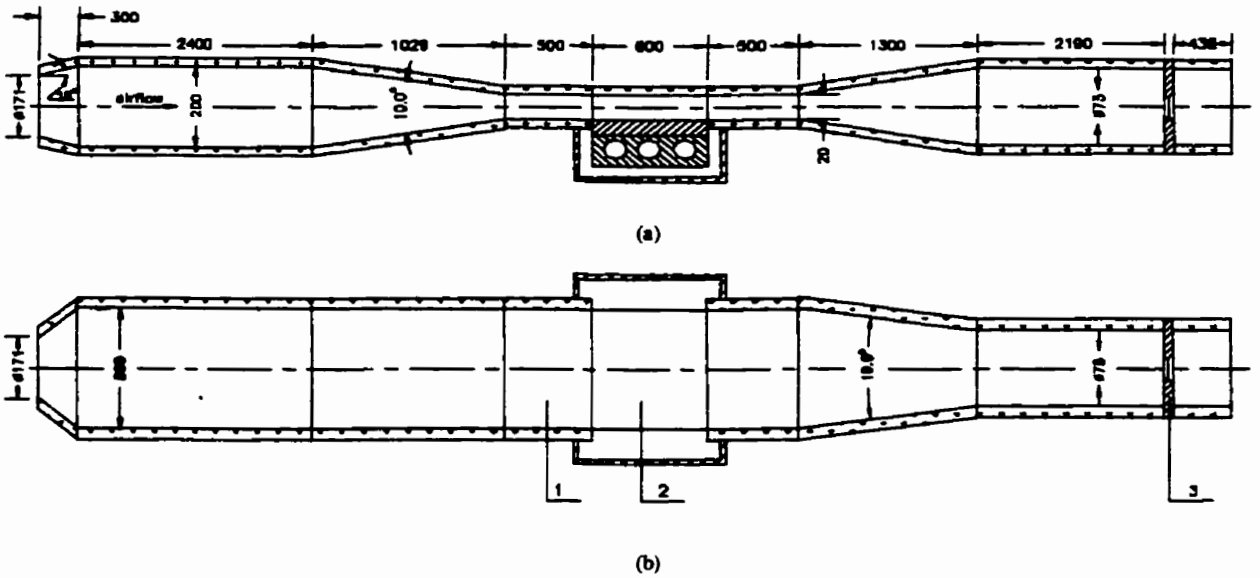

① Fully developing air flow, measuring station for air temperature and relative humidity

② Test Section

③ Orifice Plate

Dimensions (mm)

Figure 2.2 Cross sections of the test flow loop adjacent to the test section (a) side elevation (b) plan view

2.3 Previous Work of Frost Growth on Flat Plate

Mao et al. (1999) did experimental research of the frost growth on the flat plate. Figure 2.3 shows the experimental apparatus assembly. The test section was designed to allow frost growth on a large, 600×280 mm (23.6×11.0in) surface shown in Figure 2.4 which could be cooled to a temperature as low as -50°C (-58°F) using thermal-electric cooling with a heat-sink heat-exchanger cooled by an aqueous glycol flow at -20°C (-4°F).

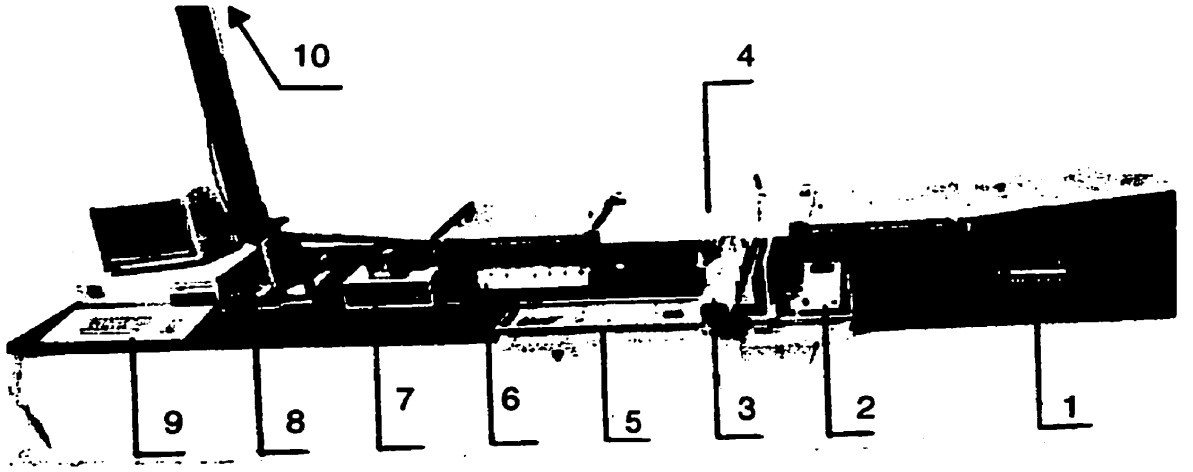

1. Temperature Indicator
2. Light Meter
3. Laser
4. Test Section
5. Laser Beam Bed
6. Frost Sample Containers
7. Data Acquisition System
8. Inclined Manometer
9. Computer
10. Orifice Meter Section

Figure 2.3 Experimental apparatus assembly for the frost growth on the flat plate

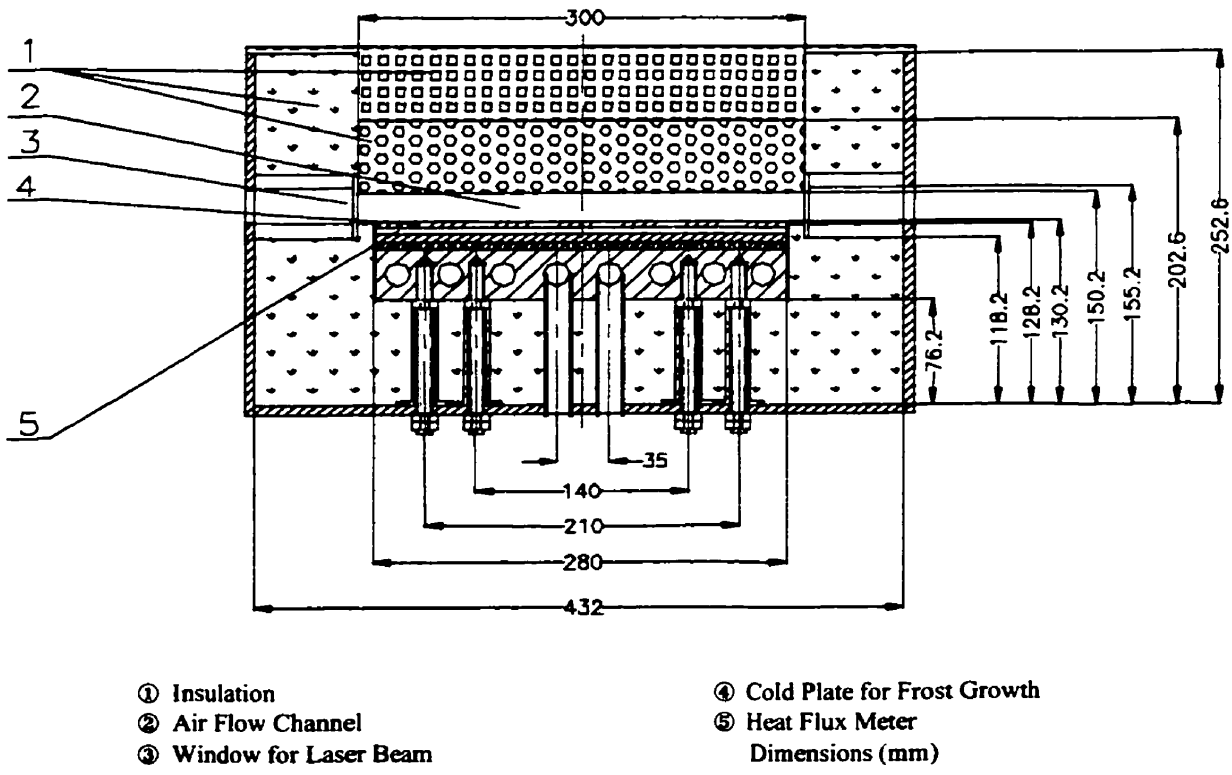

Figure 2.4 Cross Section of the test section normal to the air flow

The test section, shown in Figure 2.4, possessed three special features to permit the accurate measurement of frost thickness, frost mass accumulation, and heat rate through the base. Double glazed windows on either side of the test section permitted the use of the laser beam method of measuring frost height over the 600mm (23.6in) of length of cold plate (Mao et al., 1991). Three rows of eight (i.e. 24 in total) removable disks, each 31.9 mm (1.26 in) diameter and flush mounted in the cold base plate shown in Figure 2.5, permitted the direct measurement of mass concentration of frost at selected times during the experiment (Mao et al., 1991). The heat-flux meter was designed to be an integral part of the cold plate assembly. Thermocouples on the cold plate were used to monitor the temperature distribution on the cold plate.

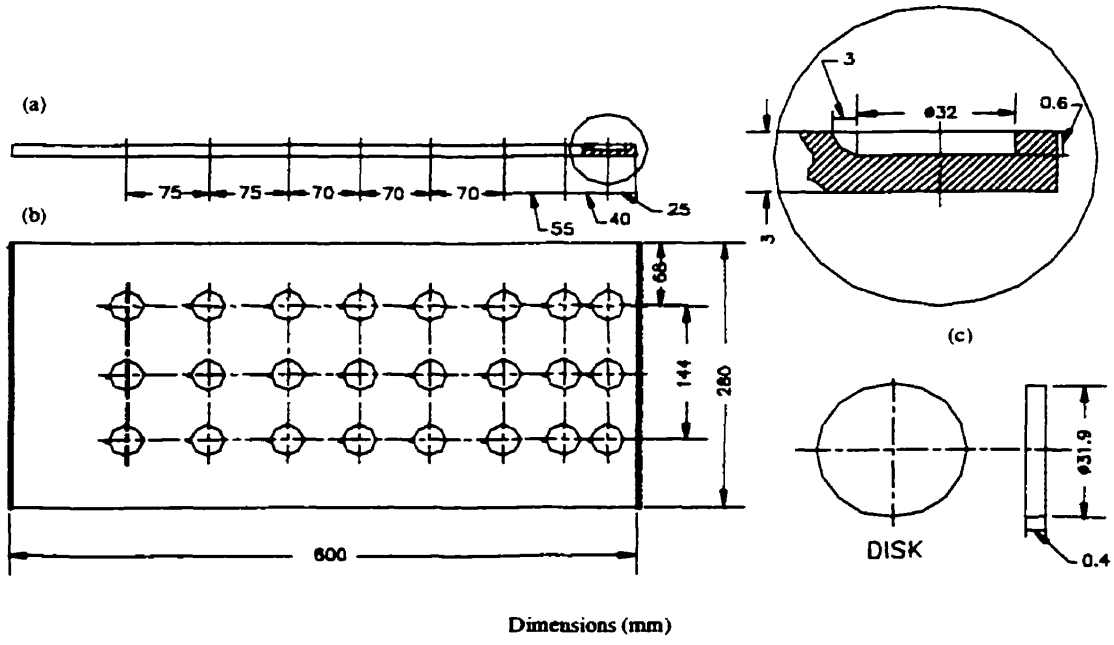

Figure 2.5 Cold test plate surface (a) side elevation and (b) plan view and their size (c) showing the positions of the removable disks

Calibration of the laser beam frost height measuring system gave an uncertainty of ±0.04mm ($\pm 1.57\times10^{-3}$in) when the frost was smooth. The uncertainty in frost height measurements for rough frost is much more difficult to quantify because very small changes in the laser beam position can cause large signal changes. This suggested that a fully automated system of measuring frost height, which can process thousands of data to get a statistical average, is desirable when the frost is rough. This automated laser scanning system is described later for the frost height measurement on heat exchanger fins. Since such an automated system was not available for measuring frost height during these tests for frost growth on a flat plate, the uncertainty in manually measuring very rough frost was estimated to be $\pm(0.3\text{mm}+0.05\delta_f)$. Isolated peaks of rough frost could be twice the size of this average height rough frost uncertainty. For frost that is somewhat

rough, the frost height uncertainty lies between the extremes of smooth and rough frost uncertainty.

Calibration of the mass concentration of frost showed that its uncertainty depends on the frost height as well as the accuracy of frost mass measurement (Mao et al., 1991). For frost heights larger than 1mm(0.04in), the uncertainty in mass concentration is between 2 and 4% and increases with frost height. Frost heights less than 0.5mm(0.02in) will result in more than 8% uncertainty.

Average frost density is more often reported in the literature rather than mass concentration. Uncertainty in the calculation of frost density is dominated by the uncertainty in frost height measurement for rough frost. For frost heights between 1 and 4mm the uncertainty in rough frost density is between 30% and 8% and decreases with frost height. For smooth frost this uncertainty in average density was between 4 and 5% and increases with frost height. For frost heights less than 0.5mm(0.02in), the uncertainty in average frost density can be higher than 60% for rough frost and 7% for smooth frost.

The test conditions used for the experiments are summarized in Table 2.1. Twenty test conditions were used to develop 480 data samples for frost thickness, frost mass concentration and heat flux through the cold plate. These data are presented in Appendix E. Each data sample includes a complete survey of these frost characteristics over the length of the cold plate surface. This data base is used to validate the numerical model for frost growth on the flat plate in Chapter 4.

Table 2.1 Ranges of Environmental Parameters Used in the Experiments for Frost Growth on the Flat Plate

Parameter	Range	Variations
Time (minutes)	0 to 360	
Distance from leading edge	0 to 500mm (0 to 19.7in)	±1mm (±0.04in)
Test surface temperature	-20.5 to –41 °C (-4.9 to –41.8° F)	±1 °C (±1.8 °F)
Supply air temperature	-10.1 to -25.8 °C (13.8 to –14.4 °F)	±1 °C (±1.8 °F)
Supply air humidity ratio	0.00019 to 0.002	±0.0001
Supply air velocity	1 to 4 m/s (198 to 786 ft/min)	±0.05m/s (±9.6 ft/min)
Inlet Reynolds number	3278 to 13112	±165

2.4 Test Section for the Frost Growth on Heat Exchanger Fins

The test section for the frost growth on heat exchanger fins was designed so that the fins could be removed at the end of a test and the height and mass of the accumulated frost could be measured. A set of aluminum fins (each 100 mm × 45 mm × 0.3mm, alloy 2024-T6) was inserted into slots built in the cold base assembly shown in Figure 2.6 and 2.7. The test facility below this base plate is described in detail in the previous section. The distance between the centerlines of adjacent fins was 9.2mm. Before each test, thermal paste was put into the slots to make good thermal contact between each fin and its cold base slot. With 5mm of each fin inside the base, the exposed surface of each fin was 100 mm x 40 mm × 0.3 mm. The cross section of the test section normal to the flow direction has a 2mm clearance above the fins. The cold base was cooled by 15 thermoelectric heat pump modules with the heat removal to an ethylene glycol cooled heat exchanger. A heat flux meter within the cold base assembly was used to measure the heat flux through the cold base as described in the previous section. The pressure drop

across the fins in the test section was measured using flush mounted static pressure taps upstream and downstream of the test section and an inclined manometer.

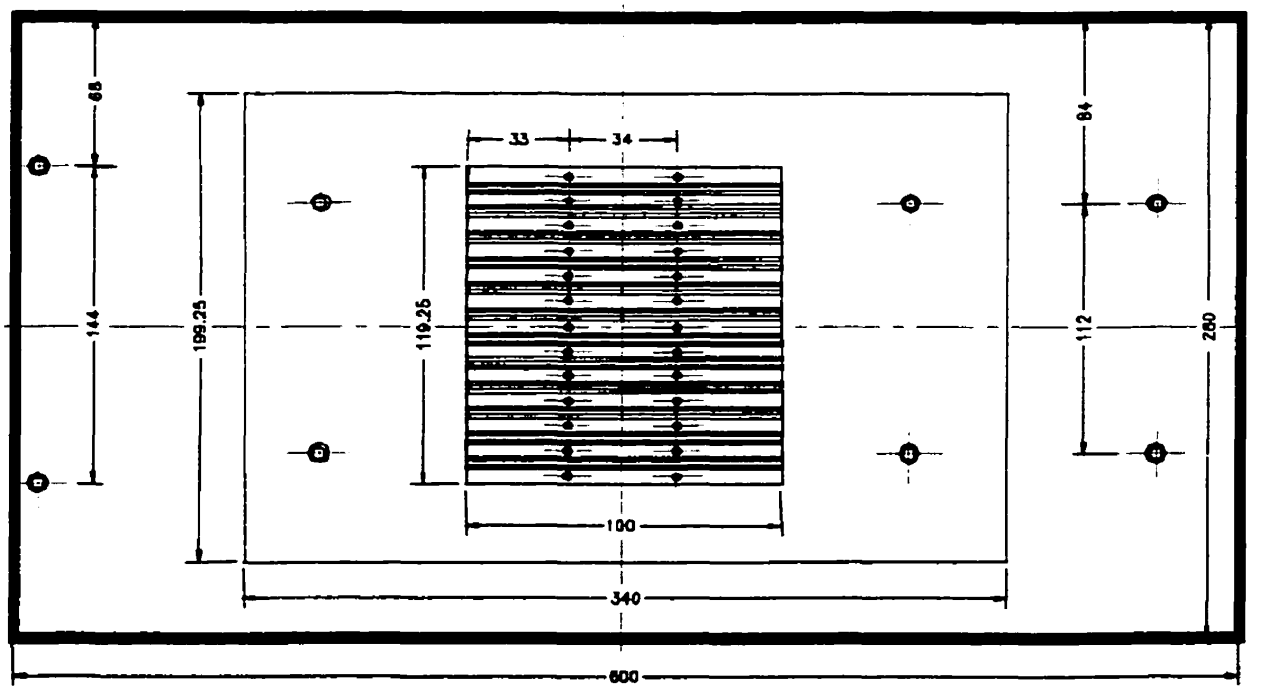

Dimensions (mm)

Figure 2.6a Plan view of base plate to hold fins

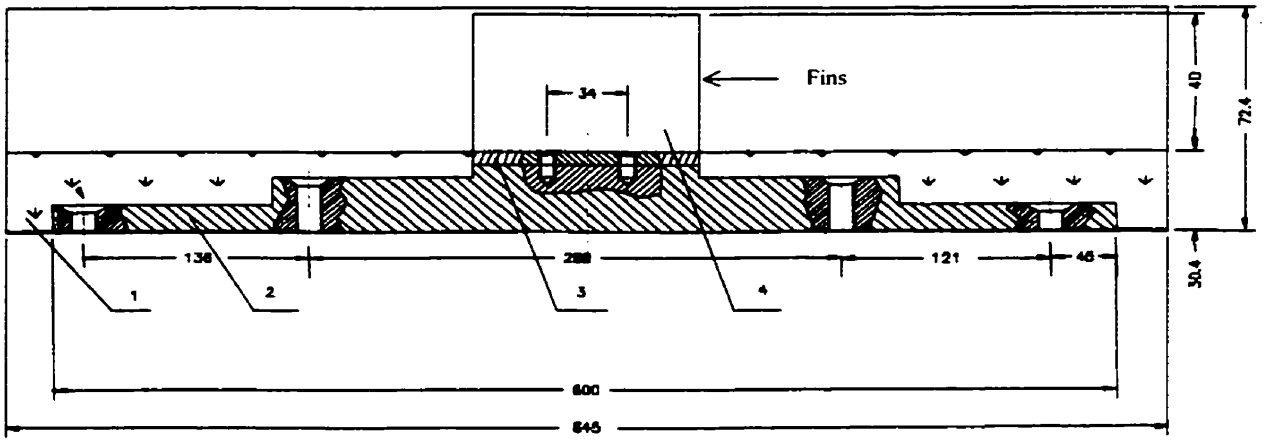

① Styrofoam insulation
② Aluminum base plate
③ Aluminum fin spacers
④ Aluminum fins
Dimensions (mm)

Figure 2.6b Side elevation view of base plate with fins installed

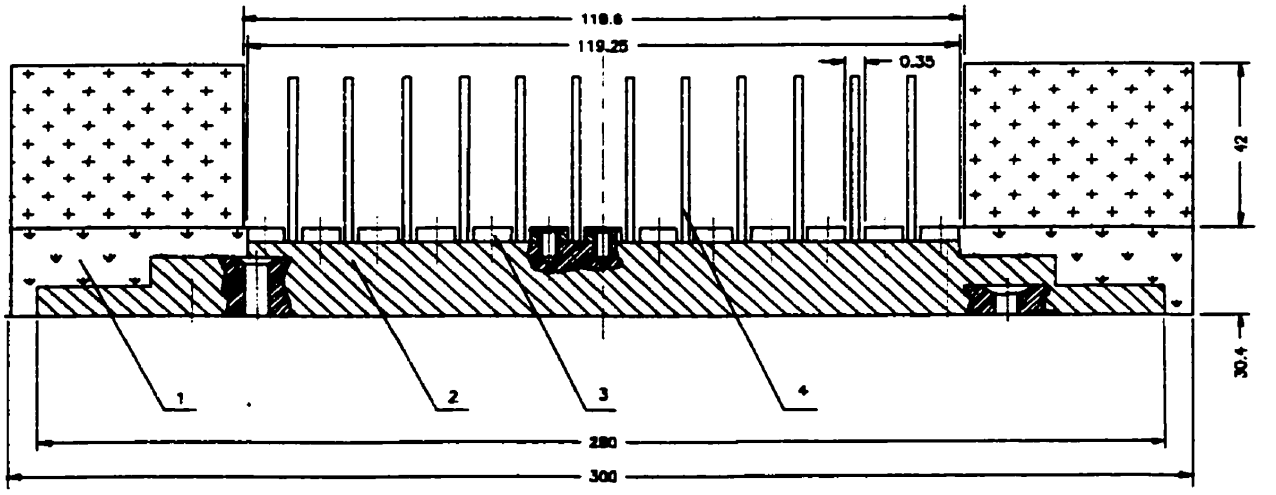

① Styrofoam insulation
② Aluminum base plate
③ Aluminum fin spaces
④ Aluminum alloy fins

Dimensions (mm)

Figure 2.6c Test section for frost growth viewed in the air flow direction

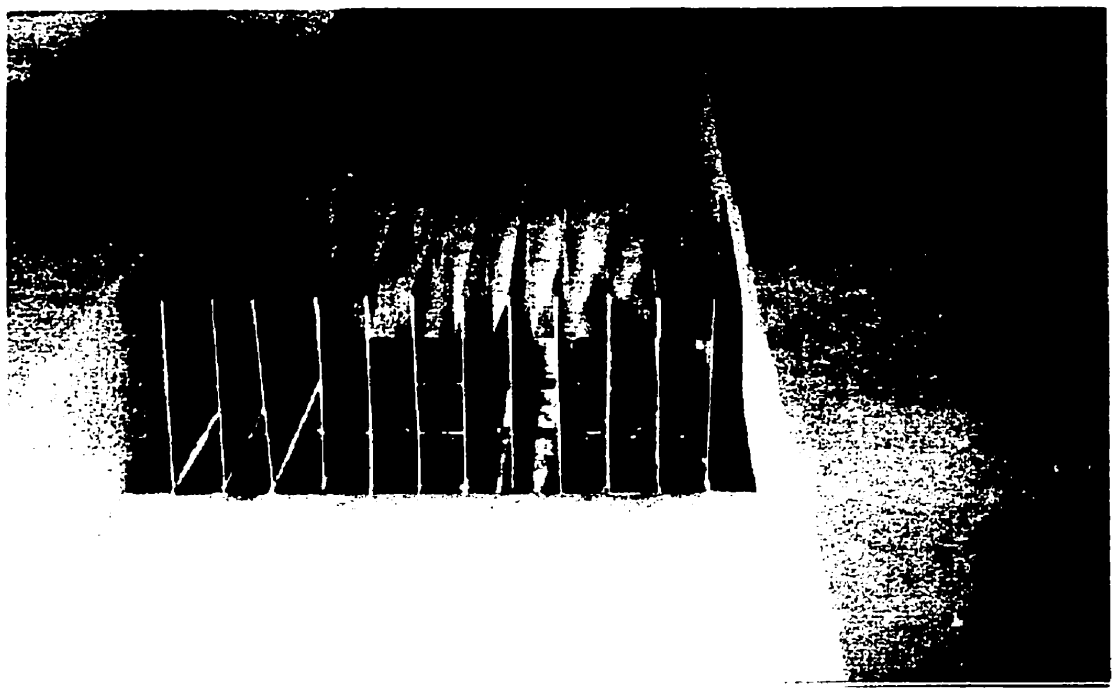

Figure 2.7a Test section before experiments

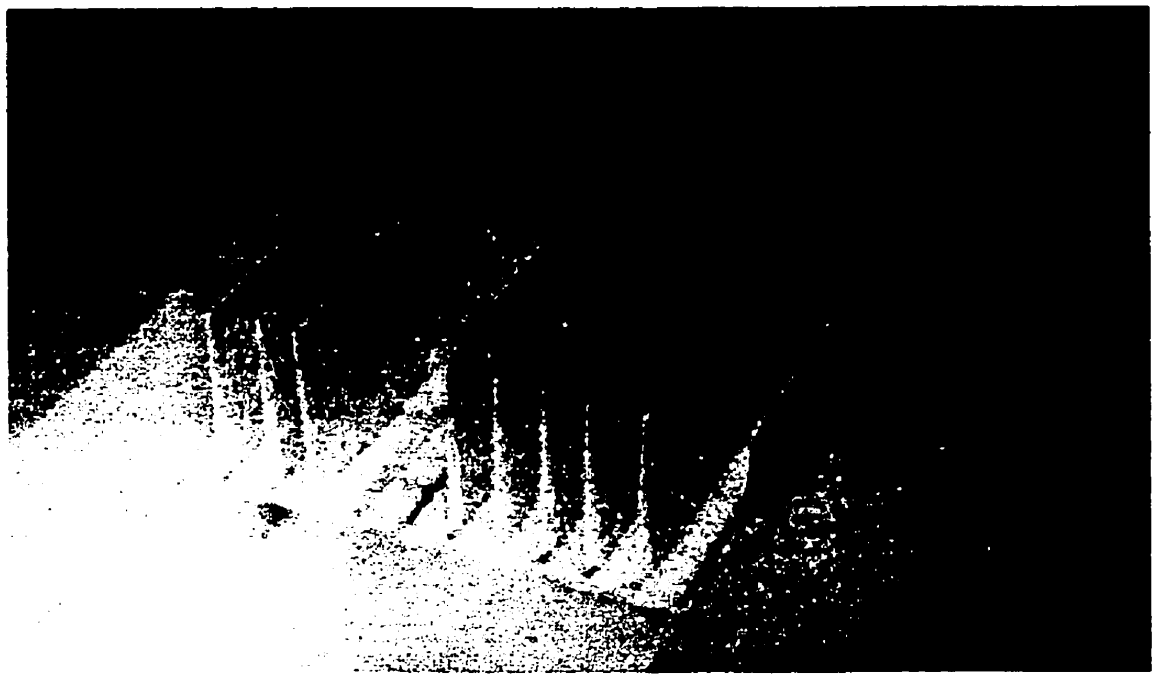

Figure 2.7b Test section after frost growth experiments with fins removed for the frost height and mass accumulation measurements

2.5 Test Procedures and Test Conditions for Frost Growth on Fins

To begin the frost growth process, certain set points such as cold base temperature, airflow dry bulb temperature, relative humidity and velocity were selected. The two environment chambers were started. The airflow was pumped into the test loop by the vacuum shown in Figure 2.1. The cold base were cooled down by starting the thermal-electric cooling with a heat-sink heat exchanger cooled by an aqueous glycol flow.

The desired test conditions were obtained by adjusting the mixing ratio of air from the two environment chambers and the electrical power to the cold base thermal-electric cooling system. Due to the very low temperatures required, it took approximately four hours for the temperatures to reach steady state. During this time, a piece of polystyrene insulation was secured across the slotted cold block to prevent any frost growth on this surface and within the slots.

Once the all temperatures reached steady state, the vacuum was shut off, the test section was opened and the insulation covering the cold block used to hold the fins was removed. Twelve clean aluminum fins were inserted into the cold block slots, 9.2mm apart as shown in Figure 2.6 and Figure 2.7. The test section was sealed and the loop was allowed to run from 3 to 5.67 hours to let enough frost growth on test fins.

During each test, small adjustments of the mixing ratio of air from two chambers were needed from time to time to keep desired test conditions. During each test, the flow velocity before entering the finned test section and mass flow rate were held constant by

manually adjusting the vacuum fan speed from time to time while the frost accumulated in the test section. The ranges of test conditions for various tests for frost growth on fins were shown in Table 2.2. The variations of test conditions were small, but sometimes significant, during any one test.

Table 2.2 Ranges of Environmental Parameters Used in the Experiments for Frost Growth on Heat Exchanger Fins

Parameter	Range	Variations
Time (min)	180 to 340	±2
Airflow Velocity (m/s)	3.3 to 6.0	±0.1
Fin Base Temperature (°C)	-39.0 to –30.5	±0.8
Airflow Temperature (°C)	-13.5 to -20.8	±0.8
Air Humidity Ratio (kg/kg)	0.00056 to 0.0011	+0.0001/-0.00005

2.6 Frost Height Measurement for Frost Growth on Heat Exchanger Fins

A new fully automated method of measuring frost growth on finned surfaces was developed. This method required the removal of a single fin from the heat exchanger after it accumulated frost for a period of time (e.g. one to six hours). The frost-coated fin (40 mm × 100 mm) was placed in a precooled fin holder where a fully-automated Laser Scanning System (LSS) permitted the measurement of both the transmitted and scattered laser light intensity. This system, shown in Figure 2.8, consisted of a helium-neon laser, two motorized positioning tables, two rotational potentiometers, and two light sensors (transmitted and scattered). All x and y position data were within ± 0.1 mm at 95% uncertainty. Vertical displacement of the laser was achieved manually within ± 0.013 mm at 95% uncertainty. Each light sensor consisted of a photo detector and amplifier which outputted a voltage that was proportional to the signal strength. The transmitted

light sensor was aligned with the laser beam while the scattered light sensor was mounted normal to the beam and was collimated through 0.1 mm apertures to exclude light from all sources except for that exactly underneath (i.e. only scattered light in the z direction was sensed). Data was collected (x-position, y-position, transmitted light and scattered light) at a rate of 1000 samples/second resulting in approximately 10^5 samples for a 40 mm × 100 mm fin. A three-dimensional representation of a frosted surface was obtained by scanning with the laser beam at different vertical heights. The apparatus and data acquisition was controlled by a dedicated PC and developed software. The fin holder was designed to maintain low operating temperatures. A thermal-electrical cooling element within the holder kept the fin base at about -20°C (-4°F) while dissipated heat was removed by water passing through a heat exchanger built into the fin holder.

The fin holder and the frost-coated fin were isolated from the warm moist surrounding air with an extruded polystyrene insulation box. Cold dry air was introduced into the insulated box to maintain a cold dry air condition surrounding the frosted fin. Figure 2.9 is a photograph showing the positions of the fin holder, fin and light sensors. The laser beam was in the negative y-direction and entered the polystyrene box through a slot from behind the scattered light sensor. The lid for the insulated box was removed for the photograph.

Legend:

① x-Direction Motor
② y-Direction Motor
③ x-Direction Table
④ y-Direction Table
⑤ x-Direction Potentiometer
⑥ y-Direction Potentiometer
⑦ Reflected Light Sensor
⑧ Transmitted Light Sensor
⑨ Helium-Neon Laser

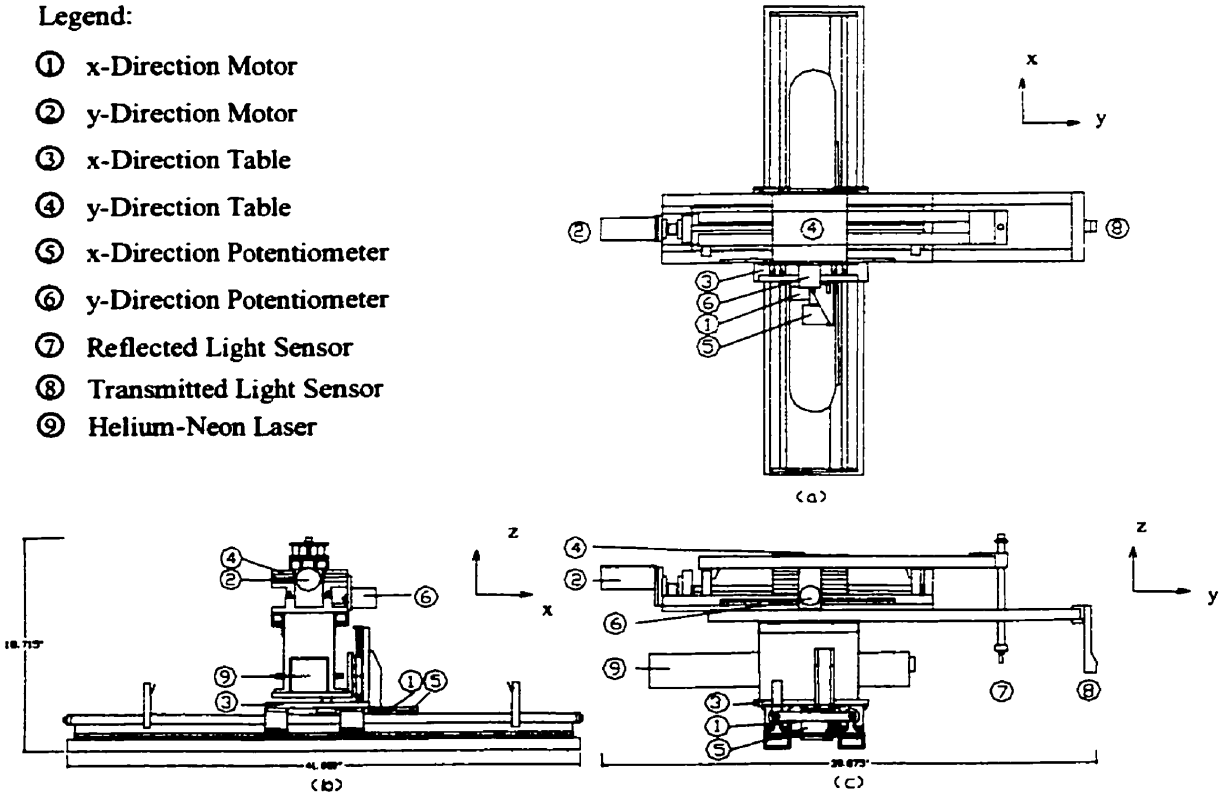

Figure 2.8 Laser Scanning System. a) plan view b) end elevation view c) side elevation view.

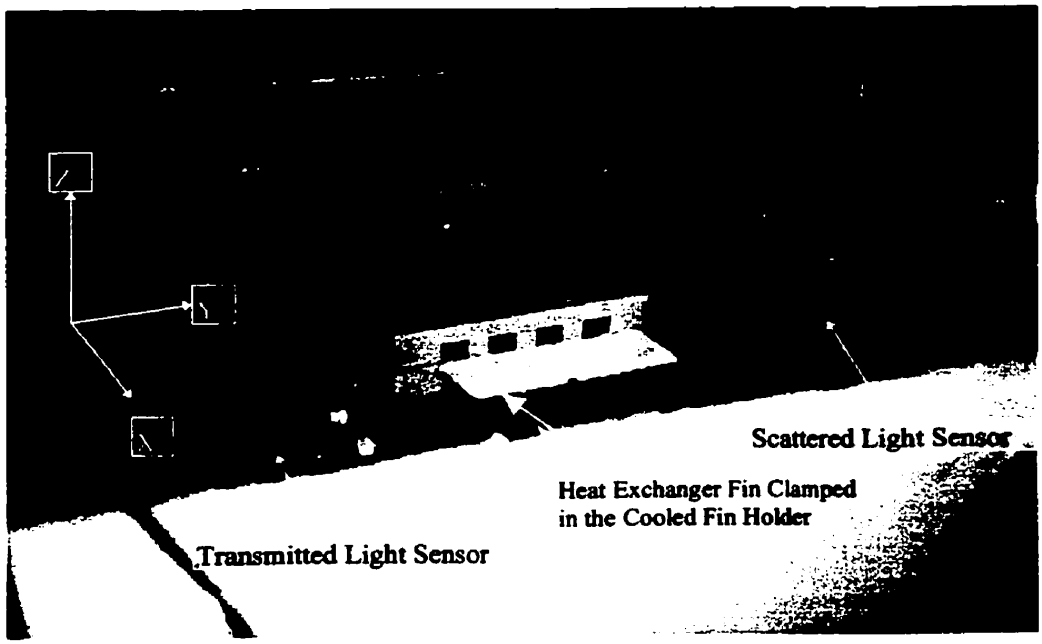

Figure 2.9 Frosted fin and fin holder in front of laser scanning system. Laser beam is in the -y direction.

Frost was grown on heat exchanger fins mounted 9.2mm apart under controlled steady state conditions in a closed loop airflow connected to two environment chambers. After enough frost accumulated on the fins (2.5 to 6 hours), one fin was removed from the center of the finned surface and placed into the pre-cooled fin holder (≈-20°C (-4°F)) using cooled pliers. The holder was then placed inside the polystyrene shroud in front of the Laser Scanning System. Cold, dry air from an environment chamber was piped into the shroud to surround the frosted fin and holder and maintain a local ambient temperature of 7 or 8°C (45 to 46°F). The relative humidity inside the shroud was measured to be quite low, at 16-20%. First, the holder was placed in front of the laser such that the laser was incident on the leading edge of the frost. The frost buildup on the leading edge was often too thick to permit the laser beam from reaching the rest of the frost on the fin. To observe the entire fin, the frost overhanging the leading edge of the fin was removed after the leading edge frost height was measured.

The maximum height profile of the frost in the x-direction (short side of the fin; normal to the laser beam) was measured first. The maximum height of the frost at any x-position was measured by adjusting the height of the laser beam so that the transmitted light sensor read at 50% of maximum laser intensity (i.e. the center of the laser beam). A dial gauge on the vertical position table was used to measure the height of the laser beam and thus, the height of the frost at this x-position. This was the same measuring procedure as outlined in Besant et al. (1990) and has a 95% level uncertainty of ± 0.03 mm.

Referring to Figure 2.10, the two tables were moved to their home positions to start the scanning process for one frost-covered fin. As the laser beam made contact with the frost, high intensity scattered light could be observed near the leading edge of the fin. Down-beam from the leading edge, less-intense scattered light peaks could be seen. The y-direction sensor scanned across the fin along the path of the laser beam, and data (x-position, y-position, transmitted light, and scattered light) was collected at a rate of 1000 samples/second. Motion in the y-direction reversed at the other side of the fin and data was collected again. Once the y-table reached its home position, it stopped and the x-direction table moved to its next position. This process was repeated until the whole fin was scanned.

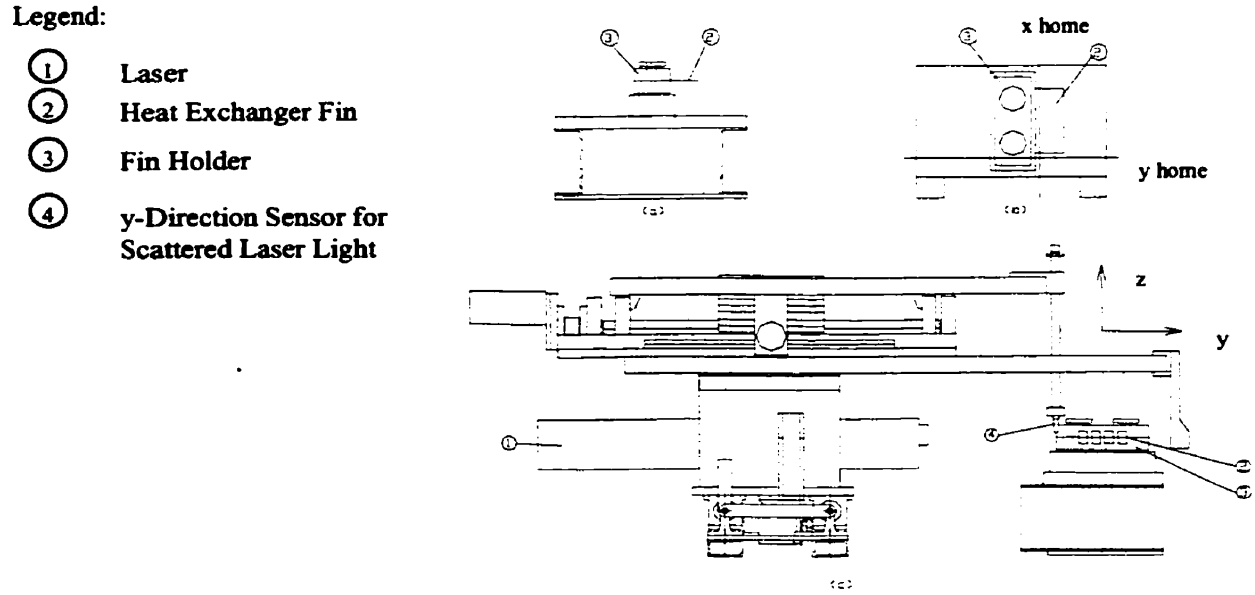

Figure 2.10 Fin Holder. a) View of fin holder, fin and mount from the x-direction.
b) Plan view of fin holder and fin showing the x- and y-home positions.
c) Placement of fin holder in relation to the Laser Scanning System.

Frost was scanned in two orientations of the laser beam, one with the laser beam incident on the leading edge of the fin and the other with the beam incident on the trailing edge. The 180° change in the direction of the laser beam was achieved by rotating the fin holder 180°. Different z-direction sections of the surface were scanned by manually moving the laser vertically. A typical test of one frosted fin consisted of four vertical laser positions spanning the range of heights indicated by the previously completed maximum height profile. All of the data were then averaged into a grid of 1mm squares for the 100 mm × 40 mm fin.

The local frost height information was based on the local scattered light signal data using a complex conversion procedure. It depends on three geometric factors: the orientation of the laser beam to the frost surface (i.e. incidence on the leading or trailing edge), the fraction of the beam hitting the frost at any x-position and the position of signal peaks in the y-direction. Each frosted fin is scanned at four heights of the laser beam with the laser beam incident on the leading and trailing edge of the fin. The detailed theory and conversion is presented in Thomas et al. (1999). A typical uncertainty error for frost height at any point is ±0.15 mm, though the maximum frost height error can be up to ±0.4 mm.

2.7 Measurement of Frost Accumulation

In order to get the frost mass concentration profile along a fin in the airflow direction, a special pre-cut fin was installed in the test section. Referring to Figure 2.11, seven tiny slots (about 0.1 mm wide and 0.3 mm deep) were etched in order to easily

break the fin into eight pieces along each slot in the flow direction. Since the majority of heat transfer was into the fin base from the top of the fin and that the heat transfer vector within each fin ranges from 80 to 90° to the base, it was determined that slots etched in this way had negligible effect on the heat flow performance and frost accumulation of the fin.

The test procedure for the mass concentration is described as follows:

1) Before each test, the cold base surface and testing fins were cleaned with an ethyl-alcohol solution to remove any dirt and moisture that might have been deposited on the surface. Thermal paste was put into each cold base slot and the fins were installed.
2) During the test, two clamps were cooled to -35°C in an environment chamber. Eight marked clean and small plastic containers with lids off were prepared.
3) Immediately after each test, the etched fin for mass measurement was pulled out by one clamp, then the other clamp was used to break the fin into eight pieces by bending along the pre-etched slot. Each fin piece with frost attached was put into one of the small containers. Each container was then sealed with its lid.
4) Each container with the fin was weighed using a high accuracy digital balance (uncertainty ±0.00001g). The lid of each container was opened and the containers were exposed to room air for about 24 hours in order to let all of the condensed water from the frost evaporate. Each container with the fin piece was weighed again. The weight difference gave the frost mass accumulation on each fin piece.

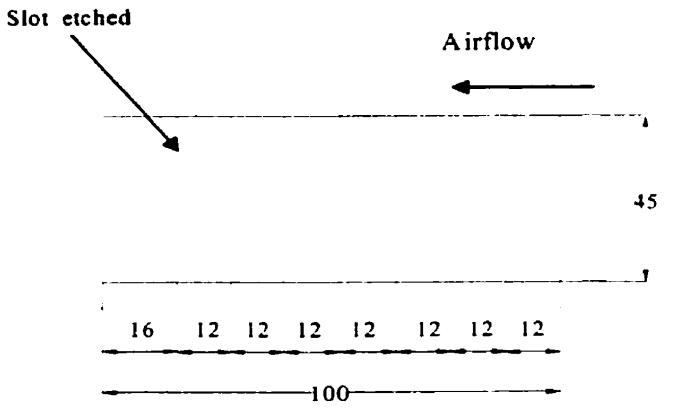

Figure 2.11 Fin for mass concentration measurement

The frost mass concentration is calculated using

$$m''_f = \frac{m_f}{A_f} \tag{2.1}$$

where m_f is frost mass accumulation on each fin piece and A_f is the surface area of each fin piece. The error of this measurement can be estimated by

$$\frac{\delta m''_f}{m''_f} = \sqrt{(\frac{\delta A_f}{A_f})^2 + (\frac{\delta m_f}{m_f})^2} \tag{2.2}$$

The relative error in frost area for a fin piece, $\delta A/A$, was estimated to be 2% and less than 1% for the entire fin. Tests were done to determine the value of the mass of frost on a fin piece, $\delta m_f / m_f$. In these tests, the mass accumulation on another fin adjacent to the etched fin was measured. This adjacent fin was pulled out and wrapped with an impermeable plastic wrap and weighed. Then the fin and its plastic wrap were exposed to room temperature for some time and when totally dry, were weighed again. The weight difference was used to obtain the total frost mass accumulation on the adjacent unetched fin. The error in this measurement was estimated to be less than 1% because

there was no handling of the whole fin other than to remove it from the cold base. This frost accumulation on the unetched fin was compared to the total frost mass accumulation for each test (i.e. sum of frost mass accumulation of eight fin pieces) on etched fin. It was found that mass of frost mass differences between two fins (etched and whole) were all within the range 8%-26% with a average 17%. The total frost mass accumulation measured on all the etched fin pieces was always less than its adjacent unetched fin. The explanation for the reduced mass on the set of fin pieces compared to the adjacent fin is that during the procedure of breaking the etched fin seven times into 8 small pieces, the fin with frost was briefly exposed to the room temperature which could result in a small amount of frost lost due to sublimation. Furthermore, when each fin piece was separated from the etched fin, the inevitable vibration and shaking force caused a small amount of frost to drop from the pre-etched fin pieces. This caused a 17% bias error and 9% random or precision error for each fin piece. In the mass accumulation test the 17% bias error was accounted for by mutiplying the frost mass on each fin piece by 1.17. The remaining random error of mass accumulation, $\delta m_f / m_f$, was then 9% for the fin pieces. The bias error of frost accumulation on the frost pieces is estimated at 2% giving a total uncertainty of 9.4%.

2.8 Air Pressure Drop and Total Heat Rate Measurement

The pressure drop across the fins in the test section was measured using flush mounted static pressure taps upstream and downstream of the test section and an inclined manometer. Measurements were taken without the fins installed to obtain the pressure drop of the flow passage for range of flows. This was then subtracted from the total

pressure drop to obtain the net pressure drop across the fins alone. The uncertainty in the net pressure across the fins was 3.8 Pa.

The transient total heat rate through cold base was measured by a heat flux meter within the cold base assembly and was recorded by a data acquisition system continuously. The uncertainty of this heat rate measurement was estimated to be ±6W.

2.9 Typical Experimental Data

Test conditions for two typical experimental data presented are listed in Table 2.3.

Table 2.3 Test Conditions For the Typical Experimental Data

Test	A	B
Dry Bulb Temperature (°C)	-15.0±0.8	-16.2±0.8
Cold Plate Temperature	-37.0±0.5	-37.0±0.5
Flow Velocity (m/s)	4.4±0.1	4.2±0.1
Humidity Ratio (kg/kg)	$(9.7+1.0/-0.5)\times10^{-4}$	$(8.3+1.0/-0.5)\times10^{-4}$
Time of Frost Growth(min)	240±2	205±2

2.9.1 Frost Height Distribution on Fins

Using the laser scanning system for measuring the distribution for air over a flat fin, a three-dimensional picture of the frost height contours can be obtained. The frost growth test conditions (data sets A and B) are displayed graphically as point, orthographic or contour views. Figures 2.12 and 2.13 present the frost height data test conditions A and B, respectively.

Figures 2.12 and 2.13 indicate that generally, after the leading edge frost has been removed, the frost closest to the fin base (x = 0 mm) and near the leading edge (y = 0 mm) is the highest and decreases with increasing x and/or y. This decrease in frost height

per unit length is much larger in the x direction than the y direction. This difference in frost gradient depends on the fin efficiency, which is discussed later. Figure 2.12 for data set A shows that the frost for this case is higher and rougher than the frost presented in Figure 2.13 for data set B. This is due to the slightly higher moisture content and airflow speed for this case as well as the larger duration of the test in case A compared to case B.

A comparison of the frost contours in Figures 2.12 and 2.13 show many similarities between the two but there are some noticeable differences, especially towards the trailing edge of the fin (i.e. y = 100 mm). Towards the trailing edge, large contour changes in frost height maybe induced by instabilities that arise due to the coupling among the mass transfer, fluid flow and heat transfer phenomena. Generally, these induced frost growth instabilities increase with distance from the leading edge of the fin where the frost density is also low.

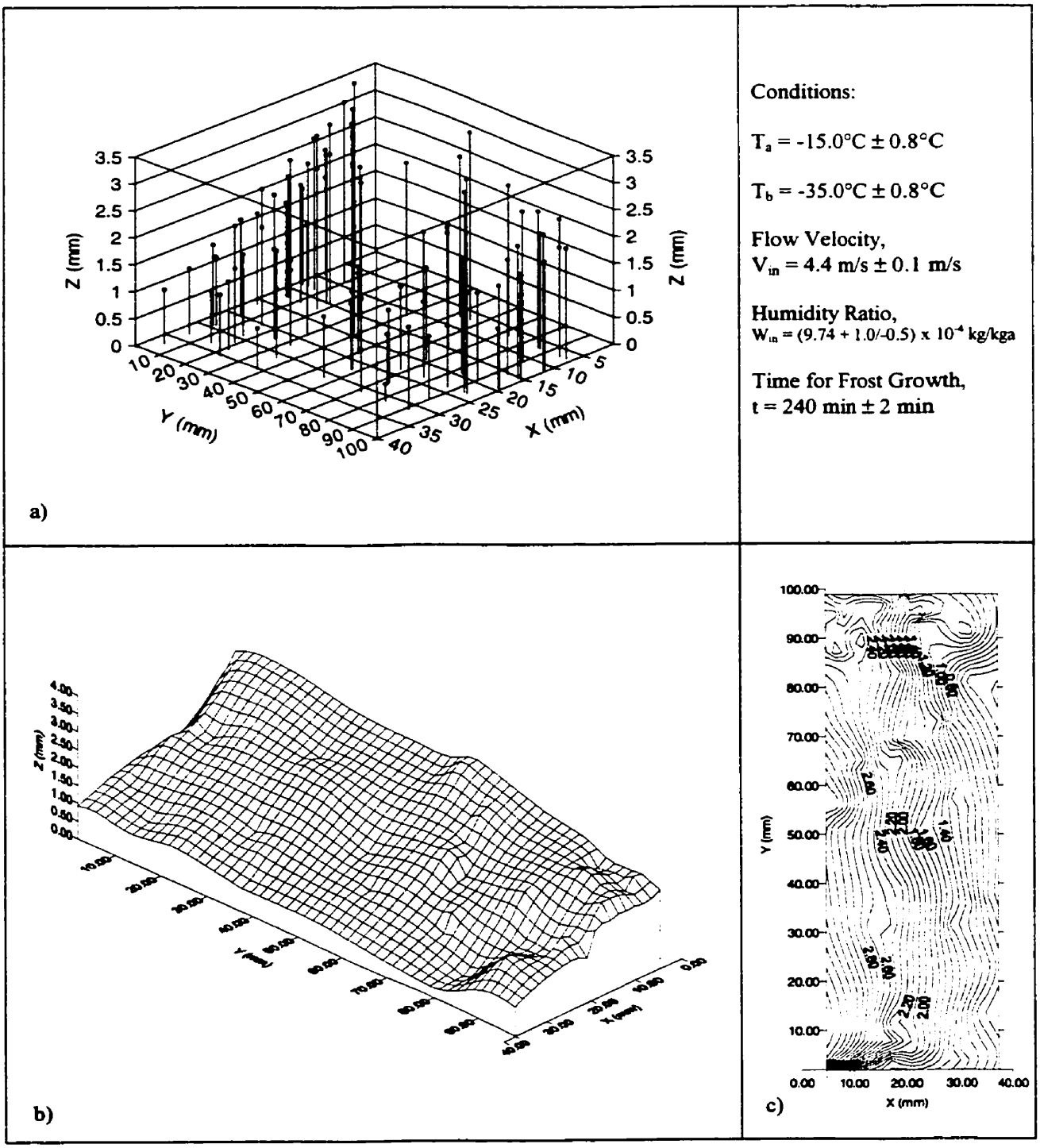

Figure 2.12 Frost Height a) data points, b) mapped surface, c) contour plot
For test condition A
(T_a = -15.0°C, T_b = -35.0°C, V_{in} = 4.4 m/s, RH = 91.2%, t = 4.0 h)

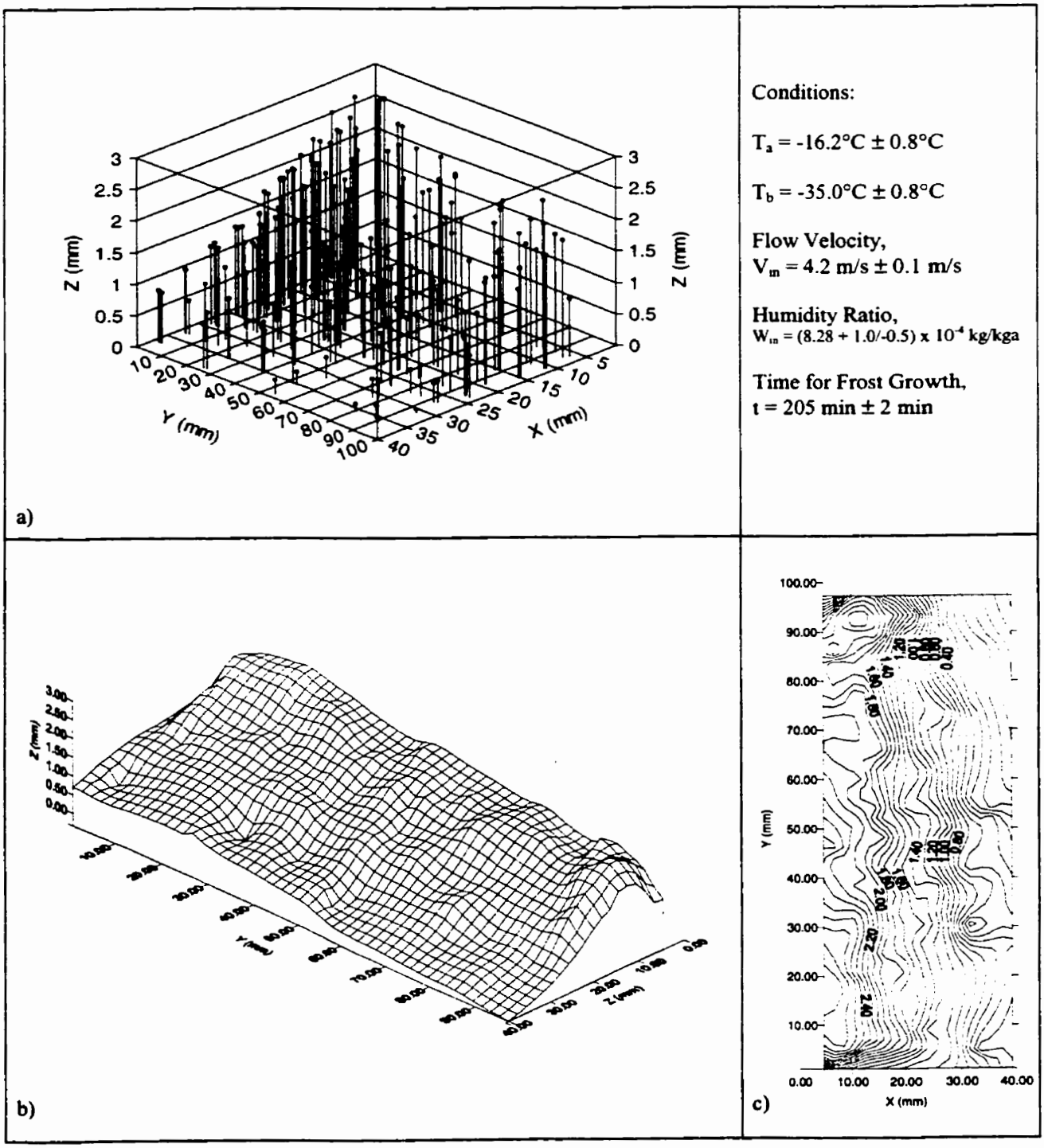

Figure 2.13 Frost Height a) data points, b) mapped surface, c) contour plot
For test condition B
(T_a = -16.2°C, T_b = -35.0°C, V_{in} = 4.2 m/s, RH = 91.0%, t = 3.42h)

2.9.2 Frost Mass Concentration and Density

The frost density is calculated by combining the mass concentration and frost height measurement data,

$$\rho_f = \frac{m''_f}{\delta_f} \tag{2.3}$$

Average frost height for each piece of fin was obtained from the frost height data. Equation (2.3) was then used to calculate the average frost density of each of the 8 fin pieces. The uncertainty error for density is calculated to be 14% using the uncertainty in m''_f and δ_f.

Figures 2.14 and 2.15 show the distributions of frost mass concentration and density versus y for the two test cases. The distribution of frost mass concentration and density in the x-direction are not directly available from the measured data. Such information could, however, be inferred from the distribution of frost height over the entire fin where both x and y coordinates are important and after assuming a certain average frost density.

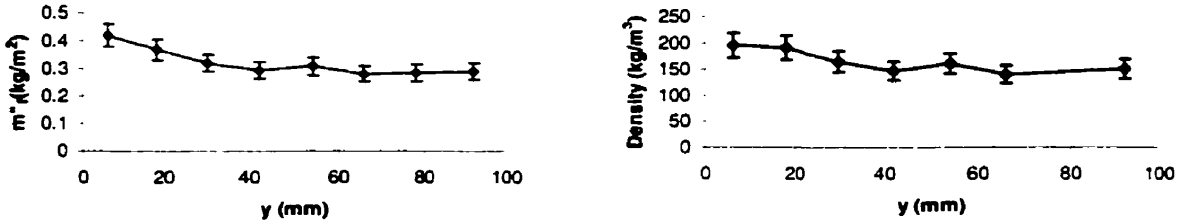

(a) (b)

Figure 2.14 Mass Concentration (a) and Density Profile (b) for Data Set A

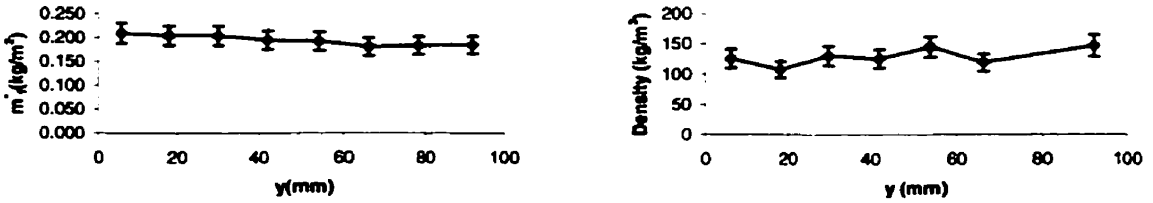

(a) (b)

Figure 2.15 Mass Concentration (a) and Density Profile (b) for Data Set B

2.9.3 Pressure Drop of Airflow through Frosted Fins

The blockage resulting from the frost growth on the fin significantly increases the air pressure drop across the fins. Figure 2.16 shows the transient pressure drop profile for Case A while Table 2.4 gives the pressure drop results for both Case A and Case B. It is shown in Figure 2.16 and Table 2.4 that frost growth results in a increase of air pressure drop across the fins by a factor of 4.6 for case A and 3.1 for Case B.

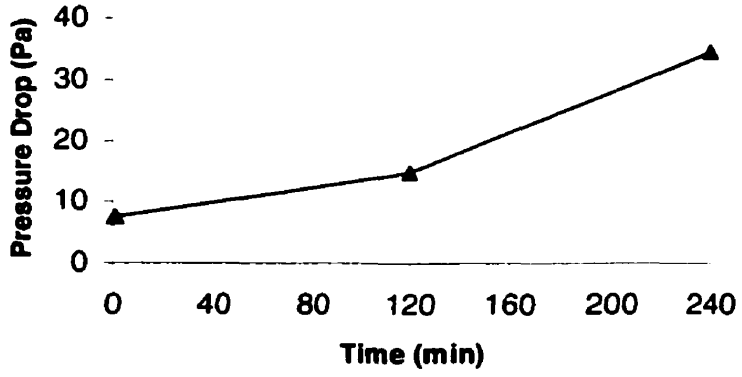

Figure 2.16 Transient pressure drop profile for test condition A
(T_a = -15.0°C, T_b = -35.0°C, V_{in} = 4.4m/s, W_{in} = 9.7x10^{-4})

Table 2.4 Pressure drop across heat exchanger fins

Test	Time (min)	Measured Pressure Drop (Pa)
A	0	7.5 ± 3.8
B	0	7.5 ± 3.8
A	240	34.6 ± 3.8
B	205	23.5 ± 3.8

2.9.4 Total Heat Rate through Cold Base

The frost growing on a fin can be considered as an additional thermal resistance on the fin, which decreases the fin heat rate. Figure 2.16 give the transient profile for the total heat rate through the cold base for test condition A. It is shown in Figure 2.16 that heat rate through cold base increase for the first 40-50 min due to the heat capacity of cold base and heat flux meter.

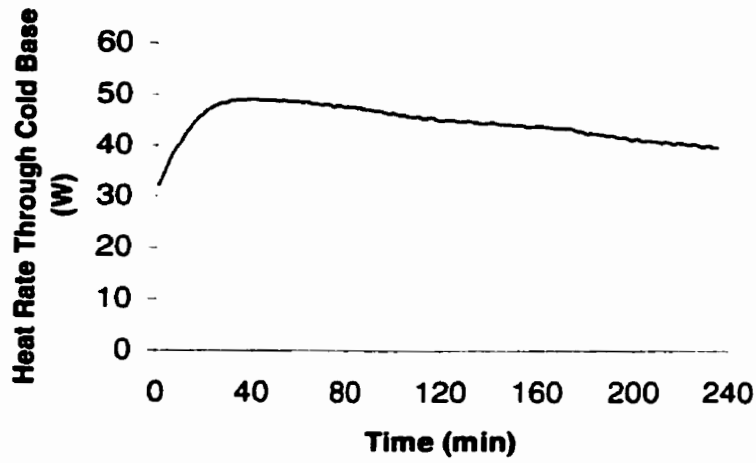

Figure 2.16 Transient heat rate through cold for Case A (T_a = -15.0°C, T_b = -35.0°C, V_{in} = 4.4m/s, W_{in} = 9.7x10^{-4})

The transient temperature effect during the early period of test is shown in Figure 2.17 for the cold base during the experiment in Case A. It is shown in Figure 2.17 that it takes 40 to 50 minutes for the cold plate temperature to reach a quasi-steady state coincident with the heat rate profiles in Figure 2.16.

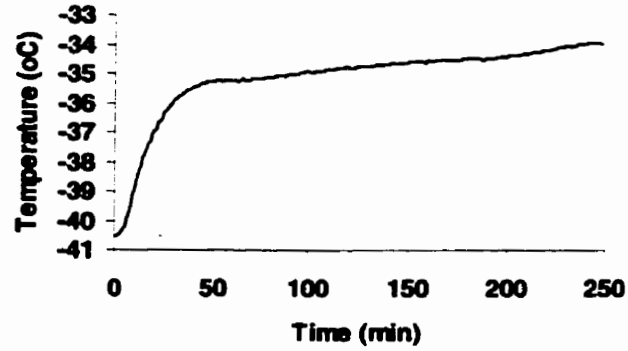

Figure 2.17 Transient temperature profile of the cold base during the experiment in Case A (T_a = -15.0°C, T_b = -35.0°C, V_{in} = 4.4m/s, W_{in} = 9.7x10^{-4}).

It is show in Figure 2.16 that, after the early period of test, the heat rate through the cold base decreases through the rest of the test period due to frost growth on the fins and un-finned base. At the end of test for Case A, the heat rate decreases by about 20%.

CHAPTER 3

PHYSICAL/NUMERICAL MODELING OF FROST GROWTH ON FLAT PLATE

In Chapter 3, a physical/numerical model is presented for predicting frost growth on flat plate under freezer operating conditions. Numerical models are important for frost growth studies because they can simulate a wider range of typical operating conditions including time variable conditions that may be impractical in experimental research. Numerical models are most useful for the design and optimization of operating conditions of heat exchangers.

In order to validate the numerical model using experimental data, the numerical model is specific to the physical test facility and boundary conditions described in Chapter 2. Alternative heat exchanger configurations and test conditions may be considered as future research.

3.1 Introduction

A schematic, detailing the geometry for the numerical model, is presented in Figure 3.1. Airflow, with known temperature, T_0, humidity ratio, W_0, and flow speed, V_0, or Reynolds number, Re, passes over a flat plate at a temperature, T_c. Both airflow temperature, T_0, and cold plate temperature, T_c, are below the freezing point while T_c is lower than the dew temperature of airflow. In the experimental study, the cold plate temperature ranges from –20°C to -41°C (-4°F to –41.8°F) while the supply air temperature ranges from –10°C to -26°C (14°F to –14.8°F) but each is held constant

during a test. As a result, a layer of frost grows on the flat plate, which is initially clean and free of frost.

The objective of the numerical model is to predict both one-dimensional spatial (z) and temporal (t) variation of the frost properties at a point, which is a distance, x, away from the leading edge of the flat plate. The frost thickness and the heat flux through the frost layer are also to be predicted. Variations in the frost properties in x-y plane are primary a consequence of variations in the boundary conditions, i.e., flat plate temperature, T_c (x, y, t), airflow temperature T_0(x, y, t), airflow humidity ratio,W_0(x, y, t) and the air stream heat and mass transfer coefficients.

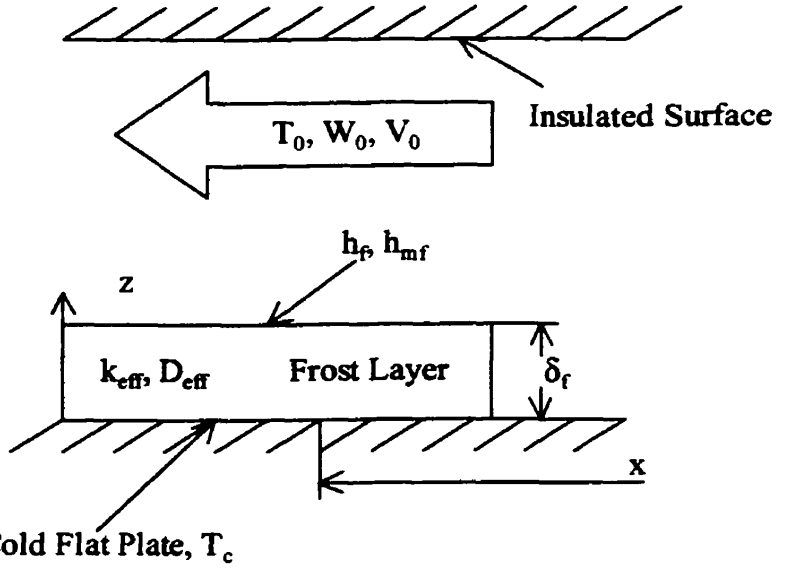

Figure 3.1 Configuration of frost growth model

Frost growth on an initially clean cold surface can be divided into two periods: an early, and relative short, droplet deposition and crystal growth period, and a fully

developed frost layer growth period (Hayashi et al., 1977). The early growth period is characterized by the condensation and subsequent freezing of small water droplets. As warm, humid air passes over a cold surface, water vapour is deposited at various nucleation sites which are usually located at microscopic surface imperfections such as scratches on the surface. These water droplets are cooled to a temperature below the freezing point (0°C) by conduction to the cold surface and freeze suddenly after 10 to 60 seconds. Ice columns then grow from the point on surface of the ice droplets furthest from the cold surface and continue normal from the cold surface. This early growth frost is characterized by dendritic crystals that grow from the top of each frozen droplet and look like trees without branches (Hayshi et al., 1997; Tokura et al., 1983; Tao et al., 1993). Then dendritic branches rapidly grow from the initial crystals on top of the frozen droplets. These branches soon form a canopy and the frost layer becomes a fully developed layer that may gradually grow over many hours without changing its essential characteristics.

Although there exist some attempts to model the early crystal growth period, for example, Seki et al. (1977) and Tao et al. (1993), it is believed that the modelling of the early crystal growth is not important to the present problem of frost growth over several hours on heat exchangers, and leads to needless complications of the formulation. The choice of the initial properties of the fully developed frost layer can be used to account for the early growth period (Le Gall et al. 1997). This is the approach used here.

The present model applied to the second or fully developed frost growth period, which represents many hours of the frost layer development and is of the greatest interest. During this period, the frost layer is characterized by a somewhat uniform canopy of frost with much branching of the dendritic ice crystals. It is modeled as a porous media made of a porous solid ice matrix with pores filled with moist air. Except adjacent to the solid surface, this porosity is typically 80% to 90%. The governing equations for the heat and mass transport processes in a porous medium were derived using the local volume averaging technique for mass, momentum, and energy transport (Kaviany 1991).

The major assumptions used to arrive at the governing equations and boundary conditions for the frost growth model are:

a) the transport of heat and mass in the frost layer is transient and macroscopically one dimensional and dependent on the boundary conditions at $z = 0$ and $z = \delta_f$,

b) the total pressure of the gaseous phase (water vapour plus air) in the frost ice matrix is constant,

c) local thermodynamic equilibrium exists in the frost layer, i.e. the gas phase temperature and solid (ice) temperature are the same,

d) gas-phase convection inside the frost layer is negligible normal to the frosted surface compared with molecular diffusion.

The justification for these assumptions is presented in Appendix A where the relative magnitude of neglected terms is shown to be small.

3.2 Governing Equations of Frost Growth on Flat Plate

The governing equations presented here are similar to those of Tao et al. (1993a). Somewhat different are the boundary conditions used for the volume fraction of ice on the cold plate and the convective heat and mass transfer coefficients at the outer edge of the frost layer. Within the frost layer, the following equations apply at every point (z, t):

Energy equation

$$\rho_f c_p \frac{\partial T}{\partial t} + \dot{m} h_{sg} = \frac{\partial}{\partial z}(k_{eff} \frac{\partial T}{\partial z}) \tag{3.1}$$

where ρ_f is the density of the frost (kg/m3),

c_p is the specific heat of the frost (J/kg K),

T is temperature (K),

t is time (s),

$\dot{m}$ is the phase change rate (kg/m^{3}s),

h_{sg} is enthalpy of sublimation (J/K),

k_{eff} is the effective thermal conductivity of frost(W/mK),

and z is position normal to the cold surface (m).

Water vapor diffusion equation

$$\frac{\partial(\varepsilon_a \rho_v)}{\partial t} - \dot{m} = \frac{\partial}{\partial z}(D_{eff} \frac{\partial \rho_v}{\partial z}) \tag{3.2}$$

where ε_a is the volume fraction of air within the frost,

and D_{eff} is the effective diffusion coefficient for water vapour within frost layer (m^2/s).

Ice phase continuity equation

$$\frac{\partial \varepsilon_\beta}{\partial t} + \frac{\dot{m}}{\rho_i} = 0 \tag{3.3}$$

where ε_β is the volume fraction of ice within the frost,

and ρ_i is the density of ice (kg/m^3).

Volumetric constraint

$$\varepsilon_\beta + \varepsilon_a = 1 \tag{3.4}$$

Thermodynamic relations

$$p_a = p_t - p_v \tag{3.5}$$

$$p_a = R_a \, \rho_a T \tag{3.6}$$

$$p_v = R_v \rho_v T \tag{3.7}$$

where p_a is the air pressure (Pa),

p_t is the total gas phase pressure (Pa),

p_v is vapour pressure (Pa),

R_a is the specific gas constant of air (J/kg K),

T is temperature (K),

ρ_a is the density of air (kg/m^3),

and R_v is the specific gas constant of water vapour (J/kg K).

For saturation conditions, the Clapeyron equation is

$$p_v = p_{ref} \exp\left[-\frac{h_{sg}}{R_v}\left(\frac{1}{T} - \frac{1}{T_{ref}}\right)\right] \tag{3.8}$$

In the governing equations, the frost properties are defined as follows,

$$\rho_f = \varepsilon_\beta \rho_i + \varepsilon_a (\rho_v + \rho_a) \tag{3.9}$$

$$c_p = \frac{\varepsilon_\beta \rho_i c_i + \varepsilon_a (c_v \rho_v + c_a \rho_a)}{\rho_f} \tag{3.10}$$

The average thermal conductivity of frost layers has been investigated by many researches. One widely used average thermal conductivity correlation used for frost in HVAC and R applications is by Yonko and Sepsy (1967) and is given by

$$k_{eff} = 0.02422 + 7.214 \times 10^{-4} \rho_f + 1.1797 \times 10^{-6} \rho_f^2 \tag{3.11a}$$

where ρ_f is the average frost density (kg/m^3).

Dietenberger (1983) has reviewed 10 independent data bases for the thermal conductivity of frost and found a wide range of calculated average thermal conductivity data (e.g. ±50% about the mean and biases up to 50% as a result of systematic errors where a wide range of frost density was reported). He found that both frost temperature and density effects are important, especially at low temperatures and densities. This equation for k_{eff} is used such that the thermal conductivity changes with height in the frost layer.

Dietenberger has recommended a complex semi-empirical relationship to calculate the local thermal conductivity of frost in the form

$$k_{eff} = f(k_{air}, k_{ice}, \rho_f, T) \tag{3.11b}$$

where the range of frost density and temperature are $50<\rho_f<600$ kg/m^3 and $136<T<267$K. The equations for this relationship are summarized in Appendix B. This equation is used such that variations in frost density and temperature will alter the local frost effective thermal conductivity.

Although no explicit uncertainty analysis was presented, the uncertainty implied in his data comparisions suggest there may be a ±15% to 20% uncertainty in k_{eff} using (3.11b).

Also,

$$D_{eff} = \varepsilon_a D_{AB} \tag{3.12}$$

where D_{AB} is the binary diffusion coefficient for water vapor in air at the film temperature (m^2/s).

3.3 Boundary and Initial Conditions

At the frost –air interface,

$$h_{mf}(x)[W_0 - W(z=\delta_f,t)] = D_{eff,s}\frac{\partial \rho_v(z=\delta_f,t)}{\partial z} + \rho_f \frac{d\delta_f}{dt} \tag{3.13}$$

where $h_{mf}(x)$ is the local convective mass transfer coefficient (kg/m^2),

W_0 is the air flow humidity ratio (kg/kg),

and W is the humidity ratio (kg/kg)

where $$W = 0.6218\frac{p_v}{p_t - p_v}. \tag{3.14}$$

The diffusion coefficient at the frost-air interface is defined as

$$D_{eff,s} = \varepsilon_a(z=\delta_f)D_{AB} \tag{3.15}$$

The boundary conditions for heat transfer are:

$$h_f(x)[T_0 - T(z=\delta_f,t)] = k_{eff}\frac{\partial T(z=\delta_f,t)}{\partial z} - h_{sg}\rho_f\frac{d\delta_f}{dt}(t) \tag{3.16}$$

$$T(z=0,t) = T_c \tag{3.17}$$

where $h_f(x)$ is the local convective heat transfer coefficient (W/m^2K), and is derived from the Gnielinski correlation.

The Gnielinski (1976) correlation for convective heat transfer for turbulent flow with low Reynolds numbers is taken to be

$$Nu_D = \frac{(f/8)(Re_D - 1000)Pr}{1+12.7(f/8)^{1/2}(Pr^{2/3}-1)} \tag{3.18}$$

where Nu_D is the Nusselt number,
Re_D is the Reynolds number,
Pr is the Prandtl number,
and f is the friction factor, taken to be 0.06 for rough frost.

Figure 14-7 in Kays and Crawford (1993) was then used to determine the local Nusselt number Nu_x. It is assumed in this study that for mass transfer

$$Sh_x = Nu_x \tag{3.19}$$

Therefore $h_{mf}(x)$ and $h_f(x)$ can be obtained from the Sh_x and Nu_x in Equation (3.18) and (3.19). At the cold plate surface

$$T(z=0,t)=T_c \tag{3.20}$$

$$\varepsilon\beta(z=0,t) = 0.3 \tag{3.21}$$

The selection of the above boundary condition (3.21) for the ice volume fraction, ε_β, needs more discussion. In their study of the early growth period of frost growth on a cold plate supplied by room air at a high relative humidity, Tao et al. (1993b) showed that a large fraction (typically 52% to 72%) of the surface on which frost grows is covered by water droplets (typically 20 to 70 μm average diameter for a plate temperature of -25°C) before these droplets suddenly freeze after a time duration of 15 to 100s. Some subcooling of the water droplets is expected during this period. Shortly after these droplets all suddenly freeze, frost crystals start to grow on these frozen droplets and a fully developed frost layer is formed after about 200s for cold plate temperatures less than -25°C (-13°F). Ramaswamy et al. (1995) showed similar results for the early growth period of frost on smooth cold surfaces with airflow at room temperature.

These early frost growth studies by Tao et al. (1993b) and Ramaswamy et al. (1995) are somewhat in conflict with the models of Tao et al. (1993a) and Le Gall et al. (1997) because the assumed boundary condition for the fraction of cold plate surface covered in frost is not modeled correctly. This boundary condition should account for the large fraction of the cold surface covered by ice during the early growth period (e.g. about 50% to 60%). This fraction of ice on the surface decreases slightly with decreasing surface temperatures. The boundary condition for the fully developed frost ice fraction on the cold plate in this study is set equal to 30% (i.e., $\varepsilon_\beta(z=0)=0.3$). This value was found to give a good fit between the theoretical simulations and the experimental data. A sensitivity study of the boundary condition did not reveal a strong sensitivity except for the case selected by Tao. It is noted that the approach of Le Gall et al. (1997) will not

permit this correction of the cold plate boundary condition because the fraction of ice on the surface is derived, not specified.

Selection of the correct ice fraction on the cold surface to start the numerical model computation of fully developed frost is not known accurately without developing a new experimental facility to investigate frost growth on surfaces for subfreezing supply air. Nonetheless, the experimental data of Tao et al. (1993b) are clear, first the volume fraction of ice droplets on the cold plate at the time of droplet freezing is at least 0.6 but this fraction decreases slightly with decreasing plate temperatures, especially for plate temperatures less than -25°C (-13°F). Secondly, the average size of frozen droplets are less than 70μm (2.76×10^{-3} in) at -25°C (-13°F) and this average ice particle size will decrease with decreasing plate temperatures. Studies of the formation of droplets on surfaces show that the shape of water droplets on surfaces depends on several factors including: surface contaminants, surface roughness, material used for the surface, the rate of growth of the droplet size and the size of the droplet. Generally, the droplet height is less than its diameter.

A qualitative confirmation of this boundary condition was investigated when a pressurized cold dry air jet was used to remove frost from a surface after it was grown on a cold plate under freezer operation conditions for a period of 2 hours. The mass accumulation results of this frost removal investigation showed that typically about 50% of the frost mass accumulation exists in the 25% of the frost layer adjacent to the surface. Furthermore, it was necessary to increase this air-jet pressure by 5 to 10 times to remove

all the bottom layer of high-density frost. Thus we should expect a thin layer of a relatively high-density frost near the cold plate on top of which exists a low-density frost.

The initial conditions are:

$$T(z,t=0)=T_c \tag{3.22}$$

$$\varepsilon_\beta(z,t=0)=0.01 \tag{3.23}$$

The sensitivity of the frost growth boundary and initial conditions is discussed in Chapter 4.

As discussed in Tao et al. (1993a), an implicit finite difference formulation of these equations was used to solve this numerical model with the properties evaluated from the previous time step.

CHAPTER 4

VALIDATION OF NUMERICAL MODEL FOR FROST GROWTH ON THE FLAT PLAT

4.1 Comparison of Numerical Simulations and Selected Data

Mao et al. (1999) presented an experimental database of the frost growth on the flat plate including 20 sets of data for 20 different test conditions. These data are presented in Appendix D. To develop an accurate numerical model, it is essential to identify those test conditions and results that would not give rise to very large uncertainties in the data. It was noted in Chapter 2, that uncertainties in the supply air humidity ratio (W) might be large when the supply air humidity ratio is low with respect to the test variations in humidity ratio (e.g. up to 0.0001). Also, it was noted that rough frost, or partially rough frost, has a large uncertainty for the height measurement when the frost layer is thin (i.e., less than 1mm or 0.04in). Uncertainty in frost mass concentration is somewhat smaller and is most significant for very thin layers of frost, similar to that for frost height. Uncertainty in the temperature difference between the airflow and flat plate was large when the temperature difference is less than 12°C (21.6°F).

There are two test conditions presented in Mao et al (1999) which are physically different tests where the supply air humidity ratio is greater than the saturation value, implying super-saturated supply air at 100% RH with airborne frost crystals or water droplets in a fog in the supply air. For airborne crystals or water droplets, frost growth is mostly by the impact of airborne frost crystals or droplets and their accretion on the outer

edge of the frost with no diffusion within the frost layer. The current molecular diffusion model does not apply to this very different physical phenomenon. For a high concentration of airborne particles, frost growth is expected to be very rapid and mostly at the air-frost interface and, depending on the airflow momentum, it can be very rough.

The above discussion implies that one should eliminate from comparisons with the model all those data sets that have common large uncertainty problems and retain those that have no problems or for which the problems may be small. With these criteria in mind, 9 data sets are selected to compare with simulations. First, simulation results are compared with one typical data set to illustrate the nature of frost growth on a flat plate then agreements with the nine data sets that possess small uncertainties in the measured frost properties are investigated.

In the presentation of results, first, typical temporal and spatial property and heat flux results are presented by comparing the simulation with one set of measured data. Figure 4.1 shows the simulated temporal variations in (a) frost height, (b) density and (c) heat flux and spatial variations in (d) density (e) mass accumulation rate and (f) temperature. These results are compared with data from one selected set. Spatial distributions of density within the frost layer are only compared with the measured average value. The selected values of the input variables for the simulation are the same as the test conditions. Given the uncertainties in the data, these comparisons illustrate reasonable agreement with measured data. The trends of property changes with time and

position are best seen in the simulation results. The spatial variation of density within the frost layer is very large even when the surface volume fraction of frost $\varepsilon_\beta(z=0)$ is only 0.3. The mass rate of accumulation of frost is large enough to cause significant coupling with heat transfer in the energy equation, especially near the cold plate. The increase in mass accumulation rate beyond $z/\delta_f=0.2$ is significant, but because it is somewhat constant over most of the frost height, the temperature profile appears to be linear over the same region. De-coupling the heat and mass transfer problem, as presented by Lee et al. (1997) and others, could lead to significant errors, especially near the cold plate surface.

All the data for the 9 tests with a low uncertainty are compared with simulation results in Figure 4.2. Generally, with the exception of a few data, good agreement is achieved because discrepancies between the simulation and data are less than 20% for most of the data. Uncertainty in the data for the smooth frost height, density and heat flux is less than 6%. For the few data with increasing frost roughness, the uncertainty in these data increases dramatically to perhaps 25% for frost thickness and density.

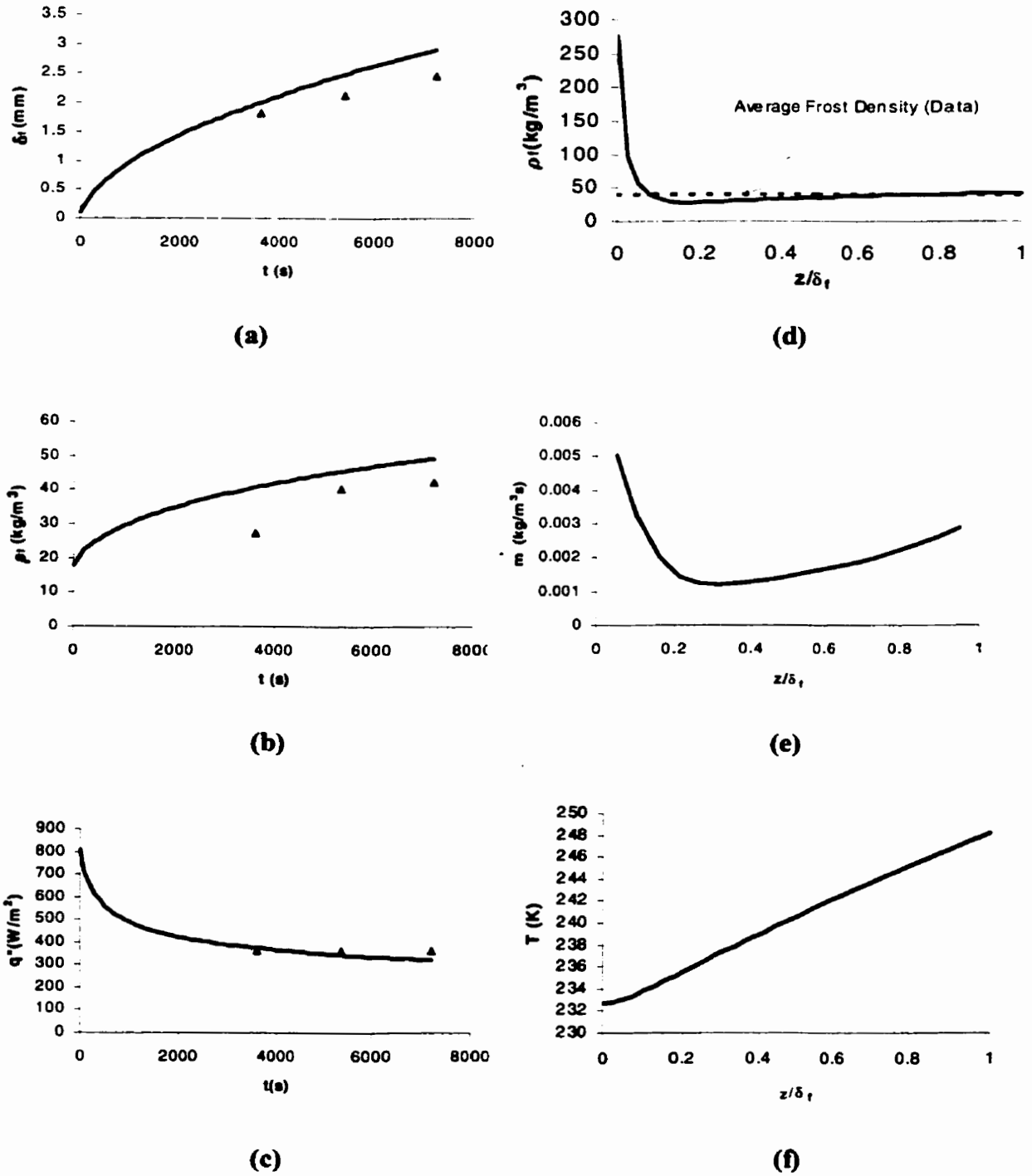

Figure 4.1 Comparison of one simulation and measured data for test conditions: T_c=-40°C, T_0=-15.4°C, W_0=0.0093, Re_d=8195, x=0.26m. Temporal distribution of (a) frost height, (b) frost density and (c) heat flux and for t =5400s spatial distribution of (d) frost density (e) mass accumulation rate (f) temperature

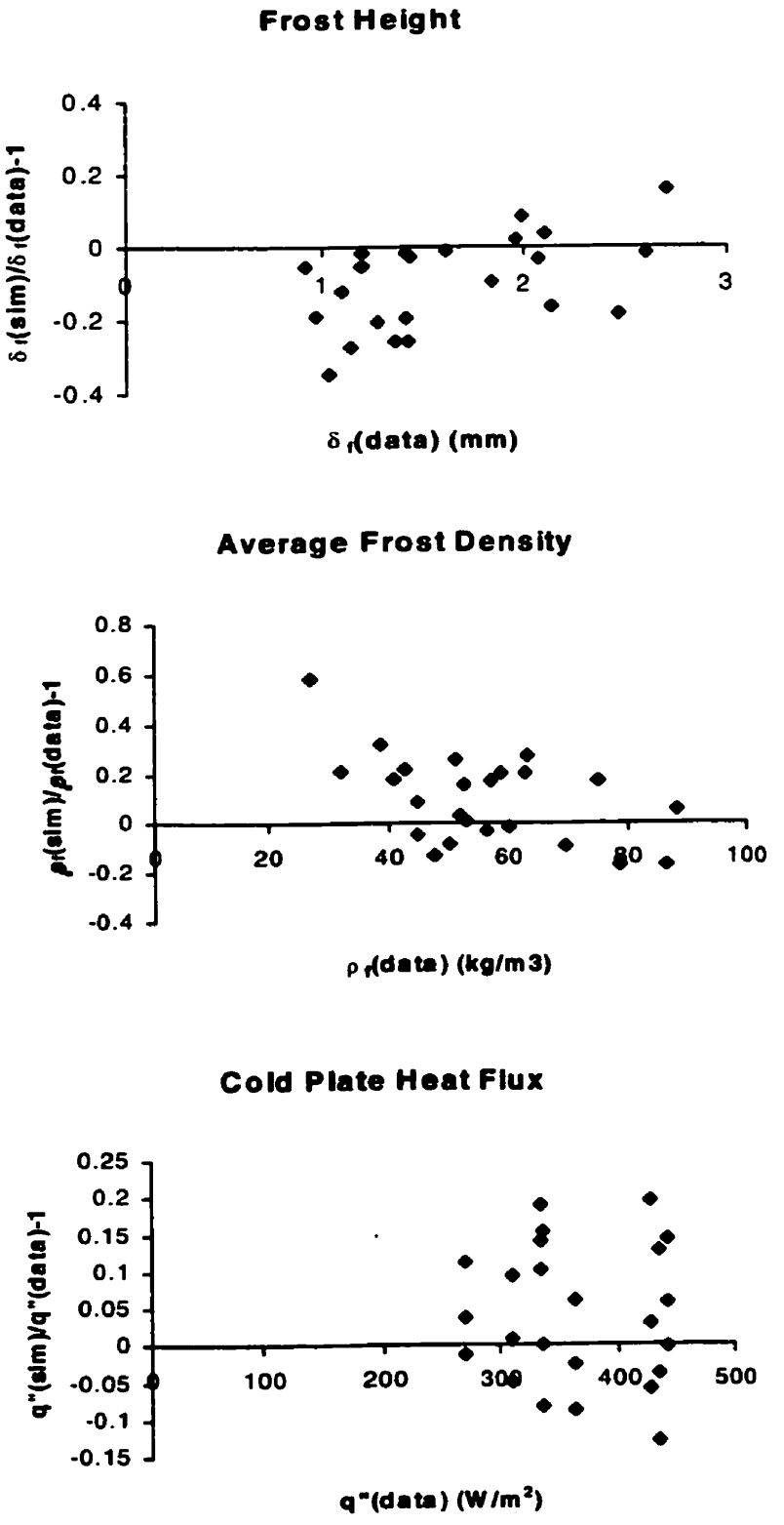

Figure 4.2 Comparison of data and the simulation using the input data for each test and simulation

4.2 Sensitivity Study of Numerical model

In Figure 4.3, the sensitivity of the simulations to surface volume fraction $\varepsilon_\beta(z=0)$ is examined. These results for the same test conditions as Figure 4.3 show that the selection of $\varepsilon_\beta(z=0)$ is an important parameter but the difference between $\varepsilon_\beta(z=0)$=0.3 and 0.6 is small. Included in the comparisons is the assumption $\partial\varepsilon_\beta / \partial z(z=0)=0$ for a boundary condition similar to Tao et al. (1993a) which gives a very low surface frost surface density and mass accumulation rate near z=0. (Comparisons with Le Gall et al. (1997) are not possible because they did not use any boundary condition for ε_β).

Ice volume fraction $\varepsilon_\beta(z=0)$=0.3 is selected for the entire test conditions with relatively low uncertainties. This value is somewhat lower than the data of Tao et al. (1993b) for the early growth of frost on a smooth surface supplied by air at room temperature. (i.e., $\varepsilon_\beta(z=0)\cong 0.6$) but as it was shown in Figure 4.3 that, aside from the average density, the results are not too sensitive to our selection. It was noted in the previous discussion that, for freezer operating conditions, somewhat lower values of $\varepsilon_\beta(z=0)$ may be expected. Secondly, the spatial step size for these computations was taken to be 25 steps across the entire frost layer which is much larger than the expected droplet size in the surface (i.e., 10 to 50 μm for surface temperature less than -25°C). This spatial step size near the surface should, perhaps, be about the same size as the expected droplet size or the surface value of ε_β should be slightly lower.

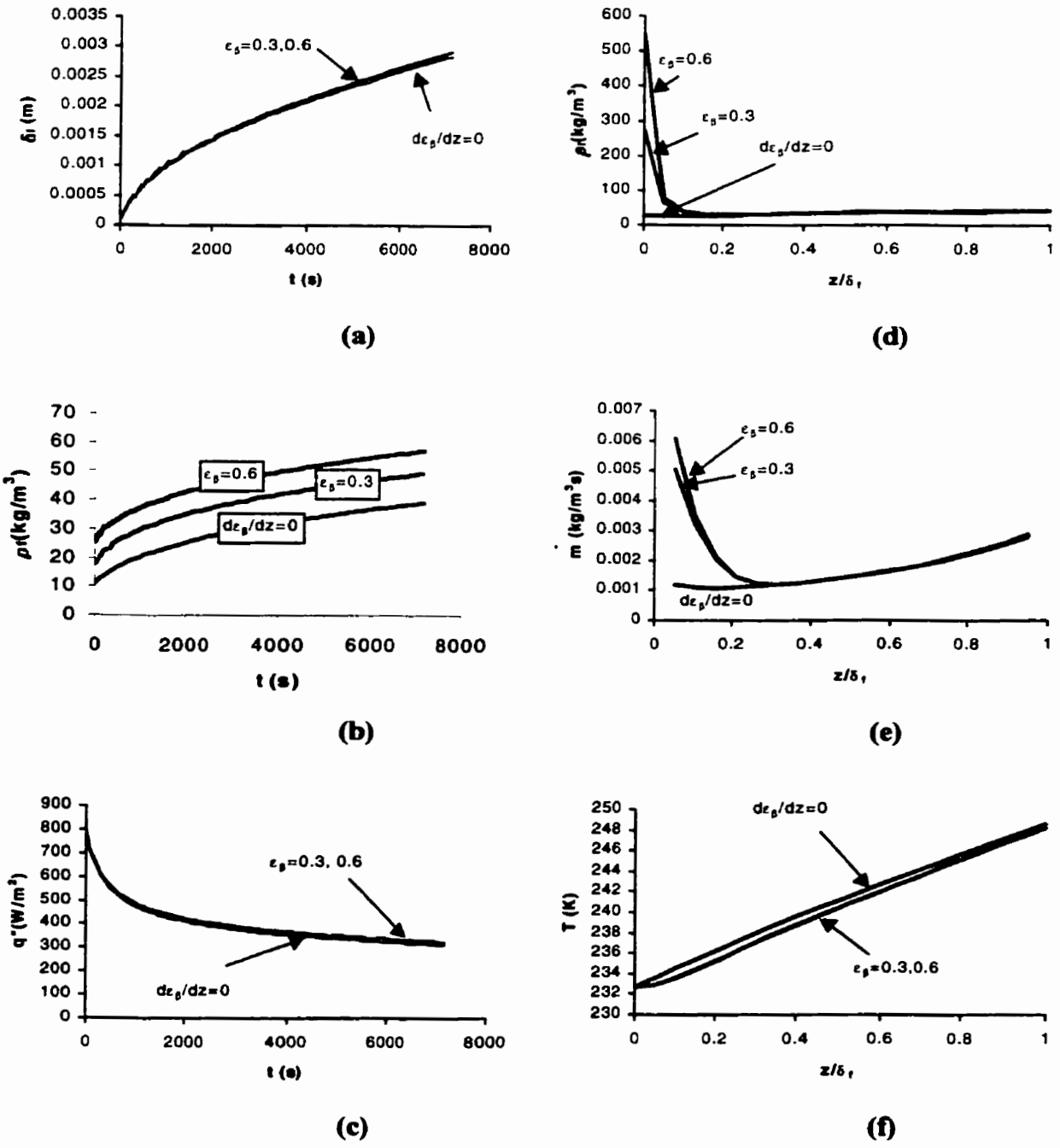

Figure 4.3 Sensitivity study for numerical model of frost growth on a flat plate using different boundary conditions for ε_β at z=0. Temporal distribution at x=0.26m of (a) frost height, (b) frost density and c) heat flux. Spatial distribution at t=5400s of (d) frost density (e) mass accumulation rate and (f) temperature

4.3 Conclusions

In this Chapter, the numerical model for the frost growth on a flat plate is validated using published experimental data. It was found that the boundary conditions on the cold plate must be selected to physically model the high surface density of frost reported in the literature. Simulation results are only compared to the measured data that are expected to have a relatively small uncertainty. Agreement between these measured data and simulations is reasonable and generally within the experimental uncertainty and the uncertainty caused by the boundary conditions selected for the model.

CHAPTER 5

PHYSICAL/NUMERICAL MODELING FOR FROST GROWTH ON HEAT EXCHANGER FINS

In this Chapter, a numerical model to simulate frost growth on a cold fin surface exposed to a forced convective flow is presented. This model will be used to predict spatial and temporal variations of the frost height, frost density, temperature and other properties over the entire surface of the fin and throughout the height of the frost. The frost mass accumulation and heat flux through the frost layer will also be predicted. The second objective is to predict the change in pressure drop across the fins for a given flow rate or, conversely, predict flow rate change for a given pressure drop across the fins with frost growth.

Unlike flat plates at a uniform cold plate temperature, heat exchanger fins give rise to frost growth that is quite non-uniform over the fin surface. The prime cause of the variations in frost properties on fins is the non-uniform surface temperatures on the fin. A secondary cause of frost non-uniformity on heat exchanger fins is due to variations in the air stream properties and heat and mass transfer coefficients. In this Chapter, frost growth on fins is first modeled as a three-dimensional layer which results from the transient growth of frost on a surface of non-uniform temperature and with non-uniform airflow properties.

5.1 Test Configuration

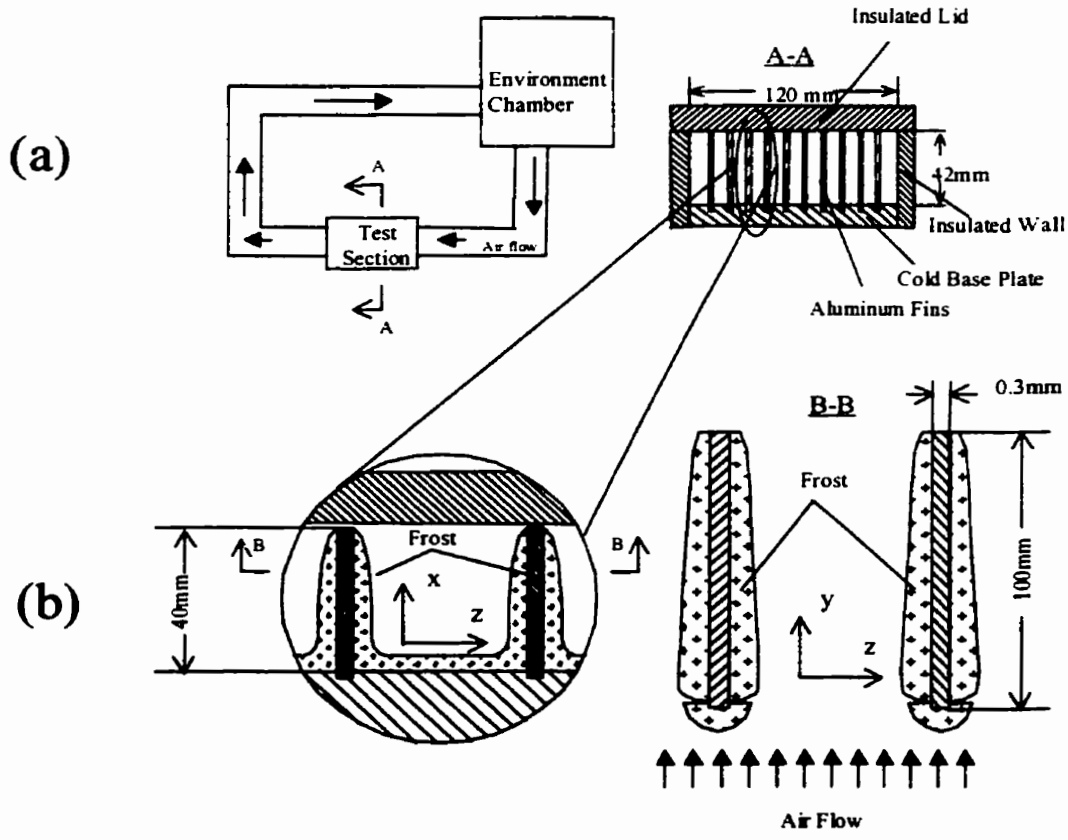

Figure 5.1 (a) Configuration of the test loop and test section
(b) Frost coated heat exchanger fins, elevation and plan views

Since the model is applicable to a particular heat exchanger configuration, it is briefly described. Figure 5.1 illustrates the test loop, test section and frost growth on the heat exchanger fins. Air is drawn from an environmental chamber at a selected temperature, humidity and volume flow rate and passes over the finned test section before being returned to the environmental chamber. The fins (40mm×100mm and 0.3mm thick) were aluminum alloy (k_{fin}=177W/mK) and placed 9.2mm apart in the cold base plate as discussed in detail in Chapter 2. Test conditions include a fin base temperature range from –30 to -41°C (-22 to –42°F), air flow temperature range from –13 to -21°C (8 to -

5°F) for the air supply with a relative humidity over 90% but less than 100%. Frost growth on the fins and base plate for periods up to 6 hours from a initial condition of no frost.

Given the operating conditions and fin geometry, the model should predict the transient frost height profile on the fins and cold base plate as well as the heat rate through the cold base and air pressure drop across the finned section. Table 5.1 lists the parameters of the operating conditions and fin geometry, which are inputs or known values for the model.

The numerical model for simulating the frost growth on plate-fin heat exchangers, illustrated in Figure 5.1, includes two parts, one is a frost growth model describing frost growth on a fin suface and unfinned base, the other is a 2-D heat conduction model describing heat transfer within each aluminum fin.

Table 5.1 Input parameters for the numerical model

Operating conditions	Fin geometry
Airflow temperature , T_{in}	Fin length, l_{fin}=100mm
Airflow humidity ratio, W_{in}	Fin height, h_{fin}=40mm
Airflow velocity, V_{in}	Fin thickness, δ_{fin}=0.3mm
Cold base temperature, T_b	Fin spacing, t_{fin}=9.2mm

5.2 Frost Growth Model

It was shown in Appendix A that frost growth on a surface can modelled as transient growth of a porous frost layer normal to the surface. The resulting equations are similar to those for grost growth on the flat plate. They duffer in the boundary conditions:

Energy equation:

$$\rho_f c_p \frac{\partial T}{\partial t} + \dot{m} h_{sg} = \frac{\partial}{\partial z}(k_{eff} \frac{\partial T}{\partial z}) \tag{5.1}$$

Vapor transport equation:

$$\frac{\partial(\varepsilon_a \rho_v)}{\partial t} - \dot{m} = \frac{\partial}{\partial z}(D_{eff} \frac{\partial \rho_v}{\partial z}) \tag{5.2}$$

Ice phase continuity equation:

$$\frac{\partial \varepsilon_\beta}{\partial t} + \frac{\dot{m}}{\rho_i} = 0 \tag{5.3}$$

Volumetric constraint:

$$\varepsilon_\beta + \varepsilon_a = 1 \tag{5.4}$$

Thermodynamic relations:

$$p_a = p_t - p_v \tag{5.5}$$

$$p_a = R_a \rho_a T \tag{5.6}$$

$$p_v = R_v \rho_v T \tag{5.7}$$

For saturation conditions, the Clapeyron equation is used:

$$p_v = p_{ref} \exp[-\frac{h_{sg}}{R_v}(\frac{1}{T} - \frac{1}{T_{ref}})] \tag{5.8}$$

In the governing equations, the frost properties are defined as follows,

$$\rho_f = \varepsilon_\beta \rho_i + \varepsilon_a(\rho_v + \rho_a) \tag{5.9}$$

$$c_{pf} = \frac{\varepsilon_\beta \rho_i c_i + \varepsilon_a(c_v \rho_v + c_a \rho_a)}{\rho_f} \tag{5.10}$$

$$k_{eff} = f(k_{air}, k_{ice}, \rho_f, T) \tag{5.11}$$

The thermal conductivity of frost, k_{eff}, is calculated using Dietenberger's model (1983) (see Appendix A).

$$D_{eff} = \varepsilon_a D_{AB} \tag{5.12}$$

Equation (5.1)-(5.12) gives a completed description of heat and mass transfer within the frost layer. Theoretically, with the proper boundary and initial conditions, the characteristics of frost layer can be solved from Equations (5.1)-(5.12).

5.2.1 Boundary Conditions for the Frost Growth Model

At the frost –air interface, the mass transfer boundary condition is

$$h_{mf}[W_0 - W(z = \delta_f, t)] = D_{eff,s} \frac{\partial \rho_v(z = \delta_f, t)}{\partial z} + \rho_f \frac{d\delta_f}{dt} \tag{5.13}$$

where h_{mf} is the local convective mass transfer coefficient (kg/m^2),

W_0 is the air flow humidity ratio (kg/kg),

and W is the humidity ratio (kg/kg)

where $$W = 0.6218 \frac{p_v}{p_t - p_v}. \tag{5.14}$$

The diffusion coefficient at the frost surface is defined as

$$D_{eff,s} = D_{AB} \varepsilon_a (z = \delta_f) \tag{5.15}$$

The boundary conditions for heat transfer are:

$$h_f[T_0 - T(z=\delta_f,t)] = k_{eff}\frac{\partial T(z=\delta_f,t)}{\partial z} - h_{sg}\rho_f\frac{d\delta_f}{dt}(t) \tag{5.16}$$

$$T(z=0,t) = T_c \tag{5.17}$$

The boundary conditions for the ice volume fraction are

$$\frac{\partial \varepsilon_\beta(z=\delta_f,t)}{\partial z} = 0 \tag{5.18}$$

and

$$\varepsilon_\beta(z=0,t) = 0.3 \tag{5.19}$$

The convective heat and mass transfer coefficients, h_f and h_{mf}, are calculated from Gnielinski correlation but modified for the entrance effect. The uncertainty in these coefficients is large (e.g.≈30%). The local cold surface temperatures, T_c, varies over the fin and is two-dimensional (x,y) and transient. T_c is determined using the fin heat conduction model.

5.2.2 Initial Conditions for Frost Growth

The initial height of frost over the entire fin is assumed to be

$$\delta_f(t=0) = 0.1mm \tag{5.20}$$

The initial temperature within the frost layer is

$$T(t=0,z) = T_c \tag{5.21}$$

The initial condition for volume fraction of ice, ε_β, within the frost layer is taken to be a constant which depends on the position on the fin,

$$\varepsilon_\beta(t=0,x,y,z)=\varepsilon_0(x,y) \tag{5.22}$$

In order to get the best fit between experimental data and simulation results, it is found that ε_0 is not a constant on the fin surface. ε_0 depends on the location on the fin surface and ranges from 0.01 to 0.23 as given by,

$$\varepsilon_0(x,y)=0.01+0.12\frac{x}{h_{fin}}+0.1\frac{y}{l_{fin}} \tag{5.23}$$

where h_{fin} is the height of the fin (m),

and l_{fin} is the length of the fin (m)

More discussion of ε_0 is presented later in the sensitivity study in Chapter 6.

Equation (5.23) states that the initial volume fraction on the fin (i.e. after the early crystal growth period of less than 100s) will be distributed with increasing values in both the x and y directions. That is, initially the frost density is higher away from the base where the temperature is warmer and downstream of the leading edge where the entrance effects are negligible. The boundary condition, equation (5.19), states that the volume fraction will be 0.3 everywhere at z=0 for t>0 (i.e. after the early growth period). The consequence of these two conditions is that there will be a large gradient in frost density near the surface and a relatively high frost density on the surface for all times larger than zero. This boundary condition appears to be consistent with the studies of early frost growth (Tao et al. 1993a) and the experimental data presented in Chapter 6.

5.3 Model for Heat Conduction in a Fin

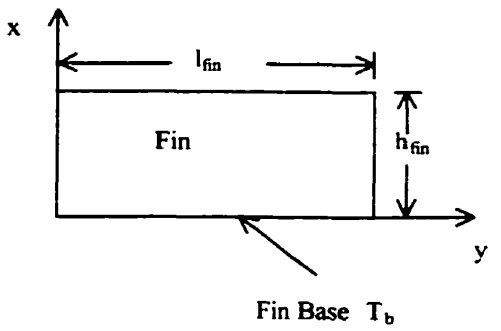

Figure 5.2 Configuration of two-dimensional heat transfer fin model

The model for heat transfer in the frost layer is coupled to the heat conduction in a fin through the boundary conditions. The governing equation for heat transfer within the fin is,

$$\rho_{fin} c_{fin} \frac{\partial T_c}{\partial t} = k_{fin} \left(\frac{\partial^2 T_c}{\partial x^2} + \frac{\partial^2 T_c}{\partial y^2} \right) + S \tag{5.24}$$

where T_c is the temperature within the fin (K),

ρ_{fin} is the density of the fin (kg/m^3),

c_{fin} is the specific heat of the fin (J/kg K),

k_{fin} is the thermal conductivity of the fin (W/m K),

and S is the heat source term (W/m^3).

S is evaluated from the frost growth model, i.e., the heat rate transferred from the frost layer to the fin surface.

$$S = \frac{2.0}{\delta_{fin}} * k_{eff} \frac{\partial T(z=0,t)}{\partial z} \tag{5.25}$$

where T is the temperature within the frost (K),

and δ_{fin} is the thickness of the fin (m).

The factor 2.0 is used to account for frost growing on both sides of each fin. At the fin base, the temperature is a constant, T_b. The fin thickness is small (0.3mm or 0.012in) so that the heat transfer at the fin edge is negligible because this area is less than 1% of the total surface. The boundary conditions for the four edges of the fin are set to be:

$$T_c(x=0,y)=T_b \tag{5.26}$$

$$\frac{\partial T_c}{\partial x}(x=h_{fin},y)=0 \tag{5.27}$$

$$\frac{\partial T_c}{\partial y}(x,y=0,l_{fin})=0 \tag{5.28}$$

The initial condition is selected to be

$$T_c(x,y,t=0)=T_b \tag{5.29}$$

5.4 Heat and Mass Transfer at the Frost-Air Interface

The local convective heat and mass transfer coefficients, $h_f(x,y,t)$ and $h_{mf}(x,y,t)$ must be estimated. The Gnielinski correlation and an entrance correction are used to estimate these convective heat and mass transfer coefficients. The Gnielinski correlation is selected since it applies to the Reynolds number range used in the experiment. This correlation was first developed for heat transfer in smooth tubes but it has been widely used for rough surfaces in ducts. Since the frost layer causes most the

resistance to heat and mass transfer, the uncertainty in this correlation plays a small role in the uncertainty in the frost growth.

To further simplify calculations of h_f and h_{mf} using Gnielinski correlation, it is assumed that frost grows uniformly on a fin surface with a frost height of $\delta_{f\text{-}ava}$ and un-finned base with a frost height of $\delta_{f\text{-}base}$. It is also assumed that h_f and h_{mf} vary only in the airflow direction, y.

The Gnielinski (1976) correlation for convective heat transfer for fully developed turbulent flow in a duct with Reynolds numbers between 3000 and 10000 is taken to be

$$Nu_D = \frac{(f/8)(Re_D - 1000)\,Pr}{1 + 12.7(f/8)^{1/2}(Pr^{2/3} - 1)} \tag{5.30}$$

where Nu_D is the Nusselt number,

Re_D is the Reynolds number,

Pr is the Prandtl number,

and f is the friction factor, taken to be 0.06 for rough frost.

A calculation of the dimensionless surface roughness, k+, of a fully developed frost layer shows that

$$30 < k^+ = \frac{k' v^*}{\nu} < 100 \tag{5.31}$$

where k′ is the estimated average frost roughness height (i.e. 0.4 to 1.2×10^{-3}m),

v* is the friction velocity and equals $(\tau_w/\rho_a)^{1/2}$ (m/s),

τ_w is the wall shear stress (N/m^2),

ρ_a is the air density (kg/m^3),

and ν is the air kinematic viscosity (m^2/s).

The above range of k+ implies the airflow near the frost-air interface is classified as a fully rough or at least a transitional rough surface. In addition, the free stream flow is turbulent with Reynolds numbers over 3000.

The Reynolds number at anytime during the frost growth is calculated from the equation

$$\mathrm{Re}_D = \frac{\rho_a D_h V}{\mu} \tag{5.32}$$

where D_h is the hydraulic diameter of the frost free area between the fins(m).

D_h is calculated using

$$D_h = \frac{4.0*(t_{fin} - 2.0*\delta_{f-avg})*(h_{fin} - \delta_{f-base})}{2.0*[(t_{fin} - 2.0*\delta_{f-avg}) + (h_{fin} - \delta_{f-base})]} \tag{5.33}$$

where t_{fin} is the fin spacing (m),

$\delta_{f\text{-}avg}$ is the average frost height on fin (m),

$\delta_{f\text{-}base}$ is the average frost height on un-finned base (m),

and V is the average air flow velocity through the finned area (m/s).

The average air speed V at any time is calculated using

$$V = \frac{V_{in} * t_{fin} * h_{fin}}{(t_{fin} - 2.0*\delta_{f-avg})*(h_{fin} - \delta_{f-base})} \tag{5.34}$$

where V_{in} is the air flow velocity before it enters the finned section (m/s).

Figure 14-7 in Kays and Crawford (1993) is used to determine the enhanced local Nusselt number Nu (y) caused by the effect of turbulent air flow entering the finned test section. Assuming heat and mass transfer similarity for this slowly varying heat and mass transfer process gives

$$Sh(y) = Nu(y) \tag{5.35}$$

where Sh is the Sherwood number.

Therefore $h_{mf}(y)$ and $h_f(y)$ is obtained from the definitions of Sh and Nu.

$$h_f(y) = \frac{Nu(y) * k_a}{D_h} \tag{5.36}$$

$$h_{mf}(y) = \frac{h_f(y)}{\rho c_p} \tag{5.37}$$

Variations in h_f and h_{mf} are assumed to be negligible in the x direction normal to the cold plate.

5.5 Pressure Drop Across the Fins

Blockage, resulting from the frost growth on the fin of a heat exchanger increases the air pressure drop across the fins. Assuming constant air density, the air pressure drop, ΔP (Pa), through the fins can be calculated using the following equation (Kays and London, 1984),

$$\Delta P = \frac{1}{2}\rho_a V^2 (K_c + C_f \frac{A}{A_c} + K_e) \tag{5.38}$$

where K_c= contraction loss coefficient for flow at heat exchanger entrance, varies with frost height,

K_e= expansion loss coefficient for air flow at heat exchanger exit, varies with frost height,

$C_f = \tau_s/(1/2\rho_{air}V^2)$, friction coefficient or Fanning friction factor,

A= exchanger total heat transfer area on one side,

A_c= exchanger minimum free-flow area, varies with frost height,

V= flow velocity entering the core of finned section (m/s),

ρ_a= density of air (kg/m^3)

In Equation (5.38), the contraction loss coefficient, K_c, and expansion loss coefficient, K_e, are for a sharp contraction at heat exchanger entrance and a sharp expansion at heat exchanger exit (Kays and London, 1984). It is observed during the experiments that after a period of frost growth, both the entrance and exit of the finned section become rounded with frost (see Figure 5.1) resulting in a reduction in the K_c and K_e. To include the effect of frost growth on the pressure loss at entrance and exit, a modified equation for the pressure drop is then used,

$$\Delta P = \frac{1}{2}\rho_a V^2[C(K_c + K_e) + C_f \frac{A}{A_c}] \qquad (5.39)$$

where C is an emperical coefficient. Coefficient C should decrease with the increase of frost height and in this study, especially when the frost layer is thin compard to the fin thickness. It is found to be

$$C = 0.5(\frac{\delta_{f-avg}}{\delta_{fin}})^{-0.65} \qquad (0.1mm<\delta_{f\text{-}avg}<\delta_{fin}) \qquad (5.40)$$

$$C=0.5 \qquad (\delta_{f\text{-}avg} \geq \delta_{fin}) \qquad (5.41)$$

5.6 Total Heat Transfer through Finned and Un-finned Base

The heat rate through each fin with frost growth is calculated using,

$$q_{fin} = \delta_{fin} \int_0^{l_{fin}} k_{fin} \left. \frac{\partial T_c}{\partial x} \right|_{x=0} dy \qquad (5.42)$$

The heat rate on base plate between the fins is calculated from the frost growth model using the equation

$$q_{base} = A_{base} k_{eff} \left. \frac{\partial T}{\partial z} \right|_{z=0} \qquad (5.43)$$

where A_{base} is the total un-finned base plate area (m^2).

The total heat transfer rate is then calculated using

$$q_{total} = n q_{fin} + q_{base} \qquad (5.44)$$

where n is the total number of the fins.

5.7 Calculation for the Bulk Air Flow Temperature T_0 and Humidity Ratio W_0

The airflow temperature, T_0, and humidity ratio, W_0, used in Equations (5.21) and (5.18) as the boundary conditions of frost growth model vary with distance from the leading edge. Heat and water vapor transfer from the airflow to the frost layer on each fin cause the airflow temperature and humidity ratio to decrease with distance from the leading edge. For our calculations, W_0 and T_0 are defined as the average airflow bulk temperature and humidity ratio within the finned section. These are:

$$W_0 = (W_{in} + W_{out})/2 \qquad (5.45)$$

$$T_0 = (T_{in} + T_{out})/2 \tag{5.46}$$

where W_{in}= air flow humidity ratio at the entrance of the finned section

W_{out}= air flow humidity ratio at the exit of the finned section

T_{in}= air flow temperature at the entrance of finned section (K)

T_{out}= air flow temperature at the exit of finned section (K)

Applying energy balance for air flow within the finned section gives,

$$\rho_{air} Q(c_p \Delta T + 2500 \Delta W) = q_{total} \tag{5.47}$$

where Q= the volume flow rate of airflow(m^3/s)

ρ_{air}= air density(kg/m^3)

c_p= specific heat of air (J/kg K)

$\Delta T = T_{in} - T_{out}$

q_{total}= the total heat transfer rate between air flow and finned section (W)

Applying mass balance of airflow within the finned section gives,

$$\rho_{air} Q \Delta W = \int h_{mf} \rho_{air} (W_0 - W_{fs}) dA \tag{5.48}$$

where $\Delta W = W_{in} - W_{out}$

W_{fs}=Humidity ratio on the frost surface

The right side of equation (5.48) indicates the total vapor transfer rate between the air flow and frost layer surface. The average bulk humidity ratio, W_0, and temperature, T_0, are obtained by combining Equation (5.45) to (5.48).

The relative humidity ratio of airflow is about 90% but less than 100% before air flow enters the finned section. With the decrease of airflow temperature within the finned section, the humidity ratio, W_0, calculated from the Equation (5.45) to (5.48) may indicate a super-saturated condition for the corresponding airflow temperature,T_0, (i.e. relative humidity ratio over 100%). The transit time for airflow through the finned section is very small (about 0.02s) so that when super-saturated air within the heat exchanger is predicted, the airflow is expected to remain super-saturated without condensation or sublimation on airborne microscopic dust particles.

5.8 Numerical Solution Procedure

The governing partial differential equations in frost growth and fin models are solved using a finite difference formulation. The two-dimensional fin surface (x-y surface) is divided into a number of continuous non-overlapping control volumes and the fin surface temperature is solved at the center point of each control volume. The frost growth model is solved at each grid point on the fin surface (x,y,t). The fin surface temperature, $T_c(x,y,t)$, provides the cold surface temperature (boundary condition) for the frost growth model at that point.

The frost growth model is also applied on the un-finned base plate. The cold surface temperature is the cold plate base temperature. It is assumed that frost growth is uniform on the un-finned cold plate surface. The algorithm for solving the whole numerical model is:

1) Use last time step fin surface temperature profile, i.e. $T_c(x,y)$, convective heat and mass transfer coefficients, i.e. h_f and h_{mf}, and average airflow humidity

ratio and temperature value, i.e. W_0 and T_0, as boundary conditions to solve the frost growth model (i.e. Equation 5.1 to 5.23) at each grid point on the fin surface. A frost height profile $\delta_f(x,y,t)$ on the fin surface is obtained along with other frost properties.

2) Solve the frost growth model on the un-finned base. A frost height, $\delta_{f\text{-}base}(t)$ is obtained.
3) Solve the fin heat conduction model (i.e. Equation 5.24 to 5.29) where the source term, S, in the fin conduction model is obtained from step 1.
4) Calculate average frost height, $\delta_{f\text{-}ava}(t)$, on the fin using known $\delta_f(x,y,t)$.
5) Calculate heat and mass transfer coefficients from Equations (5.36) and (5.37) based on the $\delta_{f\text{-}ava}(t)$ and $\delta_{f\text{-}base}(t)$ and Equations (5.30) and (5.35).
6) Calculate pressure drop across the fins, $\Delta P(t)$, using Equation (5.39).
7) Calculate heat rate through a fin and un-finned base using Equations (5.42) and (5.43).
8) Calculate the total heat rate from Equation (5.44).
9) Calculate the average airflow temperature and humidity ratio, T_0 and W_0 from Equation (5.45) to (5.48).
10) Repeat steps 1-9 and stop when the time period for frost growth is completed.

A source code of the main Fortran program used for this numerical model is listed in Appendix C.

CHAPTER 6
MODEL VALIDATION AND LIMITATIONS FOR THE FROST GROWTH ON HEAT EXCHANGER FINS

6.1 Introduction

In this chapter, the numerical model presented in Chapter 5 is used to predict frost characteristics on heat exchanger fins. To show the essential physical characteristics of frost growth on fins, simulation results for one typical operating condition are presented. Then the simulation results are compared with a wide range of experimental data for frost height, frost density, airflow pressure drop through the finned section and heat rate through the cold base.

Data are presented for typical freezer operating conditions with base plate temperatures from -31 to -38°C (-24 to -36°F) and air supply temperature from -13 to -21°C (8 to -5°F). Experimental uncertainty values are presented for all data. To complete the study, a sensitivity study of the frost growth model is used to illustrate the effects of operating and initial condition parameters on frost growth.

This validation investigation of the numerical model uses a wide range of experimental operating conditions typical of freezers. Once the model is validated, it can be used to investigate slightly different operating conditions not covered by the experimental work presented, provided a new physical phenomenon does not occur to alter the results. A sensitivity study illustrates such a data extension.

6.2 Typical Simulation Results

In this section, simulation results for one typical test condition are presented where the Ditenberger model for frost thermal conductivity is used. Table 6.1 gives the base-case test condition and Figure 6.1 to Figure 6.6 show the simulation results based on this test condition.

Table 6.1 Base case test conditions

Air Dry Bulb Temperature (°C)	-15.0
Cold Plate Temperature (°C)	-35.0
Flow Velocity Before entering Finned Section(m/s)	4.4
Humidity Ratio (kg/kg)	9.7×10^{-4}(92%RH)
Time of Frost Growth(min)	240

Figure 6.1 shows the frost height profile on a fin showing a range of frost height from 1.4 to 3.0mm. The frost is higher near the leading edge and the base and the maximum gradients in frost height are nearly 10 times higher in the x direction than in the y direction. Figure 6.2 shows the isothermal temperature profiles on a fin, indicating more than a 10°C temperature difference from the fin base (x=0) to the fin tip (x=40mm). The temperature gradient is negligible or small in the y direction.

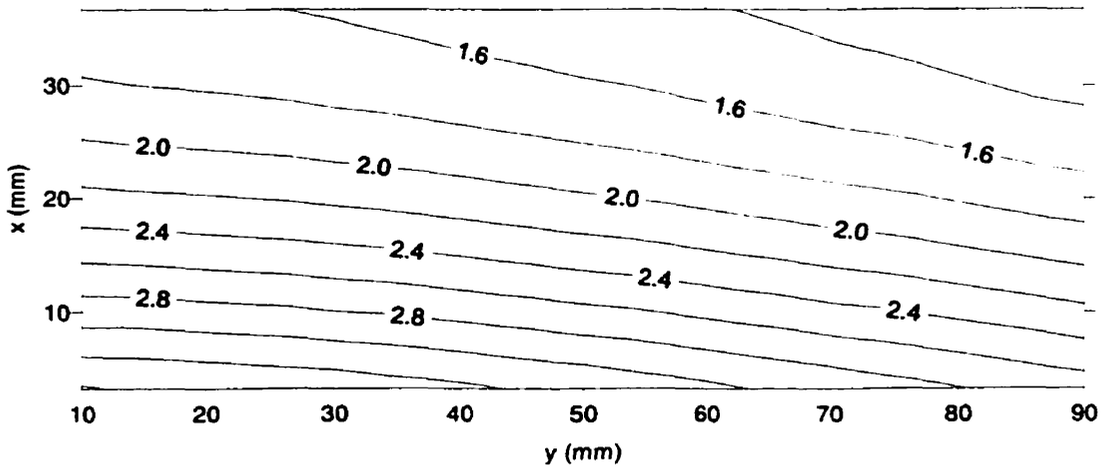

Figure 6.1 Frost height contours (mm) on the fin surface t=240min

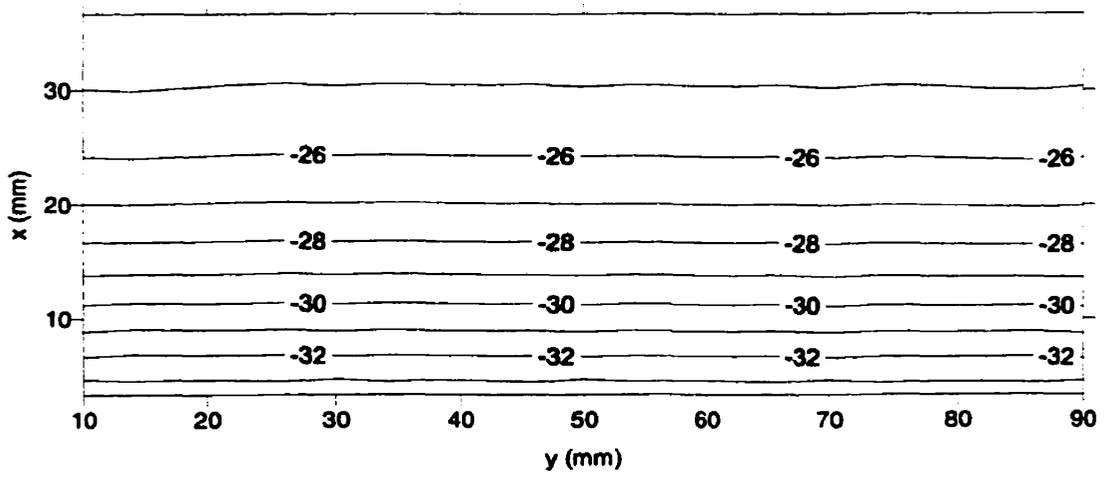

Figure 6.2 Temperature contours (°C) within the fin t=240min

Figure 6.3 shows a frost density profile within the frost layer at a particular point on the fin, showing the frost density is higher near the cold base and decreases to nearly a constant value of 17% for that of ice at z/δ_f=0.3. This type of density profile is consistent with the experimental results reported by Cremers and Hahn (1978) and others. A similar simulation result is shown in Chapter 5 and boundary conditions implied in the model are also discussed in Chapter 5.

This model does not include frost growth on the 0.3mm thick perimeter (40+100+40 mm) of the fin because this area is less than 1% of the total fin area.

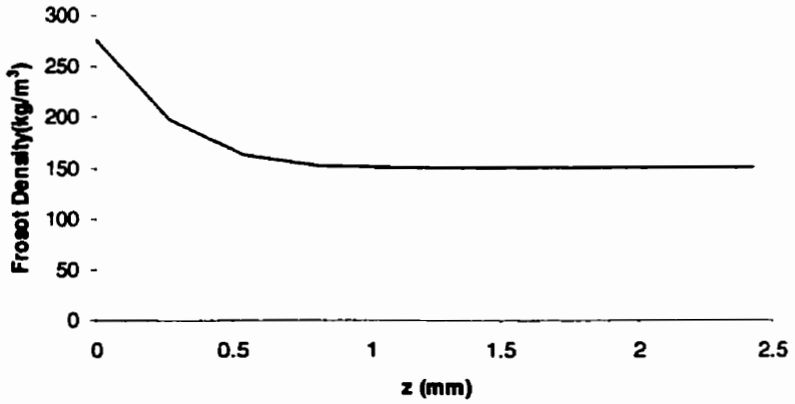

Figure 6.3 Frost density profile within frost layer at x=50mm and y=18mm, t=240min

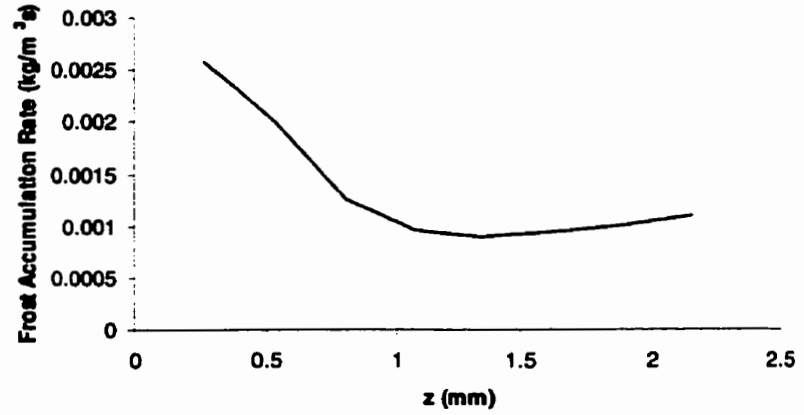

Figure 6.4 Frost accumulation rate profile within frost layer at x=50mm and y=18mm, t=240min

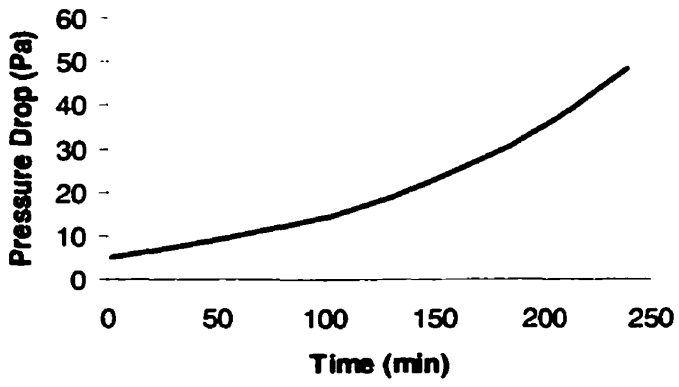

Figure 6.5 Transient pressure drop across the finned section for a constant flow rate

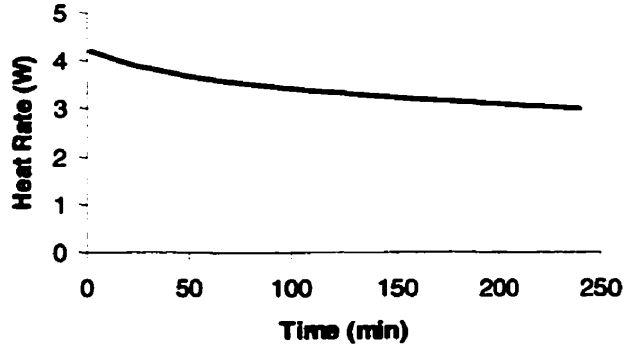

Figure 6.6 Transient heat rate profile through one fin for a constant flow rate

Figure 6.4 shows a typical profile of the frost accumulation rate or phase change rate within the frost layer at one point on the fin. This figure shows that the frost accumulation rate is highest near the cold metal surface but there is a minimum near the mid-height of the frost. This profile for mass accumulation rate causes the frost density to be somewhat uniform for $0.3<z/\delta_f<1$ at moderate duration of frost growth but for very short time or long time the frost density will be less uniform.

Figure 6.5 shows the transient pressure drop versus time which shows that the pressure drop increases dramatically with time due to frost growing on the fins while the mass flow rate of air is held constant. Figure 6.6 shows the transient heat rate profile through each fin where k_{eff} is calculated using Equation (3.11b). This figure shows that the heat rate through each fin significantly decreases with time.

6.3 Model Validation

Five data sets are used in the validation of numerical model. These data sets are selected from a large database to cover a wide range of operating conditions where the experimental uncertainty is small. The five test conditions and the maximum variations in these test conditions are listed in Table 6.2.

Table 6.2 Test Conditions for model validation

Test Conditions	Case1	Case2	Case3	Case 4	Case 5
T_a(°C)	-15.0±0.8	-16.0 ± 0.8	-18.2± 0.8	-13.5 ± 0.8	-20.8± 0.8
T_b(°C)	-35.0±0.5	-38.0 ± 0.8	-31.0 ± 0.8	-31.5 ±0.8	-39 ± 0.8
V_{in} (m/s)	4.4±0.1	4.2± 0.1	5.8 ± 0.1	5.1 ± 0.1	5.3 ± 0.1
W_{in} (kg/kg)	(9.7+1.0/-0.5) x10^{-4}	(9.3+1.0/-0.5) x 10^{-4}	(7.3+1.0/-0.5) x 10^{-4}	(11.2+1.0/-0.5) x 10^{-4}	(5.6+ 1.0/-0.5) x 10^{-4}
t (min)	240±2	220± 2	270±2	225 ± 2	210± 2

These test conditions indicate small variations in the inlet airflow speed, V_{in}, and temperature difference, T_a-T_b, but, due to the low air temperature, T_a, significant variations in the humidity ratio, W_{in}.

6.3.1 Model Validation of Frost Height

Frost height is the most important characteristic of frost growth on heat exchanger fins because it is directly related to the airflow pressure drop through finned section, heat transfer rate, and the energy required to defrost the heat exchanger. A numerical model for predicting frost growth on heat exchanger fins will not be successful if it can not predict the frost height correctly.

Figure 6.7 illustrates the comparisons of frost height between the numerical simulation results and data for case1. The other four cases showed similar frost height characteristics as Figure 6.1 as shown in Appendix E. These frost height characteristics are summarized in Table 6.3. Table 6.3 shows the comparisons of frost height between the numerical simulation results and data for all five cases by giving average frost height, $\overline{\delta}_f$, the standard error of estimate, SEE(δ_f), the standard error of simulation, SES(δ_f) and bias $\beta(\delta_f)$ between data and simulations.

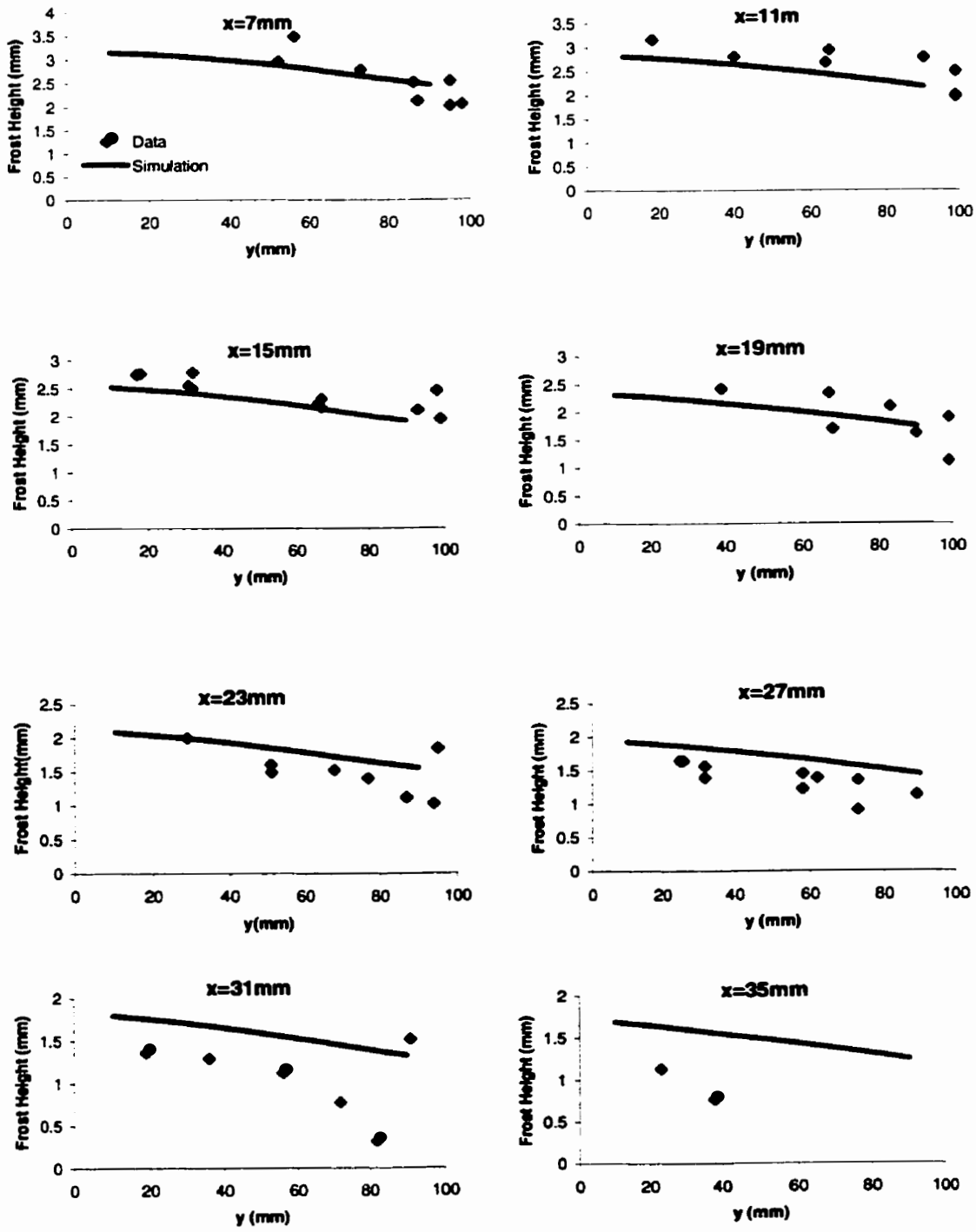

Figure 6.7 Comparison of simulated and experimental data for Case 1 (T_a = -15.0°C, T_b = -35.0°C, V_{in} = 4.4m/s, $W_0 = 9.7 \times 10^{-4}$, t = 240min)

Table 6.3 Standard error of estimate [SEE(δ_f)], standard error of simulation [SES(δ_f)] and bias [$\beta(\delta_f)$] for frost height using all data

Case 1(T_a = -15.0°C, T_b = -35.0°C, V_{in} = 4.4m/s, W_0 = 9.7x10^{-4}, t = 240min)									
x (mm)	7	11	15	19	23	27	31	35	Avg.
$\bar{\delta}_f$ (mm)	3.30	2.85	2.46	2.05	1.7	1.60	1.12	0.47	1.81
SEE(δ_f) (mm)	0.27	0.28	0.16	0.35	0.27	0.15	0.46	N/A	0.21
SES(δ_f)(mm)	0.31	0.38	0.28	0.33	0.30	0.37	0.59	0.66	0.36
$\beta(\delta_f)$(mm)	0.03	0.30	0.23	0.02	-0.17	-0.33	-0.46	-0.64	-0.12
Case 2 (T_a = -16.0°C, T_b = -38.0°C, V_{in} = 4.2 m/s, W_0=9.3x10^{-4}, t = 220 min)									
$\bar{\delta}_f$ (mm)	3.46	3.24	2.88	2.60	2.35	1.81	N/A		2.06
SEE(δ_f) (mm)	0.19	0.28	0.22	0.26	0.05	0.05			0.12
SES(δ_f)(mm)	0.33	0.50	0.41	0.32	0.22	0.20			0.22
$\beta(\delta_f)$(mm)	0.03	0.42	0.34	0.20	0.19	-0.18			0.10
Case 3 (T_a = -18.2°C, T_b = -31.0°C, V_{in} = 5.8 m/s, W_0=7.3x10^{-4}, t = 270 min)									
$\bar{\delta}_f$ (mm)	2.34	1.83	1.56	1.77	1.36	1.14	0.93	1.34	1.44
SEE(δ_f) (mm)	0.23	0.34	0.23	0.27	0.16	0.32	0.25	0.01	0.20
SES(δ_f)(mm)	0.29	0.35	0.22	0.31	0.24	0.26	0.21	0.25	0.24
$\beta(\delta_f)$(mm)	0.20	-0.01	0.03	0.21	0.19	0.07	-0.05	0.25	0.11
Case 4 (T_a = -13.5°C, T_b = -31.5°C, V_{in} = 5.1 m/s, W_0=11.2x10^{-4}, t = 225 min)									
$\bar{\delta}_f$ (mm)	3.64	2.98	2.57	2.17	1.78	1.54	0.69	0.29	1.85
SEE(δ_f) (mm)	0.28	0.30	0.24	0.21	0.23	0.16	0.07	0.14	0.19
SES(δ_f)(mm)	0.37	0.45	0.31	0.22	0.26	0.43	0.94	1.50	0.51
$\beta(\delta_f)$(mm)	0.22	0.37	0.20	0.08	-0.11	-0.30	-0.92	-1.20	-0.18
Case 5 (T_a = -20.8°C, T_b = -39.0°C, V_{in} = 5.3 m/s, W_0 = 6.1x10^{-4}, t = 210 min)									
$\bar{\delta}_f$ (mm)	2.11	2.13	1.82	1.56	1.35	0.92	0.72	0.58	1.29
SEE(δ_f) (mm)	0.28	0.33	0.27	0.20	0.34	0.19	0.25	0.27	0.24
SES(δ_f)(mm)	0.36	0.34	0.31	0.19	0.35	0.40	0.51	0.61	0.34
$\beta(\delta_f)$(mm)	-0.21	0.06	0.10	0.00	-0.13	-0.34	-0.43	-0.51	-0.17

In Table 6.3 and for n samples, SEE is standard error of estimate [ANSI/ASME PTC 19.1 (1985)] defined by

$$SEE(\delta_f) = \left[\frac{\sum_{k=1}^{n} (\delta_{f,k}(meas) - \bar{\delta}_{f,k})^2}{n-2} \right]^{1/2} \tag{6.1}$$

where

$$\bar{\delta}_{f,k} = a + bx_k \tag{6.2}$$

$$b = \frac{\sum_{k=1}^{n} (x_k - \bar{x})(\delta_{f,k}(meas) - \bar{\delta}_f(meas))}{\sum_{k=1}^{n} (x_k - \bar{x})^2} \tag{6.3}$$

$$a = \bar{\delta}_f(meas) - b\bar{x} \tag{6.4}$$

$$\bar{x} = \frac{1}{n} \sum_{k=1}^{n} x_k \tag{6.5}$$

and

$$\bar{\delta}_f(meas) = \frac{1}{n} \sum_{k=1}^{n} \delta_{f,k}(meas) \tag{6.6}$$

Using a similar form of equation (6.1), the standard error of simulation, SES, is defined as

$$SES(\delta_f) = \left[\frac{\sum_{k=1}^{n} (\delta_{f,k}(meas) - \delta_{f,k}(sim))^2}{n} \right]^{1/2} \tag{6.7}$$

and define the bias to be

$$\beta(\delta_f) = \frac{\sum_{k=1}^{n} (\delta_{f,k}(meas) - \delta_{f,k}(sim))}{n} \tag{6.8}$$

In Table 6.3, Avg. is the average value of $\overline{\delta}_f$, SEE(δ_f), SES(δ_f) and $\beta(\delta_f)$ weighted by the area in each case and is calculated using,

$$\begin{aligned} Avg(A) = {} & 7/40A_{x=7} + 4/40A_{x=11} + 4/40A_{x=15} + 4/40A_{x=19} + 4/40A_{x=23} \\ & + 4/40A_{x=27} + 4/40A_{x=31} + 5/40A_{x=35} \end{aligned} \tag{6.9}$$

where A stands for $\overline{\delta}_f$, SEE(δ_f), SES(δ_f) or $\beta(\delta_f)$ in each case. When the data is not available (N/A) in Table 6.3 Equation (6.9) is modified for the new area.

The data in Figure 6.7 and Table 6.3 for frost height on a flat fin vary significantly over the x-y fin surface and were obtained using a new laser scanning system as described in Chapter 2. The standard error of estimate (SEE) is less than 0.2mm for the average of all data and all 5 cases. The experimental uncertainty in frost measurement is less than 0.15mm (95% confidence level), for 90% of the data; i.e., less than 10% of the frost height data has a higher uncertainty. However, some height uncertainties can be as large as 1.0mm which adds considerably to the overall uncertainty and gives rise to an overall fin SEE of 0.2mm. It is shown Table 6.3 for the bias error that, with a few exceptions, the simulation results for frost height and experimental data agree within the experimental uncertainty. In general, the simulation results do not agree with the data in the tip area of the heat exchanger fins (i.e. x>27mm) where the simulation results are nearly always larger than the data for frost height. One reason for this may be that, at the fin tip, a small amount of sublimation of frost from the fin occurred towards the fin tip during the measuring process (Thomas et al., 1999). The main reason for this discrepancy near the fin tip is most likely something unrelated to experimental technique and is a

consequence of airflow channeling toward the fin tip as frost blockage increases during several hours of frost growth. This will be discussed with the comparison of pressure drop data. The discrepancy between the simulated frost height and the corresponding data is most noticeable for Case 4 for x≥27mm where the simulated frost height is significantly higher than the measured frost height. The test conditions for Case 4 included the highest supply air humidity ratio and the warmest air temperature while the entering air speed at 5.1m/s was moderately high. The other frost height simulation results are, with few exceptions, within the experimental uncertainty.

6.3.2 Model Validation of Frost Density

Figure 6.8 shows the comparisons between the local average frost density data, calculated using the measured frost mass concentration and frost height, and the simulations for case1. Test data for the other four cases were similar to Figure 6.8 which are included in Appendix E. Table 6.4 gives the comparisons for all five cases.

The uncertainty for frost density data is less than 15%. Figure 6.8 shows that the agreement between the simulation and experimental data is good except for the frost density near the leading edge (y→ 0). The experimental data of frost density is always higher than simulation results in the area of leading edge. Referring to Figure 5.1 in Chapter 5, higher density frost is accumulated ahead of the leading edge of the fin due to airflow stagnation point where y has a small negative value. The numerical model does not include this dense leading edge frost because frost accumulation near the leading edge is small relative to the total frost accumulation. In Table 6.4, the experimental data

of the leading edge are not included in the calculation. The definition of symbols used in Table 6.4 is similar to that in Table 6.3.

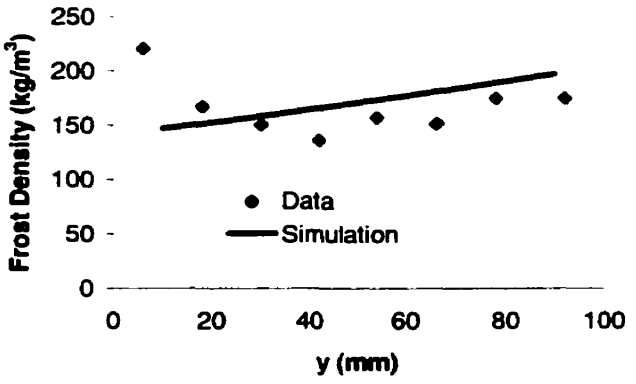

Figure 6.8 Comparisions for frost density profile between simulations and data for Case1 (T_a = -15.0°C, T_b = -35.0°C, V_{in} = 4.4m/s, $W_0 = 9.7 \times 10^{-4}$, t = 240min)

Table 6.4 Average frost density [$\bar{\rho}_f$], standard error of estimate [SEE(ρ_f)], standard error of simulation [SES(ρ_f)] and bias [$\beta(\rho_f)$] for frost density using all data

Case No.	$\bar{\rho}_f$ (kg/m^3)	SEE(ρ_f) (kg/m^3)	SES(ρ_f) (kg/m^3)	$\beta(\rho_f)$ (kg/m^3)
1	157.6	13.7	20.9	-15.1
2	129.4	10.2	27.0	-24.0
3	157.1	11.4	17.4	-13.8
4	164.3	19.0	19.3	-5.8
5	188.4	7.6	34.0	-22.2

6.3.3 Model Validation for Heat Rate Through Cold Base

Figure 6.9 shows the comparisons of transient heat rate through the cold base for Case 1. Due to the heat capacity of cold base and heat flux meter, the simulation results do not agree with the experimental data during the early stage of this test (t<40min) when

transient effects in the heat flux meter occur and the uncertainty is larger than ±6W. The transient temperature effect during the early period of test is shown in Figure 6.10 for the cold base during the experiment in Case 1. It is shown here that it takes 40 to 50 minutes for the cold plate temperature to reach a quasi-steady state coincident with the heat rate profiles in Figure 6.9

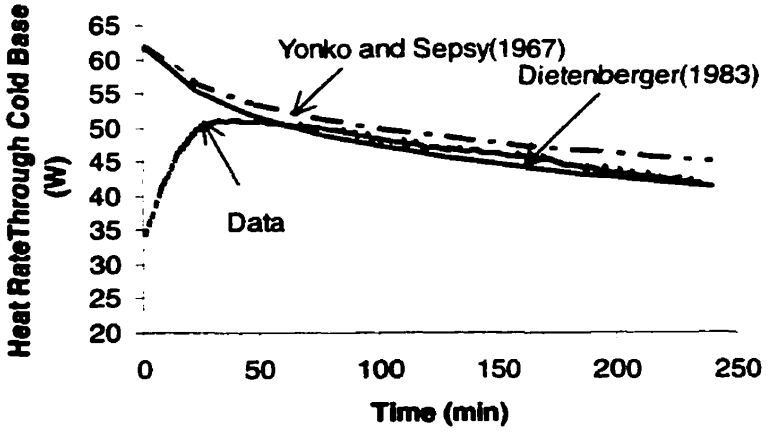

Figure 6.9 Comparisions for transient heat rate through cold base between simulations and data for case1 (T_a = -15.0°C, T_b = -35.0°C, V_{in} = 4.2m/s, $W_0 = 9.7x10^{-4}$)

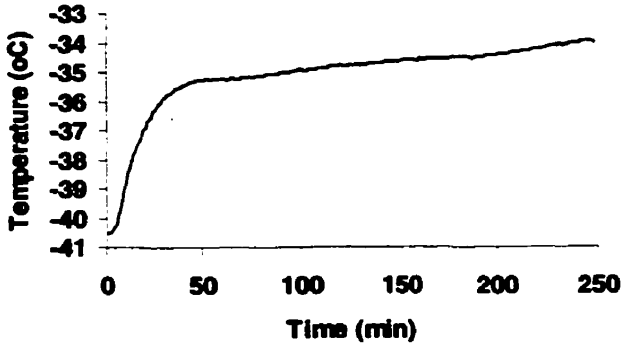

Figure 6.10 Transient temperature profile of the cold base during the experiment in case1. (T_a = -15.0°C, T_b = -35.0°C, V_{in} = 4.2m/s, $W_0 = 9.7x10^{-4}$)

It is shown in Figure 6.9, after the early period of test, that the simulation results using the correlation for k_{eff} of Yonko and Sepsy (1967), i.e. Equation (3.11a), is shown to be 5 to 10% higher than the data. Also shown is the simulation result using k_{eff} calculated with the equation set of Dietenberger (1983), i.e. Equation (3.11b). Here the simulation agrees with the experimental data within the experimental uncertainty everywhere except for t<40min.

Table 6.5 shows the comparisons of heat transfer rate through the base at the end of each test. The difference between the simulation results and experimental data is less than 10% with the more complex set of equations recommended by Dietenberger for k_{eff} giving agreement within the range of experimental uncertainty for all the data.

Table 6.5 Comparisons for heat rate through cold base at end of each test

Case No.	Measured Heat Rate Through Cold Base (W)	Simulation (W)
1	42.7±6	41.2
2	42.1±6	43.8
3	32.2±6	31.3
4	43.7±6	39.4
5	43.0±6	41.4

6.3.4 Model Validation for Airflow Pressure Drop Through Fins

Figure 6.11 shows the comparison of the simulation and experimental data for Case 1 for the transient airflow pressure drop through the fins. Table 6.6 shows comparisons of airflow pressure drop through the fins at end of each test where the uncertainty of the pressure drop is 3.8 Pa.

Agreement between the simulation pressure drop and the measured data for air flow through the frosted fins is poor for some cases in Table 6.6. The simulation results are usually larger than the experimental data. Furthermore, the graph of pressure drop versus time in Figure 6.11 for test Case 1 implies that this discrepancy between the model and data increases with time.

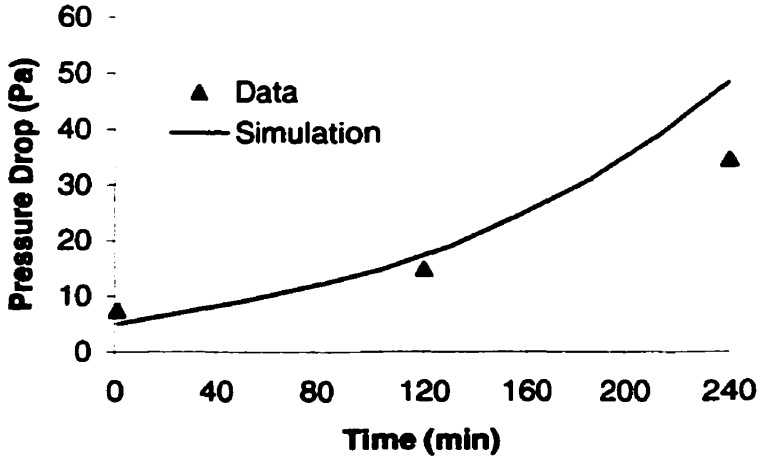

Figure 6.11 Comparisions for transient pressure drop profile between simulations and data for case1 (T_a = -15.0°C, T_b = -35.0°C, V_{in} = 4.4m/s, W_0 = 9.7x10^{-4})

Table 6.6 Pressure drop across heat exchanger fins at the end of each test

Case No.	Measured Pressure Drop (Pa)	Simulation (Pa)
1	34.6 ± 3.8	48.3
2	53.3 ± 3.8	53.0
3	39.5 ± 3.8	36.2
4	48.3± 3.8	61.0
5	32.8± 3.8	37.0

The pressure drop calculation for a finned heat exchanger with frost blockage is very sensitive to several factors, especially average frost height, frost surface roughness

and entrance and exit pressure loss coefficients. The uncertainty in this calculation is much larger than the uncertainty in the measured pressure drop. In addition, it appears that the frost height near the fin tip (i.e., $x \geq 27mm$) may, after some time, actually decrease with time, giving rise to thinner frost near the fin tip and aerodynamically smoother frost at least in this region (i.e, dimensionless surface roughness factor, $k+<30$). This appears to be an unreported physical phenomena for frost growth in narrow heat exchanger passages whereby the frost growth characteristics are self modifying in such a manner that the entropy generation rate in the heat exchanger channels due to airflow friction and heat and mass transfer is minimized (Bejan, 1997).

This self-modifying frost growth characteristic, which minimizes the rate of entropy generation, implies that, as the frost thickness starts to cause a large fraction of airflow blockage, the frost growth changes its physical character. The higher air local speeds (e.g. double the inlet air speed after 4 hours) appear to cause the rough frost peaks to be sheared off in the region of least air flow resistance and highest air speed near the fin tip, causing lower average skin friction characteristics and lower average frost growth and, therefore, pressure drop through the heat exchanger. Thus, the average rate of frost growth decreases and the skin friction decreases, especially near the fin tip.

The above discussion of the sensitivity of the pressure drop simulation and calculation implies that there should be careful restrictions placed on the simulation of pressure drop for heat exchanges with frost growth, especially when this growth causes a large fraction of blockage. Furthermore, frost growth within heat exchanger passages,

when the frost height is large relative to the heat exchanger passage width, is a very complex physical phenomenon that will require much more research, because, it appears, the entropy generation rate should be minimized for the coupled phenomena of airflow friction and heat and mass transfer. Although the numerical model presented here can accurately predict frost characteristics for many practical test conditions it can not, without empirical modifications, predict the pressure drop when the frost blockage effects are large.

6.4 Sensitivity of Parameters Used in The Numerical Model

A sensitivity study of the numerical model is performed to examine the effects of changing the six operating condition parameters and initial conditions shown in Table 6.7. Only one parameter is varied in each study and comparisons are made with the original results for the base case with operating conditions listed in the Table 6.1 (Case 1).

Table 6.7 Parameters used in the sensitivity study

Original Case	Sensitivity Study
Air Flow Temperature T_a=-15°C	T_a=-30°C
Cold Plate Temperature T_b=-35°C	T_b=-50°C
Flow Velocity Before Entering the Fined Section V_{in}=4.4 m/s	V_{in}=6.6m/s
Initial Condition of Volume Fraction of Ice on Fin Surface $\varepsilon_0(x,y)=0.01+0.1x/h_{fin}+0.1y/l_{fin}$	$\varepsilon_0(x,y)=0.5*(0.01+0.12x/h_{fin}+0.1y/l_{fin})$ $\varepsilon_0(x,y)=0.1$
Effective Thermal Conductivity of Frost K_{eff}	K_{eff}=1.2*Original K_{eff}=0.8*Original
Fin Spacing t_{fin}=9.2mm	t_{fin}=7.7mm

Figure 6.12 compares simulation results for the effect of decreasing the supply airflow temperature from -15°C to -30°C while the other sensitivity study results are

shown in Appendix F. All the sensitivity results including T_a in Table 6.7 are summarized in Table 6.8.

Since the supply air relative humidity is kept constant at 92%, the absolute humidity decreases from 9.7×10^{-4} to 2.2×10^{-4} kg/kg for air temperatures of -15°C and -30°C in Figure 6.12. Less moisture in the supply airflow results in less frost accumulation on the fins and less pressure drop across the heat exchanger. Since the temperature difference between the cold base and air temperature becomes smaller when the air supply temperature drops, the heat transfer rate through each fin decreases with a decrease in the air supply temperature.

Colder fins base temperatures result in more frost accumulation and therefore higher pressure drop across the fins as shown in Table 6.8 for T_b as a parameter. At a cold base temperature of -50°C, the airflow passage will be essentially blocked near the fin base at 240 min. Since the temperature difference between the airflow and fin is higher with the colder base temperature, the heat transfer rate through each fin is higher for the colder base temperature while the frost accumulation over 4 hours causes the heat rate to decrease by 36% at T_b=-50°C compared to 29% at T_b=-35° over 4 hours.

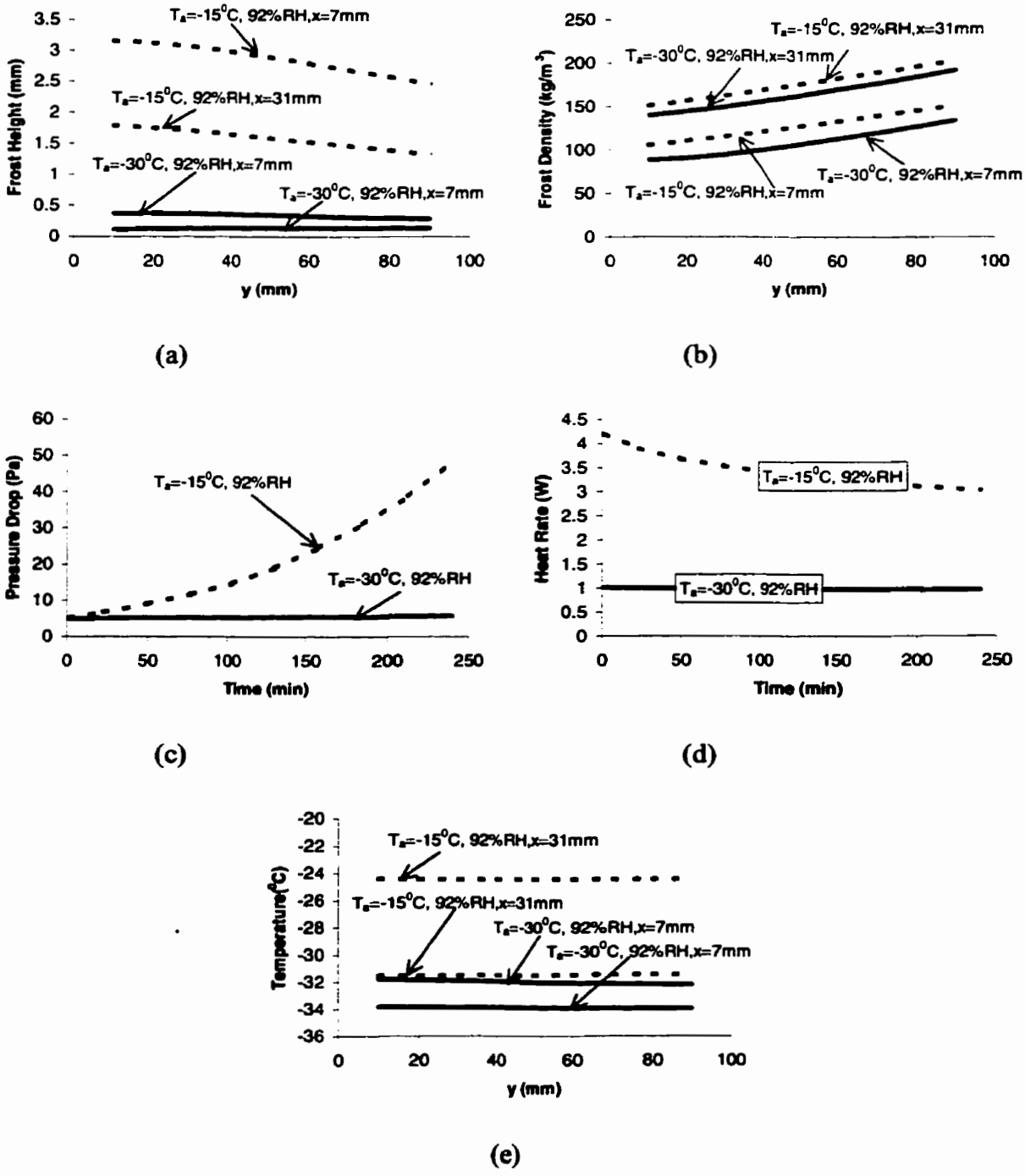

Figure 6.12 Sensitivity study for the air flow temperature, T_a a) Frost height at 240min, b) Frost density at 240min, c) Transient pressure drop, d) Transient heat rate through each fin, e) Temperature profile on the fin at 240min

Table 6.8 Sensitivity of Parameters in the Simulation using the conditions in Table 6.7

Parameter	T_a	T_b	V_{in}	ε_0		k_{eff}		t_{fin}
				Constant	$0.5*\varepsilon_0$	$0.8*k_{eff}$	$1.2*k_{eff}$	
$\Delta\delta_{f\text{-}max}$(mm) (x=7mm)	-2.8 (-88%)	1.2 (37.5%)	0.3 (10.6%)	-0.3 (-10.2%)	0.60 (24%)	-0.53 (-16.8%)	0.47 (15.2%)	-0.04 (-1.3%)
$\Delta\rho_{f\text{-}max}$(kg/m^3) (x=7mm)	-20.9 (-17.2%)	10.6 (10%)	17.0 (16%)	43.5 (41.4%)	-44.0 (-29%)	18.9 (17.9%)	-11.8 (-11.2%)	-1.5 (-1%)
ΔP_{max}(Pa) (t=240min)	-42.5 (-88%)	187.0 (387%)	60.7 (126%)	-8.0 (-16.5%)	37.7 (78%)	-14.9 (-30.7%)	19.2 (39.8%)	43.0 (89%)
Δq_{max}(W) (t=240min)	-2.0 (-67.6%)	1.6 (54.7%)	0.31 (10.3%)	-0.64 (-1.3%)	-0.36 (-12%)	-0.1 (-3.3%)	0.1 (3.3%)	0.02 (0.6%)
ΔT_{max}(°C) (x=7mm)	-2.5	-13.0	0.40	-0.3	-0.5	-0.15	0.15	0.06

It is shown in Table 6.8 that increasing the flow velocity (V_{in}) by 50% has little effect on the heat transfer rate through each fin but the pressure drop at 240min is 2.5 times higher than that for the base case. This suggests that increasing the airflow velocity may not be a suitable way to increase the heat exchanger performance under frosting condition.

It is found that the model is sensitive to the selection of this initial condition for ε_0 and this sensitivity result implies that more experimental research may be necessary to more accurately establish this initial condition. The initial condition of volume fraction of ice used in the model (i.e. Chapter 5 Equation (5.28)) is selected for the best fit with the experimental data.

Increasing the frost thermal conductivity (k_{eff}) by 20% in Table 6.8 results in a 15% increase in frost height and subsequently a 40% increase in pressure drop. The heat rate transferred to each fin only increases by 5% due to a 20% increase in the frost thermal

conductivity. Although increasing thermal conductivity of frost increases the heat rate through each fin by a small fraction, it is offset by a large increase in the frost height. This finding implies that the Dietenberger (1983) model of effective thermal conductivity for freezer operating conditions is preferred while the Yonko and Sepsy (1967) model may only be used for warmer operating conditions. This is not because k_{eff} changes the heat rate; rather, the Yonko and Sepsy model for k_{eff} causes the simulated frost height and pressure drop to be much too high.

It is found that the change in heat transfer rate for each fin is small in Table 6.8. Decreasing the fin spacing (t_{fin}) by 16% results in a 20% increase in the number of fins per unit length so that the total heat transfer rate per unit length may be expected to increase by perhaps 20%. However, at 240 min the pressure drop increases a factor of 1.9 compared to the base case and near the base of the fin the frost growth is expected to totally block the air flow path. In practice, this would imply that the defrost cycle time would have to be much shorter for a fin spacing of 7.7mm compared to a fin spacing of 9.2mm.

6.5 Conclusions

For heat and frost accumulation on a finned heat exchanger, it is shown that:

1. The numerical model simulations for frost height and density are, by and large, within the experimental uncertainty of the measured data.
2. The simulations for heat rate at the end of each test are in good agreement with the measured data.

3. The simulation results for pressure drop through the heat exchanger at the end of each test are usually higher than the experimental data. Pressure drop results is very sensitive to the frost height prediction. A small variation in the frost height causes a significant change in the pressure drop prediction, especially when frost growth results in a large blockage area fraction for airflow in the heat exchanger.

A sensitivity study has been done to investigate the effect of changing six parameters used in the numerical model. Compared to the base case and for all unspecified properties the same as the base case, a summary of sensitivity study results is shown in Table 6.9. Table 6.9 shows that changing the operating conditions usually has more than 8 times the effect on the pressure drop than on the heat rate.

Table 6.9 Summary of sensitivity study (t=240min)

New property value (base case)	Change	
	ΔP	q_{fin}
T_a=-30°C(-15°C)	-90%	-67%
T_b=-50°C(-35°C)	390%	54%
T_{fin}=9.2mm (7.7mm)	89%	0.7%
V_{in}=6.6m/s(4.4m/s)	126%	10%

The initial condition for volume fraction of ice on fin surface and the selection of equations or correlations for the calculation of effective thermal conductivity of frost are two key factors if the frost height and density are to be predicted accurately.

CHAPTER 7

SUMMARY AND CONCLUSION

7.1 Summary

In this thesis, frost growth on heat exchanger surfaces, operating under typical refrigeration conditions, is investigated experimentally and numerically. The main purpose of this research work was develop a theoretical/numerical model for predicting frost properties on heat exchanger flat plates and finned surfaces. Experimental data was used to validate this theoretical/numerical model.

7.1.1 Experimental Work

A special test facility was developed to characterize frost growing on heat exchanger flat plates and fins where the cold surfaces and the air supply conditions are similar to those experienced in freezers, i.e. cold surface temperatures ranged from –35°C to –40°C (-31°F to –40°F), air supply temperatures from –10°C to –20°C (14°F to –4°F) and humidities from 80% to 100% RH. This test facility includes a test section with removable surface disks and fins to measure the frost height and mass concentration on a flat plate and finned heat exchanger surface respectively.

Twenty tests were run by Mao et al. (1999) giving a 480 data set under a range of operating conditions for frost growth on a flat heat transfer surface and the operating conditions are given in Table 7.1

A new automated laser scanning system was developed to measure the height of frost and its distribution on heat exchanger fins. The increase in air pressure loss

resulting from frost growth on the fins was measured directly in the test loop. The frost mass accumulation distribution was measured for each test using special pre-etched fins that could be easily subdivided and weighed. The total heat rate was measured using a heat flux meter. These frost-measuring instruments were calibrated and the uncertainty of each is stated.

Table 7.1 Ranges of Environmental Parameters Used in the Experiments for Frost Growth on the Flat Plate

Parameter	Range	Variations
Time (minutes)	0 to 360	
Distance from leading edge	0 to 500mm (0 to 19.7in)	±1mm (±0.04in)
Test surface temperature	-20.5 to –41 °C (-4.9 to –41.8° F)	±1 °C (±1.8 °F)
Supply air temperature	-10.1 to -25.8 °C (13.8 to –14.4 °F)	±1 °C (±1.8 °F)
Supply air humidity ratio	0.00019 to 0.002	±0.0001
Supply air velocity	1 to 4 m/s (198 to 786 ft/min)	±0.05m/s (±9.6 ft/min)
Inlet Reynolds number	3278 to 13112	±165

Twenty-four tests were run under a range of operating conditions for the frost growth on heat exchanger fins. The ranges of operating conditions are found in Table 7.2.

Table 7.2 Operating conditions for frost experiments

Parameter	Range	Variations
Time (min)	180 to 340	±2
Supply Airflow Velocity (m/s)	3.3 to 6.0	±0.1
Fin Base Temperature (°C)	-39.0 to –30.5	±0.8
Supply Airflow Temperature (°C)	-13.5 to -20.8	±0.8
Supply Air Humidity Ratio (kg/kg)	0.00056 to 0.0011	+0.0001/-0.00005

7.1.2 Observations on Frost Growth Characteristics

Measured results for the frost growth on the flat plate showed that the frost characteristics differed significantly with frost growth data taken previously for room temperature airflow. Depending on the temperature of cold plate and the relative humidity of the subfreezing supply air, the frost could appear to be either smooth or rough. Smooth frost, which occurred at warmer plate temperatures and lower supply air relative humidities, gave rise to frost growth that was much thinner and denser than that for the rough, thick, low-density frost.

For the steady flow rate of supply over fins under freezer operating conditions, the frost height on fins was shown to decrease rapidly with distance from the cold base and less rapidly with distance from the leading edge. The air pressure drop across the fins was found to increase by a factor of 4.6. The average mass concentration profile along the fin in direction of flow was found to vary by only a small fraction.

The total heat rate remained nearly constant with time despite of the frost growth. This last finding appears to be caused by the increased heat and mass transfer coefficients caused by the frost growth while the air supply flow rate is constant.

7.1.3 Model Development and Numerical Simulations

A theoretical/numerical model was developed to simulate the frost growth on heat exchanger surfaces under freezer operating conditions. The model treats the frost as a transient, one-dimensional porous media with boundary conditions that may vary

spacially and temporally. Transient, two-dimensional heat conduction in the fin causes the frost properties to vary over the finned surfaces while variations in the air-frost interface conditions causes further changes in the frost growth patterns on both fins and flat surfaces.

The numerical model was first validated using the published experimental data for the frost growth of the flat plate comparing frost height, frost density and heat flux through cold plate. The numerical model was also validated using the experimental data for the frost growth on the heat exchanger fins for the frost height distribution on the fin surface, frost density distribution on the fin surface, pressure drop across the finned section and heat rate through the cold base. The agreements between the experimental data and simulation results were within the uncertainty bounds for most of the data.

A sensitivity study of the frost growth model was used to investigate the effects of operating and initial condition parameters that influence frost growth.

It is found that for a *constant* airflow rate through the heat exchanger over a four hour period, the blockage of air-flow resulting from the frost growth increases the pressure drop across the heat exchanger by up to a factor of 10, while heat transfer rate decreases by only 21%.

The initial condition for volume fraction of ice on finned surfaces and the selection of equations or correlations for the calculation of effective thermal conductivity of frost are two key factors if the frost height and density are to be predicted accurately.

7.2 Conclusion

It is concluded from this study that frost characteristics on heat exchangers can be modeled and simulated with a known uncertainty for test conditions similar to those investigated here and provided the frost blockage of the heat exchanger passages are small or moderate.

7.3 Future Work

There are two areas of future research. (i), (ii) and (iii) are application oriented which (iv) is a fundamental research problem

(i) This research work on frost growth on heat exchanger surfaces are based on two simple geometric shapes—flat plate and fat fins subject to the parallel flow of air. Refrigeration heat exchangers often possess more complex geometries such as tubes onto which are attached fins. These complex geometries cause the airflow speeds and directions to be more complex within heat exchangers than those studied in this research work. Future work on frost growth should investigate these more practical types of fins such as tube-finned heat exchangers.

(ii) In this study, the maximum supply air humidity was controlled to be less than 95%RH. For industrial refrigeration and freezer operation practice, the airflow humidity ratio is sometimes greater than saturation value, implying super-saturated supply air at 100% RH with airborne frost crystals or water droplets. These particles will cause accretion on the outer edge of frost with no diffusion within the frost layer. The current water vapor diffusion model for frost growth model does not apply to this very different physical phenomenon. A theoretical/numerical model should be developed to simulate

this super-saturated operating condition and this model should be confined with the experimental data.

(iii) This study is only concerned with frost growth not the removal or control of frost during a defrost cycle. The melting and removal of frost as water or ice has not been fully investigated in the literature. Frosted heated exchangers should not be overheated during a defrosting cycle so that all the water formed during a defrosting cycle is drained off. Some future research needs to be directed to this important problem where the evaporation of water and sublimation of frost needs to be minimized to some practical small fraction of total frost mass on a heat exchanger.

(iv) It was noted in this research study that the pattern of frost growth on heat exchanger fins started to show some unpredictable patterns when the frost blockage was about 50% of the original flow area. It appeared that the preferred airflow path favored some minimization of the pressure loss and perhaps some reduction in the frost surface roughness and heat and mass transfer coefficients. More research of this change in frost growth characteristics should be done.

REFERENCES

Abdel-wahed, R. M., Hifni, M.A., and Sherif, S. A., 1984, "*Heat and Mass Transfer from A Laminar Humid Air Stream to A Plate at Subfreezing Temperature*", International Journal of Refrigeration, Vol. 7, No.1.

ASME, 1990, "ANSI/ASME PTC 19.1-1985 Part I Instrumentation and Apparatus-Measurement Uncertainty", ASME New York, NY.

Bejan, A., 1997, *Advanced Engineering Thermodynamics*, 2nd Edition, John Wiley & Sons, INC.

Besant, R. W., Rezkallah, K. S., Mao, Y., and Falk, J., 1990, "*Measurement of Frost Thickness Using a Laser Beam and Light Meter*", *ASHRAE Transactions*, 96(1), pp. 519-522.

Chen, H., Besant, R. W. and Tao, Y. X., 1999a, "*Frost Characteristics and Heat Transfer on a Flat Plate under Freezer Operating Conditions, Part II Numerical Modeling and Comparisons with Data*", ASHRAE Transactions, 105(2)

Chen, H., Thomas, L. and Besant, R. W., 1999b, "*Measurement of Frost Characteristics on Heat Exchanger Fins, Part II: Data and Analysis*" ASHRAE Transaction, 105 (2).

Cremers, C. J. and Hahn, O. J., 1978, "*Frost Density Measurement on Vertical Cylinders by Gamma-Ray Attenuation*", *Adv. Cryogen. Engng.* 23, pp. 371-375.

Dietenberger, M. A., 1983, "*Generalized Correlation of the Water Frost Thermal Conductivity*", Int. J. Heat Mass Transfer, Vol. 26, No. 4, pp. 607-619.

Gates, P. R., Sepsy, C. F. and Huffman, G. D., 1973, "*Heat Transfer and Pressure Loss in Extended Surface Heat Exchangers Operating under Frosting Conditions Part I: Literature Survey, Test Apparatus And Preliminary Results*", *ASHRAE Transactions*, 73(2), pp. I.2.1-I.2.13.

Gnielinski, V., 1976, "*New Equations For Heat And Mass Transfer In Turbulent Pipe And Channel Flow, Int. Chem. Eng.*, 16, pp.359-368.

Hayashi, Y., Aoki, A., Adachi, S. and Hori, K., 1977. *Study of Frost Properties Correlating with Frost Formation Types*. Transactions of the ASME: Journal of Heat Transfer, 99(5), pp. 239-245.

Kaviany, M. 1991, *Principles of Heat Transfer in Porous Media*. Springer, New York

Kays, W. M. and Crawford, M. E., 1993, *Convective Heat Transfer*, Third Edition. Toronto: McGraw-Hill, Inc.

Kays, W. M. and London, A. L., 1984, *Compact Heat Exchangers*, Third Edition, Toronto: McGraw-Hill Book Company.

Kondepudi, S. N., and O'Neal, D. L., 1989, "*Effect of Frost Growth on the Performance of Louvered Finned Tube Heat Exchangers*". *International Journal of Refrigeration* 12: 151-158.

Le Gall, R., Grillot, J. M. and Jallut, C., 1997, *Modeling Of Frost Growth And Densification*, Int. J. Heat Mass Transfer, Vol. 40, No. 13, pp.3177-3187.

Lee, K-S, Kim, W-S and Lee T-H, 1997, *A one-dimensional Model For Frost Formation On A Cold Flat Plate Surface*, Int. J. Heat Mass Trans. 40 (18), pp.4359-5365.

Mao, Y., Besant, R. W. and Rezkallah, K. S., 1991, "*A Method of Measuring Frost Density using Flush-Mounted Removable Disks*", *ASHRAE Transactions*, 97 (1), pp. 26-30.

Mao, Y., Besant, R. W. and Rezkallah, K. S., 1992, *"Measurement and Correlations of Frost Properties with Airflow over a Flat Plate", ASHRAE Transactions,* 98 (1), pp. 65-78.

Mao, Y., Besant, R. W. and Chen, H., 1999, *"Frost Characteristics and Heat Transfer on a Flat Plate under Freezer Operating Conditions. Part I: Experimentation and Correlations", ASHRAE Transactions*, 105 (2).

Niederer, D. H., 1976, *"Frosting and Defrosting Effects on Coil Heat Transfer"*, ASHRAE Transactions, 82(1), pp. 467-473.

Ogawa, K., Tanaka, N. and Takeshita, M. 1993, *"Performance Improvement of Plate Fin-and Tube Heat Exchanger under Frosting Conditions", ASHRAE Transactions*, 99(1), pp. 762-771

O' Neal, D. L. and Tree, D. R., 1985, *"A Review of Frost Formation in Simple Geometries". ASHRAE Transactions*, 91, pp.267-281.

O' Neal, D. L. and Tree, D. R., 1984, *"Measurement of Frost Growth and density in A Parallel Plate Geometry", ASHRAE Transactions*, 90 (2A), pp.278-290.

Padki, M.M., Sherif, S. A. and Nelson, R. M., 1989, *"A simple method for modeling the frost formation phenomenon in different geometries"*, ASHRAE Trans. 95(2), pp.1127-1137.

Parish, H.C., and Sepsy, C. F., 1972, *"A Numerical Analysis of Frost Formation under Forced Convection"*, ASHRAE Transactions, Vol. 79, Pt.1.

Ramaswumy, M. Georgiadis, J.G., and Tenbusch A.1995, *"Microscopic Study Of Frost Inception: Effects Of Substrate, Supercooling, And Grazing Flow"*, Proceedings of 1995 ASME Int, Mechanical Engineering Congress and Exposition.

Rite, R. W. and Crawford, R. R., 1991, *"A Parametric Study of the Factors Governing the Rate of Frost Accumulation on Domestic Refrigerator-Freezer Finned-Tube Evaporator", ASHRAE Transactions*, 97(2), pp. 438-446.

Stoecker, W. F., 1957, *"How Frost Formation on Coils Affects Refrigeration System"*, Refrigeration Engrg., Feb. 1957, pp. 42.

Stoecker, W. F., 1960, *"Frost Formation on Refrigeration Coils"*, ASHRAE Trans., Vol (66), pp. 91.

Senshu, T., Yasuda, H., Oguni, K. and Ishibane, K.1990, *"Heat Pump Performance under Frosting Conditions: Part I-Heat and Mass Transfer on Cross-Finned Tube Heat Exchangers under Frosting Conditions". ASHRAE Transactions* 96(1).

Seki, N., Fukusako, S., Matsuo, K. and Hori, K., *"Incipient Phenomena of Frost Formation"*, Bulletin of the JSME, 1984, 27, (233), 2476-2482.

Tao, Y-X, Besant, R.W. and Mao, Y., 1993a, *Characteristics of Frost Growth on A Flat Plate During The Early Period*, ASHRAE Transactions, Vol. 99(1), pp. 739-745.

Tao, Y-X, Besant, R.W. and Rezkallah, K. S., 1993b, *A Mathematical Model For Predicting The Densification And Growth Of Frost On A Flat Plate.* Int. J. Heat Mass Transfer. Vol. 36, No.2, pp. 353-363.

Thomas, L., Chen, H. and Besant, R. W., 1999, *Measurement of Frost Characteristics on Heat Exchanger Fins Part I: Test Facility and Instrumentation, ASHRAE Transactions*, 105(2).

Tokura, I., Saito, H., and Kishinami, K., 1983, *"Study on Properties and Growth Rate of Frost Layers on Cold Surfaces"*, Transactions of the ASME: *Journal of Heat transfer*, 105(11), pp. 895-901.

Wagner, W. B., 1963, "Frost Formation on An Extended Surface Heat Exchanger in Crossflow of Humid Air", M. Sc. Thesis, The Ohio State University.

Yonko, J. D and Sepsy, C. F., 1967, "*An Investigation of The Thermal Conductivity of Frost While Forming on A Flat Horizontal Plate*", ASHRAE Trans. 73, Part II, pp. I.1.1-I.1.11.

APPENDIX A

SIMPLIFICATION OF GOVERNING EQUATIONS OF FROST GROWTH ON THE COLD SURFACE

Frost growth on a cold surface can be illustrated in Figure A1. The following equations apply at every point within frost layer.

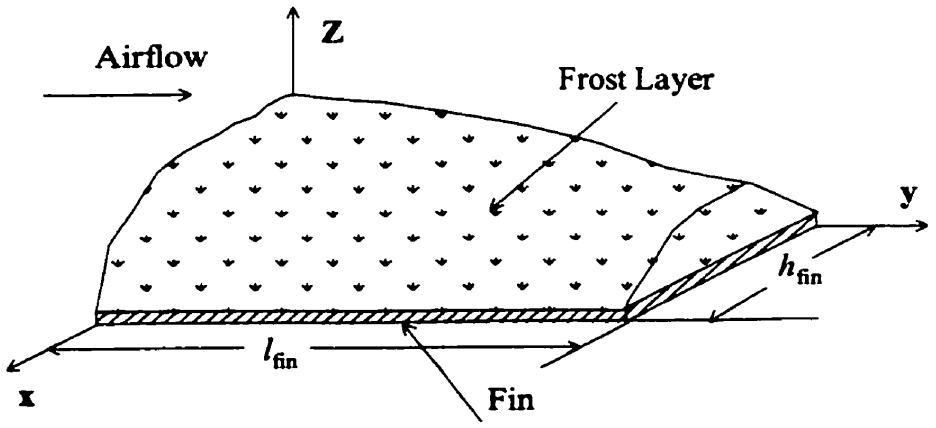

Figure A1 Confiuration of frost growth model

Momentum equation for aiflow within frost layer (Darcy's Law):

$$u_x = -\frac{K}{\mu}\frac{\partial P}{\partial x} \tag{A1}$$

$$u_y = -\frac{K}{\mu}\frac{\partial P}{\partial y} \tag{A2}$$

$$u_z = -\frac{K}{\mu}\frac{\partial P}{\partial z} \tag{A3}$$

where K is the permeability of the frost which is assumed to be isotropic and u_x,u_y and u_z are airflow velocity within the frost layer.

Energy equation:

$$\frac{\partial(\rho_f c_{pf} T)}{\partial t} + \dot{m} h_{sg} + \frac{\partial(\rho_{air} c_{pa} u_x T)}{\partial x} + \frac{\partial(\rho_{air} c_{pa} u_y T)}{\partial y} + \frac{\partial(\rho_{air} c_{pa} u_z T)}{\partial z}$$
$$= \frac{\partial}{\partial x}(k_{eff} \frac{\partial T}{\partial x}) + \frac{\partial}{\partial y}(k_{eff} \frac{\partial T}{\partial y}) + \frac{\partial}{\partial z}(k_{eff} \frac{\partial T}{\partial z}) \tag{A4}$$

Water vapor transport equation:

$$\frac{\partial(\varepsilon_a \rho_v)}{\partial t} - \dot{m} + \frac{\partial(\rho_v u_x)}{\partial x} + \frac{\partial(\rho_v u_y)}{\partial y} + \frac{\partial(\rho_v u_z)}{\partial z}$$
$$= \frac{\partial}{\partial x}(D_{eff} \frac{\partial \rho_v}{\partial x}) + \frac{\partial}{\partial y}(D_{eff} \frac{\partial \rho_v}{\partial y}) + \frac{\partial}{\partial z}(D_{eff} \frac{\partial \rho_v}{\partial z}) \tag{A5}$$

Ice phase continuity equation:

$$\frac{\partial \varepsilon_\beta}{\partial t} + \frac{\dot{m}}{\rho_i} = 0 \tag{A6}$$

The above governing equation imply that all the terms for a three dimensional space are equally important. Now a quantitative analysis is used to establish the relative size of each term in Equations (A4) and (A5). The relative magnitude of each term in Equation (A4) and Equation (A5) is estimated using experimental or simulation results presented in Chen et al. (1999a and 1999b). Terms that are relatively small will be dropped.

Since the total air pressure drop must be essentially zero in x and z direction, the air velocity within the porous frost layer (u_x and u_z) are assumed to be negligible. The air velocity in y direction within the porous frost layer is estimated to be 1mm/s initially but as the frost grows this Darcy velocity increases and after 3.5 hours it is estimate to be about 10mm/s. Experimentally, the temperature distribution on fin surface is measured. It is assumed that temperature distribution within frost layer in the region near the fin surface in the (x,y) plane follows same pattern as that on the fin surface while at the frost-air interface, the bulk air temperature is uniform in the (x,z) plane. The mass accumulation rate, $\dot{m}$, can be estimated from the frost accumulation data. Table A1 shows a comparison of all terms in the energy equation throughout the frost layer (i.e., Equation (A4)) with respect to the source term $\dot{m} h_{sg}$ where the size of each term is estimated from experimental data. Table A2 gives the quantitative analysis for vapor transfer equation, Equation (A5), and all terms are given as a ratio to the source term $\dot{m}$.

Table A1 Comparison of terms in the energy equation with respect to the source term

$\frac{\partial(\rho_{air} c_{pa} u_x T)}{\partial x} \Big/ \dot{m} h_{sg}$	$\frac{\partial(\rho_{air} c_{pa} u_y T)}{\partial y} \Big/ \dot{m} h_{sg}$	$\frac{\partial(\rho_{air} c_{pa} u_z T)}{\partial y} \Big/ \dot{m} h_{sg}$
≈0	≈0.005 at u_y=1mm/s ≈0.05 at u_y=10mm/s	≈0
$\frac{\partial}{\partial x}(k_{eff} \frac{\partial T}{\partial x}) \Big/ \dot{m} h_{sg}$	$\frac{\partial}{\partial y}(k_{eff} \frac{\partial T}{\partial y}) \Big/ \dot{m} h_{sg}$	$\left[\frac{\partial(\rho_f c_{pf} T)}{\partial t} + \frac{\partial}{\partial z}(k_{eff} \frac{\partial T}{\partial z})\right] \Big/ \dot{m} h_{sg}$
≈0.25 at z=0 ≈0 at z=δ_f	≈0	≈1

The term, $\frac{\partial}{\partial z}(k_{eff}\frac{\partial T}{\partial z})$, is somewhat small but it is essential to obtain the temperature distribution in the z direction. This temperature distribution is needed to get the mass transfer rate in Equations (A4), (A5) and (A6).

Table A2 Comparison of terms in the vapor transport equation with respect to the source term

$\frac{\partial(\rho_v u_x)}{\partial x}\Big/\dot{m}$	$\frac{\partial(\rho_v u_y)}{\partial y}\Big/\dot{m}$	$\frac{\partial(\rho_v u_z)}{\partial y}\Big/\dot{m}$
≈0	≈0.007 at u_y=1mm/s ≈0.07 at u_y=10mm/s	≈0
$\frac{\partial}{\partial x}(D_{eff}\frac{\partial \rho_v}{\partial x})\Big/\dot{m}$	$\frac{\partial}{\partial y}(D_{eff}\frac{\partial \rho_v}{\partial y})\Big/\dot{m}$	$\left[\frac{\partial(\rho_v \varepsilon_a)}{\partial t}+\frac{\partial}{\partial z}(D_{eff}\frac{\partial \rho_v}{\partial z})\right]\Big/\dot{m}$
≈0.004	≈0	≈1

Based on the comparisons of the ratios in Tables A1 and A2, Equations (A4) and (A5) for frost growth on fins can be simplified to one-dimensional transient diffusion equations. These are:

Energy equation,

$$\rho_f c_p \frac{\partial T}{\partial t} + \dot{m} h_{sg} = \frac{\partial}{\partial z}(k_{eff}\frac{\partial T}{\partial z}) \qquad \text{(A7)}$$

Vapor transport equation,

$$\frac{\partial(\varepsilon_a \rho_v)}{\partial t} - \dot{m} = \frac{\partial}{\partial z}(D_{eff} \frac{\partial \rho_v}{\partial z}) \qquad \text{(A8)}$$

Equations (A7), (A8) and (A6) are the final major governing equations for the frost growth model on the heat exchanger fins.. This evaluation of terms in the frost growth model has allowed an experimental justification for the assumptions made by Tao et al. (1993a).

APPENDIX B

CALCULATION OF THERMAL CONDUCTIVITY OF FROST

The calculation algorithm of effective thermal conductivity of frost is based on the work by Dietenberger (1983). According to Dietenberger, at low frost density, the total structure of the frost is the random mixture of ice cylinders and ice spheres. At high frost density, the total structure of frost is a random mixture of air bubbles and ice layers. Through a complex semi-empirical derivation, the final set of equations for the calculation of the air–ice thermal conductivity of frost are given as follows:

$$k_{eff} = 1/4((3B_c - 1)k_l + (3\Theta_c - 1)k_u + \{[(3B-1)k_l + (3\Theta_c - 1)k_u]^2 + 8k_l k_u\}^{1/2}) \quad \text{(B1)}$$

where

$$\Theta_c = 1 - B_c \quad \text{(B2)}$$

and

$$B_c = 13.6(B_2 - B_1)(B - B_1)^2 \times [1 - \frac{2}{3}(\frac{B - B_1}{B_3 - B_1} + \frac{B - B_1}{B_2 - B_1}) + \frac{(B - B_1)^2}{2(B_3 - B_1)(B_2 - B_1)}] \quad \text{(B3)}$$

$$\text{for } B > B_1$$

$$B_c = 0 \text{ for } B_c \le B_1 \quad \text{(B4)}$$

B is the porosity of frost, defined by the equation

$$B = \frac{\rho_i - \rho_f}{\rho_i - \rho_a} \quad \text{(B5)}$$

$$B_1 = 0.1726(T/273.16) \quad \text{(B6)}$$

$$B_2 = 0.751 \quad \text{(B7)}$$

B_1 is a temperature dependent variable and is defined by

k_u in equation (B1) is calculated using.

$$k_u = (1-B)k_b + Bk_c \quad \text{(B8)}$$

where k_b is a thermal conductivity factor which includes the thermal conductivity of pure ice (k_i) and air (k_a)

$$k_b = k_i[1-2B(\frac{1-a}{2+a})]\Big/[1+B((\frac{1-a}{2+a})] \quad \text{(B9)}$$

$$a = k_a / k_i \quad \text{(B10)}$$

$$k_c = (1-B)k_i + Bk_a \quad \text{(B11)}$$

k_l in equation (B1) is calculated using,

$$k_l = (1-B)k_p + Bk_s \quad \text{(B12)}$$

where

$$k_s = k_i[3+2B(a-1)]/[3-B(\frac{a-1}{a})] \quad \text{(B13)}$$

and

$$k_p = \frac{k_i k_a}{(1-B)k_a + k_i B} \quad \text{(B14)}$$

Equations (B2) to (B14) are substitutes into (B1) to give the effective thermal conductivity for any frost condition.

APPENDIX C
FORTRAN PROGRAM FOR FROST GROWTH ON FINNED SURFACES

```
************************************
* This is my frost growth model    *
* on fin under convection conditions*
*                                  *
************************************

      implicit none
      integer mm,nn,kk
      parameter(mm=9)
      parameter(nn=11)
      parameter(kk=10)
      integer lt,ltt,ls,count,count1,itera,I,J,k,ll
      real*8  kfin          !thermal conductivity of fin
      real*8  rhofin        !density of fin
      real*8  cpfin         !specific heat of fin
      real*8  q1(mm,nn),h_flux    !heat flux from frost to fin
      real*8  dt            !time step
      real*8  dx,x(mm)            !grid spacing in x direction fin
      real*8  dy,y(nn)            !grid spacing in y direction fin
      real*8  length        !length of the fin
      real*8  height        !height of the fin
      real*8  thick         !thickness of the fin
      real*8  dis         !distance between two fins
      real*8  a(100),b(100),c(100),d(100),p(100),q(100),t(100)
      real*8  T_cold        !cold base temperature
      real*8  T_new(mm,nn),t_old(mm,nn)
      real*8  t_new1(mm,nn)!temperature to be solved
      real*8  z(kk)
      real*8  t_lead(nn)!temperaturature at leading edge
      real*8  tfr_lead(nn,kk)!frost temperature at leading edge
      real*8  ft_lead(nn)!frost hight at leading edge
      real*8  ebsb_lead(nn,kk)!volume fraction of ice at leading edge
      real*8  q_lead(nn) !heat flux from frost to fin at leading edge
      real*8  h_lead(nn)     !heat transfer coeff. at leading edge
      real*8  hm_lead(nn)    !heat transfer coeff. at leading edge
      real*8  density_lead(nn) !density of frost at leading edge
     real*8  qfin
      real*8  t_base(kk)
      real*8  ebsb_base(kk)
      real*8  ft_base
      real*8  q_base,density_base
      real*8  alfa          !dx*dx/(dy*dy)
      real*8  diff1
      real*8  diff
      real*8  a1
      real*8 h1,hm1,ta,w0,h0,hm0
      real*8 h(mm,nn),hm(mm,nn)
      real*8 tfrost(mm,nn,kk),t_frost(kk)
      real*8 ebsb(mm,nn,kk),ebsb_old(kk)
      real*8 ft_old(mm,nn),ft
      real*8 density(mm,nn),fdensity
      real*8 tbase,qbase
      real*8 dh,re,v,v0

      real*8 pre_drop,dfbase,dffin

      real*8 m_dot1(mm,nn,kk),m_dot(kk),rhof1(mm,nn,kk),rhof(kk)

     real*8 tin,tout,win,wout,qin,w_drop,t_drop
      real*8 m_rate,m_ratebase,m_ratefin(mm,nn)

************************************
* Fin part, fin is a two-dimensional*
************************************

      open(unit=1,file='t.dat',status='new')
```

```
          open(unit=5,file='flux.dat',status='unknown',access='append')
          open (unit=11,file='qfin.dat',status='unknown',access='append')
          open(unit=12,file='p.dat',status='unknown',access='append')

          ll=16200

          tin=-15.0+273.15
          tout=-15.0+273.15

          ta=0.5*(tin+tout)

          win=9.7e-4
          wout=9.7e-4
          w0=0.5*(win+wout)
          t_cold=-35.0+273.15
          dh=16e-3
          v0=4.4

*****************
*Volume flow rate*
*****************

          qin=v0*40*119*1e-6

          kfin=177
          rhofin=2702
          cpfin=903
          dt=0.5
          count=3

          length=0.1
          height=0.04
          dis=0.009
          thick=0.308e-3

          dx=length/(mm+1)
          dy=height/(nn+1)

          do i=1,mm
            x(i)=i*dx
          enddo


          do j=1,nn
            y(j)=j*dy
          enddo



          alfa=(dx*dx)/(dy*dy)
          a1=dx*dx*rhofin*cpfin/(kfin*dt)


****************************************
*Initial condition*
****************************************
         do i=1,mm
           do j=1,nn
             do k=1,kk
               ebsb(i,j,k)=(0.05+x(i)/length*0.1)+y(j)/height*0.1
               tfrost(i,j,k)=t_cold
             enddo
           enddo
         enddo

        do i=1,mm
         do j=1,nn
           ft_old(i,j)=1e-4
         enddo
        enddo
```

```
            do i=1,mm
             do j=1,nn
               t_new(i,j)=t_cold
               t_new1(i,j)=t_cold
               t_old(i,j)=t_cold
              enddo
            enddo

           do i=1,nn
             t_lead(i)=t_cold
             ft_lead(i)=1e-4
           enddo

           do i=1,nn
             do j=1,kk
               tfr_lead(i,j)=t_cold
             enddo
           enddo

           do i=1,nn
            do j=1,kk
              ebsb_lead(i,j)=0.05
            enddo
           enddo

           do j=1,kk
            t_base(j)=t_cold
           enddo

           do j=1,kk
             ebsb_base(j)=0.05
           enddo

           ft_base=1e-4


**********
*solving *
**********


       count1=0

       do lt=1,100

       do ltt=1,11/100

           ta=0.5*(tout+tin)
          w0=0.5*(win+wout)
         count1=count1+1

          if(count1.eq.3600)then
          dt=1.0
         endif

         dffin=0.0
         do i=1,mm
          do j=1,nn
            dffin=dffin+ft_old(i,j)/(mm*nn)
          enddo
         enddo

      v=v0*dis*height/((dis-2.0*dffin)*(height-ft_base))

        dh=2.0*(dis-2.0*dffin)*(height-ft_base)/
    $(height+dis-2.0*dffin-ft_base)

        call cal_re(dh,v,re)

        call cal_h0(dh,re,h0,hm0)
```

```
          call cal_h(dh,mm,nn,h,hm,x,h0,hm0)


*************
*unfined base*
*************
         h1=h0*0.8
         hm1=hm0*0.8
         tbase=t_cold
         ft=ft_base
           do k=1,kk
              ebsb_old(k)=ebsb_base(k)
              t_frost(k)=t_base(k)
           enddo

           call base(kk,dt,tbase,h1,hm1,ta,w0,t_frost,ebsb_old,
     $ft,h_flux,fdensity,m_dot,rhof,m_rate)
           do k=1,kk
             t_base(k)=t_frost(k)
             ebsb_base(k)=ebsb_old(k)
           enddo

           ft_base=ft
           density_base=fdensity
           q_base=h_flux
           m_ratebase=m_rate


        do i=1,mm
          do j=1,nn

           h1=h(i,j)*(0.8+y(j)/height*0.2)
           hm1=hm(i,j)*(0.8+y(j)/height*0.2)
            h1=h(i,j)
            hm1=hm(i,j)
           tbase=t_new(i,j)
           ft=ft_old(i,j)

           do k=1,kk
              ebsb_old(k)=ebsb(i,j,k)
              t_frost(k)=tfrost(i,j,k)
           enddo

           call base(kk,dt,tbase,h1,hm1,ta,w0,t_frost,ebsb_old,
     $ft,h_flux,fdensity,m_dot,rhof,m_rate)
           do k=1,kk
             tfrost(i,j,k)=t_frost(k)
             ebsb(i,j,k)=ebsb_old(k)
             m_dot1(i,j,k)=m_dot(k)
             rhof1(i,j,k)=rhof(k)

            enddo
           ft_old(i,j)=ft
           density(i,j)=fdensity
           q1(i,j)=h_flux
           m_ratefin(i,j)=m_rate

         enddo
        enddo

*************************
*Leading edge frost growth*
*************************

        call cal_hlead(nn,v,ft_lead,h_lead,hm_lead)

        do i=1,nn
           h1=h_lead(i)
           hm1=hm_lead(i)
           tbase=t_lead(i)
```

```
            ft=ft_lead(i)

            do k=1,kk
               ebsb_old(k)=ebsb_lead(i,k)
               t_frost(k)=tfr_lead(i,k)
            enddo

            call lead_base(kk,dt,tbase,hl,hml,ta,w0,t_frost,ebsb_old,
     Sft,h_flux,fdensity)
            do k=1,kk
              tfr_lead(i,k)=t_frost(k)
              ebsb_lead(i,k)=ebsb_old(k)
            enddo

            ft_lead(i)=ft
            density_lead(i)=fdensity
            q_lead(i)=h_flux

          enddo


*****************************************
*Line by line solver from bottom to the top *
*****************************************
           itera=1

1000       do ls=1,count

              do j=1,nn
                if(j.eq.1)then
                  do i=1,mm
                   if(i.eq.1)then
                    a(i)=A1+1.0+2.0*alfa
                    b(i)=1.0
                    c(i)=0.0
                    d(i)=alfa*t_new(i,j+1)+alfa*t_cold
     $              +A1*t_old(i,j)+2.0*q1(i,j)/(kfin*thick)*dx*dx
     $              +q_lead(j)*dx/kfin
                   else if (i.eq.mm)then
                     a(i)=A1+1.0+2.0*alfa
                     b(i)=0.0
                     c(i)=1.0
                     d(i)=alfa*t_new(i,j+1)+alfa*t_cold
     $               +a1*t_old(i,j)+2.0*q1(i,j)/(thick*kfin)*dx*dx
                   else
                     a(i)=a1+2.0+2.0*alfa
                     b(i)=1.0
                     c(i)=1.0
                     d(i)=alfa*t_new(i,j+1)+alfa*t_cold
     $                +a1*t_old(i,j)+2.0*q1(i,j)/(thick*kfin)*dx*dx
                   endif
                  enddo
                   call tdma(mm,a,b,c,d,p,q,t)
                   do i=1,mm
                    t_new(i,j)=t(i)
                   enddo
                 else if(j.eq.nn)then
                    do i=1,mm
                      if (i.eq.1)then
                        a(i)=a1+1.0+1.0*alfa
                        b(i)=1.0
                        c(i)=0.0
                        d(i)=alfa*t_new(i,j-1)+a1*t_old(i,j)
     $                  +2.0*q1(i,j)/(thick*kfin)*dx*dx
     $                  +q_lead(j)*dx/kfin

                      else if (i.eq.mm)then
                        a(i)=a1+1.0+1.0*alfa
                        b(i)=0.0
                        c(i)=1.0
                        d(i)=alfa*t_new(i,j-1)+a1*t_old(i,j)
```

```
$                +q1(i,j)*2.0/(thick*kfin)*dx*dx
                 else
                   a(i)=a1+2.0+1.0*alfa
                   b(i)=1.0
                   c(i)=1.0
                   d(i)=alfa*t_new(i,j-1)+a1*t_old(i,j)
$                  +2.0*q1(i,j)/(thick*kfin)*dx*dx
                 endif
               enddo
               call tdma(mm,a,b,c,d,p,q,t)
               do i=1,mm
                T_new(i,j)=t(i)
               enddo
             else
               do i=1,mm
                 if(i.eq.1)then
                   a(i)=a1+1.0+2.0*alfa
                   b(i)=1.0
                   c(i)=0.0
                   d(i)=alfa*t_new(i,j-1)+alfa*t_new(i,j+1)
$                  +2.0*q1(i,j)/(thick*kfin)*dx*dx+a1*t_old(i,j)
$                  +q_lead(j)*dx/kfin

                 else if (i.eq.mm)then
                   a(i)=a1+1.0+2.0*alfa
                   b(i)=0.0
                   c(i)=1.0
                   d(i)=alfa*t_new(i,j-1)+alfa*t_new(i,j+1)
$                  +2.0*q1(i,j)/(thick*kfin)*dx*dx+a1*t_old(i,j)
                 else
                   a(i)=a1+2.0+2.0*alfa
                   b(i)=1.0
                   c(i)=1.0
                   d(i)=alfa*t_new(i,j-1)+alfa*t_new(i,j+1)
$                  +2.0*q1(i,j)/(kfin*thick)*dx*dx+a1*t_old(i,j)
                 endif
               enddo
               call tdma(mm,a,b,c,d,p,q,t)
               do i=1,mm
                 t_new(i,j)=t(i)
               enddo
             endif

           enddo

            i=1
            do j=1,nn
             t_lead(j)=t_new(i,j)+q_lead(j)*dx/kfin
            enddo

          if (ls.eq.count)then
            diff1=0.0
            do i=1,mm
             do j=1,nn

              diff=abs(t_new(i,j)-t_new1(i,j))/t_new(i,j)
              if(diff.ge.diff1)then
                diff1=diff
              endif
             enddo
            enddo
          endif
          do i=1,mm
           do j=1,nn
            t_new1(i,j)=t_new(i,j)
           enddo
          enddo
        enddo!ls

         if(diff1.ge.1d-9)then
           itera=itera+1
```

```
              goto 1000
            endif


            do i=1,mm
              do j=1,nn
               t_old(i,j)=t_new(i,j)
              enddo
            enddo

             dffin=0.0
            do i=1,mm
             do j=1,nn
               dffin=dffin+ft_old(i,j)/(mm*nn)
             enddo
            enddo

            dfbase=ft_base

            call p_drop(dffin,dfbase,height,length,dis,pre_drop,v0)

          qfin=0
           do i=2,mm-1
            qfin=qfin+t_new(i,1)/(mm-2)
           enddo
          qfin=(qfin-t_cold)/dy*kfin*0.3084*100*1e-6
          qbase=qfin*12+q_base*(120-12*0.35)*110*1e-6

****************
*Wout calculation*
****************

* Average mass transfer rateon one fin side

            m_rate=0.0
            do i=1,mm
             do j=1,nn
               m_rate=m_rate+m_ratefin(i,j)/(mm*nn)
             enddo
            enddo

*Total mass transfer rate through fins (kg/s)

            m_rate=m_rate*12*2*40*100*1e-6

*Total mass transfer rate throu unfinned base

            m_ratebase=m_ratebase*115*110*1e-6

*wdrop calculation

            w_drop=(m_rate+m_ratebase)/(1.39*qin)
            wout=win-w_drop

*temperature drop  calculation

            t_drop=qbase/(1.39*qin)-2500*w_drop
            t_drop=t_drop/1006
            tout=tin-t_drop

*           write(*,*)pre_drop,t_drop,w_drop


         enddo


          write(5,*)count1,qbase
          write(12,*)count1,pre_drop
          write(11,*)count1,qfin

          enddo
```

```
      open(unit=4,file='den.dat',status='new')
      open(unit=2,file='ft.dat',status='new')

      do i=1,mm
        do j=1,nn
         write(1,*)x(i),y(j),t_new(i,j)
         write(2,*)x(i),y(j),ft_old(i,j)

         enddo
       enddo

      open(unit=3,file='infrost.dat',status='new')
        z(1)=0
        do i=2,kk
          z(i)=z(i-1)+ft_old(5,5)/9
        enddo
        do i=1,kk
          write(3,*)z(i),rhof1(5,5,i),m_dot1(5,5,i)
        enddo
        do i=1,mm
         do j=1,nn
            write(4,*)x(i),y(j),density(i,j)
         enddo
        enddo
      CLOSE(1)
      close(2)
      close(3)
      close(4)

     end
      include'base.for' !Frost growth model
      include'lead_base.for'!frost growth model used on leading edge
      include'cal_h.for'    !Convective heat and mass transfer
      include'cal_re.for'   !Reynolds number
      include'cal_h0.for'
      include'cal_hlead.for' !Heat and mass transfer on leading edge
      include'pre_drop.for'  !Pressure Drop
      include'cal_kcke.for'  !Entrance and exit pressure loss coefficient


*       Frost growth model

      subroutine base(kk,dt,t_cold,h1,hm1,t0,w0,t_old,ebsb_old,
     $ft_old,h_flux,density,m_dot,rhof,m_rate)

      implicit none
      integer mm,kk
      integer i,nn,ls,lss,chen
      real*8 t_old(kk)
      real*8 t(kk,2)      !temperature
                          !1,current,2,last iteration
     real*8 h_flux        !heat flux into the base
     real*8 kf,kf1        !last node frost thermal conductivity
     real*8 d_mdot        !
     real*8 density
     real*8 rhocg(kk)     !density of vapor gas
     real*8 rhong(kk)     !density of dry air

     real*8 rhocg_old(kk)!last time step vapor density
     real*8 ebsb(kk),ebsb1(kk)
     real*8 ebsb_old(kk) !volume fraction of ice
     real*8 m_dot(kk),m_dot1(kk)    !phase change rate
     real*8 cpcg          !specific heat of vapor
     real*8 cpng          !specific heat of dry air
     real*8 z(kk)         !z coordinate
     real*8 new_z(kk)     !updated z cordinate
     real*8 hsg          !latent heat

     real*8 ap(kk),an(kk),as(kk),s(kk)
```

```
                    !used for solving energy equaiton
real*8 ft,ft1       !frost tree thickness
real*8 ft_old       !last time step frost tree thickness
real*8 dt           !time step


real*8 rhof(kk)     !density of frost
real*8 spheat(kk)   !specific heat of frost
real*8 rhoice       !density of ice
real*8 cpice        !specific heat of ice
real*8 kef(kk)      !effect thermal conductivity of tree
real*8 deff(kk)     !effect vapor diffusion co.
real*8 deffm
real*8 f            !co. used for calculating deff
real*8 fs           !co. used for calculating surface deff
real*8 t0           !air flow temperature
real*8 w0           !air flow humidity
real*8 tfs          !surface temperature of frost
real*8 wfs          !surface humidty of frost
real*8 t_cold       !cold plate temperature
real*8 hl           !convection heat transfer co.
real*8 hml          !convection mass transfer co.
real*8 h, hm
real*8 rcg, rng     !constant
real*8 pcg,png,p0   !pressure of vapor, dry air, and total air
real*8 tcri         !triple point (0c)
real*8 relax1,relax2
                    !relaxation
real*8 dz,var1,var2

real*8 a(100),b(100),c(100),d(100),p(100),q(100),y(100)

real*8 diff_set, diff
real*8 dif_set, dif

real*8 ebsb0
real*8 m_rate

ebsb0=0.3




mm=kk
hm=hml*1.30
f=-0.1
fs=0.1



hsg=2.8e+6
tcri=273.15         !freezing point
p0=96.458*1000      !local air pressure



rcg=461.5
rng=287.0



rhoice=920.00
cpice=2025.00
cpcg=2050.0
cpng=1007.0

relax1=0.5
relax2=0.05
ft=ft_old
```

```
      ft1=ft


*Grid information

      dz=ft_old/(mm-1)
      z(1)=0.0

      do i=2,mm
        z(i)=z(i-1)+dz
      enddo

*initial condition
      do i=1,mm
       t(i,1)=t_old(i)
       t(i,2)=t_old(i)
      enddo

      do i=1,mm
        ebsb(i)=ebsb_old(i)
        ebsb1(i)=ebsb(i)
        m_dot(i)=1e-6
        m_dot1(i)=m_dot(i)
      enddo

      do i=1,mm
       var1=t_old(i)
       call psat(var1,tcri,pcg)
       rhocg(i)=pcg/(rcg*var1)
       rhocg_old(i)=rhocg(i)

       png=p0-pcg
       rhong(i)=png/(rng*var1)
      enddo


      ls=0
      h=h1


100   do lss=1,10


*************************
* properties calculation*
*************************

         call ava_den(rhocg,rhong,rhoice,ebsb,rhof,mm)


         call sph(mm,rhoice,rhof,rhocg,rhong,ebsb,cpcg,
     $cpng,cpice,spheat)
         call keff(mm,kef,rhof,t_old)
         call cal_deff(t,mm,ebsb,deff,f,fs,deffm)
         call bT_coeff(kef,rhof,dt,dz,t_old,
     *m_dot,ap,an,as,s,mm,spheat)
         call bT_bound(t_cold,rhof,kef,t0,h,dt,dz,
     *ap,an,as,s,mm,ft,ft_old,spheat,t_old)

        kf=2.0*kef(1)*kef(2)/(kef(1)+kef(2))

*************************
* solving Energy equation*
*************************

      do I=2,mm
         if (i.eq.2)then
           a(i-1)=ap(i)
           b(i-1)=an(i)
           c(i-1)=0.0
           d(i-1)=s(i)
```

```
          else if (i.eq.mm)then
            a(i-1)=ap(i)
            b(i-1)=0.0
            c(i-1)=as(i)
            d(i-1)=s(i)
           else
             a(i-1)=ap(i)
             b(i-1)=an(i)
             c(i-1)=as(i)
             d(i-1)=s(i)
           endif
           if(a(i-1).lt.0.0)then
             write(*,*)'a wrong',i-1,a(i-1),ap(i)
             pause
           else if(b(i-1).lt.0.0)then
             write(*,*)'b wrong',i-1,b(i-1),an(i)
            else if(c(i-1).lt.0.0)then
             write(*,*)'c wrong',i-1,c(i-1),as(i)
            else if(d(i-1).lt.0.0)then
             write(*,*)'d wrong',i-1,d(i-1),s(i)
             pause
            endif

      enddo


      nn=mm-1

      t(1,1)=t_cold

      call tdma(nn,a,b,c,d,p,q,y)

      do i=1,nn
       t(i+1,1)=y(i)
      enddo

      do i=1,mm
       t(i,1)=t(i,2)+relax1*(t(i,1)-t(i,2))


      enddo

*****************************************************************
* Calculating vapor and dry air density at each control volume*
*****************************************************************
      do i=1,mm
       var1=t(i,1)
       call psat(var1,tcri,pcg)
       rhocg(i)=pcg/(rcg*var1)
       png=p0-pcg
       rhong(i)=png/(rng*var1)
      enddo

*****************************************************************
*calculating phase change rate on each control volume, 2 to mm-1*
*****************************************************************
      call  cal_mdot(mm,deff,rhocg,dt,dz,rhocg_old,
     *m_dot,ebsb,ebsb_old)
        do i=1,mm
         m_dot(i)=m_dot1(i)+relax2*(m_dot(i)-m_dot1(i))
        enddo

***********************************
* solve for volume fraction of ice*
***********************************
      do i=1,mm
       ebsb(i)=-m_dot(i)/rhoice*dt+ebsb_old(i)
       if(ebsb(i).lt.0)then
         write(*,*)'ebsb<0',i,ebsb(i),-M_dot(i),ebsb_old(i)
         pause
       endif
```

```
      enddo
      i=1
      ebsb(i)=ebsb0

      i=mm
      ebsb(i)=ebsb(i-1)

      do i=1,mm
       ebsb(i)=ebsb1(i)+relax1*(ebsb(i)-ebsb1(I))
      enddo

*****************************
*frost height calculation   *
*****************************

      tfs=t(mm,1)

      call cal_w(tfs,wfs)
      var1=hm*(w0-wfs)-deffm*(rhocg(mm)-rhocg(mm-1))/dz
      ft=ft_old+var1/rhof(mm)*dt
      ft=ft1+relax1*(ft-ft1)

      diff_set=0.0

      do i=1,mm
       diff=abs(t(i,1)-t(i,2))/t(i,1)
       if(diff.ge.diff_set)then
         diff_set=diff
       endif
      enddo

      dif_set=0.0
      do i=1,mm
       dif=abs(ebsb(i)-ebsb1(i))/ebsb(i)
       if(dif.ge.dif_set)then
         dif_set=dif
       endif
      enddo

      d_mdot=0.0
        do i=2,mm-1
          if(m_dot(i).eq.0)then
             dif=0
          else

         dif=abs(m_dot(i)-m_dot1(i))/abs(m_dot(i))
          endif  *

          if(dif.ge.d_mdot)then
             d_mdot=dif
          endif
        enddo

      do i=1,mm
       t(i,2)=t(i,1)
       ebsb1(i)=ebsb(i)
       m_dot1(i)=m_dot(i)
      enddo

       ft1=ft

      enddo      !lss
*      write(*,*)d_mdot
      if(d_mdot.ge.1e-4)then
        ls=ls+1
        if(ls.ge.1000)then
         write(*,*)'d_mdot not conver'
         stop
        endif
        goto 100
      endif
```

```
      if(diff_set.ge.1e-7)then
       ls=ls+1
       if(ls.gt.100)then
        write(*,*)'not conver.'
        stop
       endif
       goto 100
      endif

      if(dif_set.ge.1e-9)then
       ls=ls+1
       if(ls.gt.100)then
        write(*,*)'not conver.'
        stop
       endif
       goto 100
      endif

       density=0.0

      do i=2,mm-1
       density=density+rhof(i)*dz
      enddo
      density=density+rhof(1)*0.5*dz+rhof(mm)*0.5*dz
      density=density/ft

      h_flux=kf*(t(2,1)-t_cold)/dz-m_dot(2)*hsg*0.5*dz

      ft_old=ft

*******************************
* update grid  based on new ft*
*******************************

      new_z(1)=0.0
      dz=ft/(mm-1)

      do i=2,mm
       new_z(i)=new_z(i-1)+dz
      enddo

      if(new_z(mm-1).gt.z(mm))then
       write(*,*)'Dear Hong sth is wrong? :)'
       stop
      endif

*******************************
*Update temperature           *
*******************************
       do i=1,mm
        t_old(i)=t(i,1)
       enddo


      do i=2,mm-1
       var1=new_z(i)

       call lgrg2(z,T_old,mm,var1,var2)
       t(i,1)=var2
       t_old(i)=t(i,1)
       t(i,2)=t(i,1)
      enddo

*************************
* Update ebsb           *
*************************

      do i=1,mm
       ebsb_old(i)=ebsb(i)
      enddo
```

```
      do i=2,mm-1
       var1=new_z(i)
       call lgrg2(z,ebsb_old,mm,var1,var2)

       ebsb(i)=var2
       if(ebsb(i).lt.0)then
          write(*,*)'ebsb<1 in interpo',i,ebsb(i)
         chen=1

       endif
      enddo
             if(chen.eq.1)then
                 write(*,*)'ebsb<0 in intep'
      do i=1,mm

         write(*,*)ebsb_old(i),ebsb(i)

      enddo

           pause
            endif
         do i=1,mm
             ebsb_old(i)=ebsb(i)
           enddo

      m_rate=hm*(w0-wfs)

      return
      end

      include'ava_den.for'  !Frost density
      include'sph.for'      !Frost specific heat
      include'keff.for'     !Frost thermal conductivity
      include'kdeff.for'    !Vapor diffusion coefficient
      include'bt_coeff.for' !Coefficient for the energy equation
      include'bt_bound.for' !Boundary condition for the energy equation
      include'intepl.for'   !Interpolation
      include'psat.for'     !Saturation condition
      include'tdma.for'     !TDMA solver
      include'newcal_mdot.for' !Phase change rate
      include'cal_w.for'       !Humidity ratio
```

APPENDIX D
EXPERIMENTAL DATA FOR THE FROST GROWTH ON THE FLAT PLATE

Test No.	x	W	R_{ed}	T_a	Ts	t	m_f	δ_f	q^*
	(m)	(kg/kg)		(°C)	(°C)	(s)	(kg/m^2)	(m)	(W/m^2)
1	0.025	1.22E-03	13112	-11.6	-20.05	3600	6.72E-02	8.13E-04	276.7
	0.065	1.22E-03	13112	-11.6	-20.25	3600	5.97E-02	8.89E-04	296.1
	0.12	1.22E-03	13112	-11.6	-20.27	3600	5.47E-02	7.87E-04	269.8
	0.19	1.22E-03	13112	-11.6	-20.39	3600	5.60E-02	8.64E-04	296.1
	0.26	1.22E-03	13112	-11.6	-20.4	3600	4.98E-02	7.87E-04	269.8
	0.33	1.22E-03	13112	-11.6	-20.46	3600	4.85E-02	9.14E-04	269.8
	0.405	1.22E-03	13112	-11.6	-20.5	3600	4.73E-02	7.62E-04	293.3
	0.48	1.22E-03	13112	-11.6	-20.45	3600	4.73E-02	8.13E-04	251.8
	0.025	1.22E-03	13112	-11.6	-20.05	5400	1.18E-01	1.19E-03	276.7
	0.065	1.22E-03	13112	-11.6	-20.25	5400	1.06E-01	1.25E-03	296.1
	0.12	1.22E-03	13112	-11.6	-20.27	5400	9.83E-02	1.17E-03	269.8
	0.19	1.22E-03	13112	-11.6	-20.39	5400	9.45E-02	1.17E-03	296.1
	0.26	1.22E-03	13112	-11.6	-20.4	5400	8.96E-02	1.19E-03	269.8
	0.33	1.22E-03	13112	-11.6	-20.46	5400	8.83E-02	1.25E-03	269.8
	0.405	1.22E-03	13112	-11.6	-20.5	5400	8.46E-02	1.25E-03	293.3
	0.48	1.22E-03	13112	-11.6	-20.45	5400	8.34E-02	1.17E-03	251.8
	0.025	1.22E-03	13112	-11.6	-20.05	7200	1.59E-01	1.43E-03	276.7
	0.065	1.22E-03	13112	-11.6	-20.25	7200	1.42E-01	1.42E-03	296.1
	0.12	1.22E-03	13112	-11.6	-20.27	7200	1.22E-01	1.19E-03	269.8
	0.19	1.22E-03	13112	-11.6	-20.39	7200	1.24E-01	1.19E-03	296.1
	0.26	1.22E-03	13112	-11.6	-20.4	7200	1.23E-01	1.40E-03	269.8
	0.33	1.22E-03	13112	-11.6	-20.46	7200	1.21E-01	1.30E-03	269.8
	0.405	1.22E-03	13112	-11.6	-20.5	7200	1.13E-01	1.36E-03	293.3
	0.48	1.22E-03	13112	-11.6	-20.45	7200	1.11E-01	1.41E-03	251.8
2	0.025	1.00E-03	8195	-10.3	-30.5	4200	6.72E-02	1.33E-03	319.6
	0.065	1.00E-03	8195	-10.3	-30.65	4200	5.35E-02	1.21E-03	344.5
	0.12	1.00E-03	8195	-10.3	-30.52	4200	4.85E-02	8.13E-04	268.4
	0.19	1.00E-03	8195	-10.3	-30.42	4200	5.10E-02	8.38E-04	386.0
	0.26	1.00E-03	8195	-10.3	-30.2	4200	5.23E-02	1.03E-03	336.2
	0.33	1.00E-03	8195	-10.3	-30.17	4200	5.35E-02	8.59E-04	336.3
	0.405	1.00E-03	8195	-10.3	-30.16	4200	5.35E-02	1.02E-03	379.1
	0.48	1.00E-03	8195	-10.3	-29.59	4200	5.35E-02	9.35E-04	283.7
	0.025	1.00E-03	8195	-10.3	-30.5	6000	9.08E-02	1.70E-03	319.6
	0.065	1.00E-03	8195	-10.3	-30.65	6000	8.46E-02	1.56E-03	344.5
	0.12	1.00E-03	8195	-10.3	-30.52	6000	8.09E-02	1.31E-03	268.4
	0.19	1.00E-03	8195	-10.3	-30.42	6000	8.09E-02	1.35E-03	386.0
	0.26	1.00E-03	8195	-10.3	-30.2	6000	8.21E-02	1.40E-03	336.2
	0.33	1.00E-03	8195	-10.3	-30.17	6000	8.71E-02	1.36E-03	336.3
	0.405	1.00E-03	8195	-10.3	-30.16	6000	8.46E-02	1.60E-03	379.1
	0.48	1.00E-03	8195	-10.3	-29.59	6000	8.71E-02	1.42E-03	283.7
	0.025	1.00E-03	8195	-10.3	-30.5	7800	1.52E-01	2.05E-03	319.6
	0.065	1.00E-03	8195	-10.3	-30.65	7800	1.47E-01	2.02E-03	344.5
	0.12	1.00E-03	8195	-10.3	-30.52	7800	1.32E-01	1.83E-03	268.4
	0.19	1.00E-03	8195	-10.3	-30.42	7800	1.36E-01	1.78E-03	386.0
	0.26	1.00E-03	8195	-10.3	-30.2	7800	1.23E-01	1.96E-03	336.2
	0.33	1.00E-03	8195	-10.3	-30.17	7800	1.19E-01	1.86E-03	336.3

	0.405	1.00E-03	8195	-10.3	-30.16	7800	1.18E-01	2.01E-03	379.1
	0.48	1.00E-03	8195	-10.3	-29.59	7800	1.11E-01	1.80E-03	283.7
3	0.025	7.30E-04	3278	-10.1	-39.22	3600	4.73E-02	1.14E-03	319.0
	0.065	7.30E-04	3278	-10.1	-39.69	3600	3.23E-02	9.40E-04	321.6
	0.12	7.30E-04	3278	-10.1	-39.47	3600	2.74E-02	5.71E-04	269.5
	0.19	7.30E-04	3278	-10.1	-40.21	3600	2.61E-02	6.86E-04	306.3
	0.26	7.30E-04	3278	-10.1	-40.23	3600	2.49E-02	7.62E-04	247.3
	0.33	7.30E-04	3278	-10.1	-40.33	3600	2.24E-02	5.59E-04	239.1
	0.405	7.30E-04	3278	-10.1	-40.22	3600	2.24E-02	6.25E-04	285.8
	0.48	7.30E-04	3278	-10.1	-39.49	3600	2.36E-02	7.11E-04	182.9
	0.025	7.30E-04	3278	-10.1	-39.22	5400	6.35E-02	1.26E-03	319.0
	0.065	7.30E-04	3278	-10.1	-39.69	5400	4.98E-02	1.23E-03	321.6
	0.12	7.30E-04	3278	-10.1	-39.47	5400	3.98E-02	8.76E-04	269.5
	0.19	7.30E-04	3278	-10.1	-40.21	5400	3.73E-02	1.03E-03	306.3
	0.26	7.30E-04	3278	-10.1	-40.23	5400	3.36E-02	1.17E-03	247.3
	0.33	7.30E-04	3278	-10.1	-40.33	5400	3.23E-02	9.14E-04	239.1
	0.405	7.30E-04	3278	-10.1	-40.22	5400	3.98E-02	1.12E-03	285.8
	0.48	7.30E-04	3278	-10.1	-39.49	5400	3.23E-02	9.91E-04	182.9
	0.025	7.30E-04	3278	-10.1	-39.22	7200	8.71E-02	1.30E-03	319.0
	0.065	7.30E-04	3278	-10.1	-39.69	7200	6.84E-02	1.38E-03	321.6
	0.12	7.30E-04	3278	-10.1	-39.47	7200	5.60E-02	9.02E-04	269.5
	0.19	7.30E-04	3278	-10.1	-40.21	7200	5.23E-02	1.07E-03	306.3
	0.26	7.30E-04	3278	-10.1	-40.23	7200	4.48E-02	1.22E-03	247.3
	0.33	7.30E-04	3278	-10.1	-40.33	7200	4.73E-02	9.65E-04	239.1
	0.405	7.30E-04	3278	-10.1	-40.22	7200	4.35E-02	1.19E-03	285.8
	0.48	7.30E-04	3278	-10.1	-39.49	7200	4.48E-02	1.18E-03	182.9
4	0.025	1.90E-04	8195	-25.8	-40.97	3600	1.37E-02	4.57E-04	307.5
	0.065	1.90E-04	8195	-25.8	-41.41	3600	1.87E-02	3.05E-04	303.2
	0.12	1.90E-04	8195	-25.8	-41.35	3600	8.70E-03	1.75E-04	221.0
	0.19	1.90E-04	8195	-25.8	-41.68	3600	9.90E-03	1.78E-04	305.8
	0.26	1.90E-04	8195	-25.8	-41.61	3600	9.90E-03	1.65E-04	255.2
	0.33	1.90E-04	8195	-25.8	-41.63	3600	8.70E-03	2.29E-04	246.9
	0.405	1.90E-04	8195	-25.8	-41.5	3600	1.12E-02	3.30E-04	296.3
	0.48	1.90E-04	8195	-25.8	-40.91	3600	2.61E-02	4.57E-04	189.5
	0.025	1.90E-04	8195	-25.8	-40.97	5400	2.12E-02	5.33E-04	307.5
	0.065	1.90E-04	8195	-25.8	-41.41	5400	2.36E-02	3.43E-04	303.2
	0.12	1.90E-04	8195	-25.8	-41.35	5400	1.62E-02	2.45E-04	221.0
	0.19	1.90E-04	8195	-25.8	-41.68	5400	1.62E-02	2.54E-04	305.8
	0.26	1.90E-04	8195	-25.8	-41.61	5400	1.49E-02	2.16E-04	255.2
	0.33	1.90E-04	8195	-25.8	-41.63	5400	1.62E-02	2.54E-04	246.9
	0.405	1.90E-04	8195	-25.8	-41.5	5400	1.37E-02	4.32E-04	296.3
	0.48	1.90E-04	8195	-25.8	-40.91	5400	1.99E-02	4.70E-04	189.5
	0.025	1.90E-04	8195	-25.8	-40.97	7200	3.48E-02	5.46E-04	307.5
	0.065	1.90E-04	8195	-25.8	-41.41	7200	2.74E-02	3.56E-04	303.2
	0.12	1.90E-04	8195	-25.8	-41.35	7200	2.12E-02	2.55E-04	221.0
	0.19	1.90E-04	8195	-25.8	-41.68	7200	2.12E-02	2.79E-04	305.8
	0.26	1.90E-04	8195	-25.8	-41.61	7200	1.99E-02	4.19E-04	255.2
	0.33	1.90E-04	8195	-25.8	-41.63	7200	1.87E-02	3.05E-04	246.9
	0.405	1.90E-04	8195	-25.8	-41.5	7200	1.74E-02	4.57E-04	296.3
	0.48	1.90E-04	8195	-25.8	-40.91	7200	2.12E-02	6.10E-04	189.5
5	0.025	7.50E-04	8195	-15.9	-27.81	3600	4.11E-02	5.59E-04	211.9

	0.065	7.50E-04	8195	-15.9	-28.05	3600	3.11E-02	5.97E-04	200.8
	0.12	7.50E-04	8195	-15.9	-28.27	3600	2.74E-02	5.33E-04	171.7
	0.19	7.50E-04	8195	-15.9	-28.18	3600	2.61E-02	5.33E-04	221.5
	0.26	7.50E-04	8195	-15.9	-28.04	3600	2.36E-02	5.97E-04	196.6
	0.33	7.50E-04	8195	-15.9	-28.07	3600	2.49E-02	5.33E-04	184.2
	0.405	7.50E-04	8195	-15.9	-28.22	3600	2.61E-02	6.60E-04	196.6
	0.48	7.50E-04	8195	-15.9	-27.93	3600	2.74E-02	4.93E-04	185.6
	0.025	7.50E-04	8195	-15.9	-27.81	5400	5.72E-02	7.24E-04	211.9
	0.065	7.50E-04	8195	-15.9	-28.05	5400	4.85E-02	8.08E-04	200.8
	0.12	7.50E-04	8195	-15.9	-28.27	5400	4.35E-02	7.11E-04	171.7
	0.19	7.50E-04	8195	-15.9	-28.18	5400	4.11E-02	6.86E-04	221.5
	0.26	7.50E-04	8195	-15.9	-28.04	5400	4.23E-02	7.87E-04	196.6
	0.33	7.50E-04	8195	-15.9	-28.07	5400	3.98E-02	7.24E-04	184.2
	0.405	7.50E-04	8195	-15.9	-28.22	5400	4.60E-02	7.49E-04	196.6
	0.48	7.50E-04	8195	-15.9	-27.93	5400	4.23E-02	6.60E-04	185.6
	0.025	7.50E-04	8195	-15.9	-27.81	7200	9.08E-02	9.98E-04	211.9
	0.065	7.50E-04	8195	-15.9	-28.05	7200	7.71E-02	1.02E-03	200.8
	0.12	7.50E-04	8195	-15.9	-28.27	7200	6.84E-02	9.10E-04	171.7
	0.19	7.50E-04	8195	-15.9	-28.18	7200	6.72E-02	8.38E-04	221.5
	0.26	7.50E-04	8195	-15.9	-28.04	7200	6.10E-02	1.07E-03	196.6
	0.33	7.50E-04	8195	-15.9	-28.07	7200	5.97E-02	8.89E-04	184.2
	0.405	7.50E-04	8195	-15.9	-28.22	7200	5.72E-02	9.40E-04	196.6
	0.48	7.50E-04	8195	-15.9	-27.93	7200	5.35E-02	8.89E-04	185.6
6	0.025	1.03E-03	8195	-13.1	-21.71	3600	4.48E-02	3.30E-04	174.4
	0.065	1.03E-03	8195	-13.1	-21.91	3600	3.11E-02	2.52E-04	164.7
	0.12	1.03E-03	8195	-13.1	-22.2	3600	2.61E-02	2.03E-04	141.2
	0.19	1.03E-03	8195	-13.1	-22.18	3600	2.49E-02	1.40E-04	171.6
	0.26	1.03E-03	8195	-13.1	-22.12	3600	2.36E-02	1.27E-04	155.0
	0.33	1.03E-03	8195	-13.1	-22.18	3600	2.49E-02	1.80E-04	142.6
	0.405	1.03E-03	8195	-13.1	-22.33	3600	2.61E-02	1.91E-04	146.7
	0.48	1.03E-03	8195	-13.1	-22.13	3600	2.61E-02	1.82E-04	150.9
	0.025	1.03E-03	8195	-13.1	-21.71	5400	6.34E-02	5.08E-04	174.4
	0.065	1.03E-03	8195	-13.1	-21.91	5400	5.10E-02	2.79E-04	164.7
	0.12	1.03E-03	8195	-13.1	-22.2	5400	4.35E-02	3.81E-04	141.2
	0.19	1.03E-03	8195	-13.1	-22.18	5400	4.48E-02	3.18E-04	171.6
	0.26	1.03E-03	8195	-13.1	-22.12	5400	4.23E-02	3.68E-04	155.0
	0.33	1.03E-03	8195	-13.1	-22.18	5400	4.23E-02	2.16E-04	142.6
	0.405	1.03E-03	8195	-13.1	-22.33	5400	4.35E-02	3.94E-04	146.7
	0.48	1.03E-03	8195	-13.1	-22.13	5400	4.35E-02	2.54E-04	150.9
	0.025	1.03E-03	8195	-13.1	-21.71	7200	1.01E-01	6.48E-04	174.4
	0.065	1.03E-03	8195	-13.1	-21.91	7200	8.46E-02	7.62E-04	164.7
	0.12	1.03E-03	8195	-13.1	-22.2	7200	7.46E-02	4.08E-04	141.2
	0.19	1.03E-03	8195	-13.1	-22.18	7200	7.22E-02	4.70E-04	171.6
	0.26	1.03E-03	8195	-13.1	-22.12	7200	6.47E-02	6.22E-04	155.0
	0.33	1.03E-03	8195	-13.1	-22.18	7200	6.34E-02	3.94E-04	142.6
	0.405	1.03E-03	8195	-13.1	-22.33	7200	5.97E-02	6.86E-04	146.7
	0.48	1.03E-03	8195	-13.1	-22.13	7200	5.72E-02	5.84E-04	150.9
7	0.025	7.20E-04	13112	-18.1	-25.22	3600	4.98E-02	6.22E-04	231.3
	0.065	7.20E-04	13112	-18.1	-25.43	3600	4.23E-02	5.97E-04	225.7
	0.12	7.20E-04	13112	-18.1	-25.74	3600	3.61E-02	4.95E-04	184.2
	0.19	7.20E-04	13112	-18.1	-25.83	3600	3.61E-02	5.21E-04	231.3

	0.26	7.20E-04	13112	-18.1	-25.85	3600	2.99E-02	3.56E-04	202.2
	0.33	7.20E-04	13112	-18.1	-26	3600	2.99E-02	3.45E-04	187.0
	0.405	7.20E-04	13112	-18.1	-26.23	3600	2.74E-02	4.19E-04	188.4
	0.48	7.20E-04	13112	-18.1	-26.02	3600	2.61E-02	3.88E-04	173.1
	0.025	7.20E-04	13112	-18.1	-25.22	5400	7.59E-02	1.00E-03	231.3
	0.065	7.20E-04	13112	-18.1	-25.43	5400	6.34E-02	9.65E-04	225.7
	0.12	7.20E-04	13112	-18.1	-25.74	5400	5.72E-02	9.53E-04	184.2
	0.19	7.20E-04	13112	-18.1	-25.83	5400	5.60E-02	9.02E-04	231.3
	0.26	7.20E-04	13112	-18.1	-25.85	5400	5.10E-02	7.24E-04	202.2
	0.33	7.20E-04	13112	-18.1	-26	5400	4.85E-02	5.33E-04	187.0
	0.405	7.20E-04	13112	-18.1	-26.23	5400	4.60E-02	8.13E-04	188.4
	0.48	7.20E-04	13112	-18.1	-26.02	5400	4.35E-02	5.79E-04	173.1
	0.025	7.20E-04	13112	-18.1	-25.22	7200	1.00E-01	1.12E-03	231.3
	0.065	7.20E-04	13112	-18.1	-25.43	7200	8.71E-02	1.19E-03	225.7
	0.12	7.20E-04	13112	-18.1	-25.74	7200	7.71E-02	1.08E-03	184.2
	0.19	7.20E-04	13112	-18.1	-25.83	7200	7.22E-02	1.04E-03	231.3
	0.26	7.20E-04	13112	-18.1	-25.85	7200	6.72E-02	9.70E-04	202.2
	0.33	7.20E-04	13112	-18.1	-26	7200	6.47E-02	8.56E-04	187.0
	0.405	7.20E-04	13112	-18.1	-26.23	7200	6.10E-02	1.02E-03	188.4
	0.48	7.20E-04	13112	-18.1	-26.02	7200	5.97E-02	8.71E-04	173.1
8	0.025	1.03E-03	4917	-12.9	-20.16	3600	3.36E-02	1.65E-04	163.2
	0.065	1.03E-03	4917	-12.9	-20.4	3600	2.11E-02	1.02E-04	142.5
	0.12	1.03E-03	4917	-12.9	-20.68	3600	1.87E-02	9.60E-05	121.7
	0.19	1.03E-03	4917	-12.9	-20.69	3600	1.87E-02	8.90E-05	152.2
	0.26	1.03E-03	4917	-12.9	-20.68	3600	1.87E-02	1.78E-04	132.8
	0.33	1.03E-03	4917	-12.9	-20.72	3600	1.87E-02	1.50E-04	123.1
	0.405	1.03E-03	4917	-12.9	-20.92	3600	1.74E-02	1.51E-04	121.8
	0.48	1.03E-03	4917	-12.9	-20.71	3600	1.87E-02	1.65E-04	128.7
	0.025	1.03E-03	4917	-12.9	-20.16	3600	5.10E-02	2.92E-04	163.2
	0.065	1.03E-03	4917	-12.9	-20.4	5400	3.98E-02	2.67E-04	142.5
	0.12	1.03E-03	4917	-12.9	-20.68	5400	3.73E-02	2.54E-04	121.7
	0.19	1.03E-03	4917	-12.9	-20.69	5400	3.73E-02	2.29E-04	152.2
	0.26	1.03E-03	4917	-12.9	-20.68	5400	3.48E-02	2.56E-04	132.8
	0.33	1.03E-03	4917	-12.9	-20.72	5400	3.36E-02	2.45E-04	123.1
	0.405	1.03E-03	4917	-12.9	-20.92	5400	3.61E-02	2.94E-04	121.8
	0.48	1.03E-03	4917	-12.9	-20.71	5400	3.48E-02	3.18E-04	128.7
	0.025	1.03E-03	4917	-12.9	-20.16	5400	8.58E-02	4.32E-04	163.2
	0.065	1.03E-03	4917	-12.9	-20.4	7200	7.22E-02	3.56E-04	142.5
	0.12	1.03E-03	4917	-12.9	-20.68	7200	6.22E-02	2.67E-04	121.7
	0.19	1.03E-03	4917	-12.9	-20.69	7200	5.85E-02	2.63E-04	152.2
	0.26	1.03E-03	4917	-12.9	-20.68	7200	5.35E-02	3.75E-04	132.8
	0.33	1.03E-03	4917	-12.9	-20.72	7200	5.22E-02	2.82E-04	123.1
	0.405	1.03E-03	4917	-12.9	-20.92	7200	4.73E-02	5.08E-04	121.8
	0.48	1.03E-03	4917	-12.9	-20.71	7200	4.48E-02	4.89E-04	128.7
9	0.025	8.40E-04	8195	-13.5	-30.81	3600	4.85E-02	1.00E-03	282.2
	0.065	8.40E-04	8195	-13.5	-31.05	3600	3.86E-02	1.05E-03	276.7
	0.12	8.40E-04	8195	-13.5	-31.23	3600	2.99E-02	1.04E-03	231.0
	0.19	8.40E-04	8195	-13.5	-31.28	3600	3.23E-02	9.27E-04	294.6
	0.26	8.40E-04	8195	-13.5	-31.13	3600	3.11E-02	7.11E-04	262.8
	0.33	8.40E-04	8195	-13.5	-31.17	3600	3.23E-02	5.59E-04	257.3
	0.405	8.40E-04	8195	-13.5	-31.36	3600	3.36E-02	6.48E-04	231.0

	0.48	8.40E-04	8195	-13.5	-30.97	3600	3.36E-02	6.99E-04	240.7
	0.025	8.40E-04	8195	-13.5	-30.81	5400	6.34E-02	1.21E-03	282.2
	0.065	8.40E-04	8195	-13.5	-31.05	5400	4.85E-02	1.19E-03	276.7
	0.12	8.40E-04	8195	-13.5	-31.23	5400	4.73E-02	1.23E-03	231.0
	0.19	8.40E-04	8195	-13.5	-31.28	5400	4.73E-02	1.05E-03	294.6
	0.26	8.40E-04	8195	-13.5	-31.13	5400	5.10E-02	9.78E-04	262.8
	0.33	8.40E-04	8195	-13.5	-31.17	5400	5.35E-02	6.86E-04	257.3
	0.405	8.40E-04	8195	-13.5	-31.36	5400	5.60E-02	8.38E-04	231.0
	0.48	8.40E-04	8195	-13.5	-30.97	5400	5.35E-02	8.13E-04	240.7
10	0.025	6.20E-04	8195	-13.9	-38.81	3600	4.48E-02	1.52E-03	338.4
	0.065	6.20E-04	8195	-13.9	-39.06	3600	3.11E-02	1.35E-03	341.1
	0.12	6.20E-04	8195	-13.9	-39.19	3600	2.86E-02	1.17E-03	260.0
	0.19	6.20E-04	8195	-13.9	-39.14	3600	3.36E-02	9.65E-04	382.2
	0.26	6.20E-04	8195	-13.9	-38.92	3600	2.99E-02	9.27E-04	326.0
	0.33	6.20E-04	8195	-13.9	-38.87	3600	2.86E-02	6.99E-04	324.6
	0.405	6.20E-04	8195	-13.9	-38.93	3600	2.99E-02	8.13E-04	359.0
	0.48	6.20E-04	8195	-13.9	-38.22	3600	2.86E-02	8.20E-04	289.1
	0.025	6.20E-04	8195	-13.9	-38.81	5400	6.34E-02	1.56E-03	338.4
	0.065	6.20E-04	8195	-13.9	-39.06	5400	5.72E-02	1.55E-03	341.1
	0.12	6.20E-04	8195	-13.9	-39.19	5400	5.22E-02	1.44E-03	260.0
	0.19	6.20E-04	8195	-13.9	-39.14	5400	5.35E-02	1.33E-03	382.2
	0.26	6.20E-04	8195	-13.9	-38.92	5400	5.60E-02	1.31E-03	326.0
	0.33	6.20E-04	8195	-13.9	-38.87	5400	5.47E-02	1.95E-03	324.6
	0.405	6.20E-04	8195	-13.9	-38.93	5400	5.35E-02	1.19E-03	359.0
	0.48	6.20E-04	8195	-13.9	-38.22	5400	4.98E-02	1.21E-03	289.1
	0.025	6.20E-04	8195	-13.9	-38.81	7200	9.95E-02	1.72E-03	338.4
	0.065	6.20E-04	8195	-13.9	-39.06	7200	8.71E-02	1.65E-03	341.1
	0.12	6.20E-04	8195	-13.9	-39.19	7200	7.71E-02	1.45E-03	260.0
	0.19	6.20E-04	8195	-13.9	-39.14	7200	7.34E-02	1.31E-03	382.2
	0.26	6.20E-04	8195	-13.9	-38.92	7200	7.09E-02	1.50E-03	326.0
	0.33	6.20E-04	8195	-13.9	-38.87	7200	6.84E-02	1.09E-03	324.6
	0.405	6.20E-04	8195	-13.9	-38.93	7200	6.59E-02	1.32E-03	359.0
	0.48	6.20E-04	8195	-13.9	-38.22	7200	6.34E-02	1.34E-03	289.1
11	0.025	2.00E-03	13112	-12.9	-39.81	1800	8.34E-02	2.20E-03	399.8
	0.065	2.00E-03	13112	-12.9	-40.11	1800	7.21E-02	2.24E-03	427.1
	0.12	2.00E-03	13112	-12.9	-39.53	1800	6.72E-02	2.20E-03	391.7
	0.19	2.00E-03	13112	-12.9	-40.08	1800	6.47E-02	2.10E-03	442.2
	0.26	2.00E-03	13112	-12.9	-39.81	1800	6.22E-02	2.21E-03	390.2
	0.33	2.00E-03	13112	-12.9	-39.65	1800	5.85E-02	2.15E-03	393.0
	0.405	2.00E-03	13112	-12.9	-39.33	1800	5.60E-02	2.31E-03	459.0
	0.48	2.00E-03	13112	-12.9	-38.44	1800	5.60E-02	2.44E-03	344.0
	0.025	2.00E-03	13112	-12.9	-39.81	3600	1.46E-01	2.85E-03	399.8
	0.065	2.00E-03	13112	-12.9	-40.11	3600	1.26E-01	3.05E-03	427.1
	0.12	2.00E-03	13112	-12.9	-39.53	3600	1.22E-01	2.92E-03	391.7
	0.19	2.00E-03	13112	-12.9	-40.08	3600	1.16E-01	2.99E-03	442.2
	0.26	2.00E-03	13112	-12.9	-39.81	3600	1.11E-01	2.91E-03	390.2
	0.33	2.00E-03	13112	-12.9	-39.65	3600	1.06E-01	2.92E-03	393.0
	0.405	2.00E-03	13112	-12.9	-39.33	3600	1.08E-01	3.02E-03	459.0
	0.48	2.00E-03	13112	-12.9	-38.44	3600	1.03E-01	2.97E-03	344.0
	0.025	2.00E-03	13112	-12.9	-39.81	5400	1.99E-01	3.07E-03	399.8
	0.065	2.00E-03	13112	-12.9	-40.11	5400	1.64E-01	3.51E-03	427.1

	0.12	2.00E-03	13112	-12.9	-39.53	5400	1.69E-01	3.34E-03	391.7
	0.19	2.00E-03	13112	-12.9	-40.08	5400	1.53E-01	3.11E-03	442.2
	0.26	2.00E-03	13112	-12.9	-39.81	5400	1.53E-01	3.38E-03	390.2
	0.33	2.00E-03	13112	-12.9	-39.65	5400	1.44E-01	3.14E-03	393.0
	0.405	2.00E-03	13112	-12.9	-39.33	5400	1.43E-01	3.71E-03	459.0
	0.48	2.00E-03	13112	-12.9	-38.44	5400	1.64E-01	3.40E-03	344.0
12	0.025	1.16E-03	13112	-12.3	-39.87	3600	8.34E-02	2.67E-03	419.0
	0.065	1.16E-03	13112	-12.3	-40.04	3600	8.09E-02	2.82E-03	460.0
	0.12	1.16E-03	13112	-12.3	-39.5	3600	7.83E-02	2.62E-03	416.4
	0.19	1.16E-03	13112	-12.3	-39.92	3600	9.21E-02	2.79E-03	484.7
	0.26	1.16E-03	13112	-12.3	-39.58	3600	9.21E-02	2.69E-03	423.2
	0.33	1.16E-03	13112	-12.3	-39.43	3600	7.96E-02	2.64E-03	428.8
	0.405	1.16E-03	13112	-12.3	-39.19	3600	8.83E-02	2.92E-03	497.5
	0.48	1.16E-03	13112	-12.3	-38.16	3600	9.45E-02	2.81E-03	408.7
	0.025	1.16E-03	13112	-12.3	-39.87	5400	1.70E-01	3.15E-03	419.0
	0.065	1.16E-03	13112	-12.3	-40.04	5400	1.68E-01	3.30E-03	460.0
	0.12	1.16E-03	13112	-12.3	-39.5	5400	1.64E-01	3.20E-03	416.4
	0.19	1.16E-03	13112	-12.3	-39.92	5400	1.39E-01	3.56E-03	484.7
	0.26	1.16E-03	13112	-12.3	-39.58	5400	1.63E-01	3.38E-03	423.2
	0.33	1.16E-03	13112	-12.3	-39.43	5400	1.56E-01	3.25E-03	428.8
	0.405	1.16E-03	13112	-12.3	-39.19	5400	1.39E-01	3.46E-03	497.5
	0.48	1.16E-03	13112	-12.3	-38.16	5400	1.47E-01	3.28E-03	408.7
	0.025	1.16E-03	13112	-12.3	-39.87	7200	2.36E-01	3.51E-03	419.0
	0.065	1.16E-03	13112	-12.3	-40.04	7200	2.25E-01	3.58E-03	460.0
	0.12	1.16E-03	13112	-12.3	-39.5	7200	2.24E-01	3.63E-03	416.4
	0.19	1.16E-03	13112	-12.3	-39.92	7200	2.24E-01	3.52E-03	484.7
	0.26	1.16E-03	13112	-12.3	-39.58	7200	2.08E-01	4.13E-03	423.2
	0.33	1.16E-03	13112	-12.3	-39.43	7200	1.97E-01	3.87E-03	428.8
	0.405	1.16E-03	13112	-12.3	-39.19	7200	1.93E-01	3.99E-03	497.5
	0.48	1.16E-03	13112	-12.3	-38.16	7200	1.95E-01	3.67E-03	408.7
13	0.025	1.07E-03	13112	-13.8	-32.74	1800	6.47E-02	1.58E-03	402.1
	0.065	1.07E-03	13112	-13.8	-32.94	1800	5.85E-02	1.55E-03	439.4
	0.12	1.07E-03	13112	-13.8	-32.63	1800	5.35E-02	1.52E-03	364.9
	0.19	1.07E-03	13112	-13.8	-32.72	1800	5.23E-02	1.35E-03	473.9
	0.26	1.07E-03	13112	-13.8	-32.33	1800	4.60E-02	1.19E-03	427.1
	0.33	1.07E-03	13112	-13.8	-32.23	1800	4.35E-02	8.13E-04	431.3
	0.405	1.07E-03	13112	-13.8	-31.99	1800	4.10E-02	1.07E-03	493.5
	0.48	1.07E-03	13112	-13.8	-31.2	1800	3.98E-02	1.17E-03	388.6
	0.025	1.07E-03	13112	-13.8	-32.74	3600	1.31E-01	2.49E-03	402.1
	0.065	1.07E-03	13112	-13.8	-32.94	3600	1.19E-01	2.44E-03	439.4
	0.12	1.07E-03	13112	-13.8	-32.63	3600	1.11E-01	2.34E-03	364.9
	0.19	1.07E-03	13112	-13.8	-32.72	3600	1.08E-01	2.24E-03	473.9
	0.26	1.07E-03	13112	-13.8	-32.33	3600	1.05E-01	1.99E-03	427.1
	0.33	1.07E-03	13112	-13.8	-32.23	3600	9.95E-02	1.88E-03	431.3
	0.405	1.07E-03	13112	-13.8	-31.99	3600	9.83E-02	2.34E-03	493.5
	0.48	1.07E-03	13112	-13.8	-31.2	3600	9.70E-02	1.91E-03	388.6
	0.025	1.07E-03	13112	-13.8	-32.74	5400	1.92E-01	2.92E-03	402.1
	0.065	1.07E-03	13112	-13.8	-32.94	5400	1.77E-01	3.08E-03	439.4
	0.12	1.07E-03	13112	-13.8	-32.63	5400	1.61E-01	2.82E-03	364.9
	0.19	1.07E-03	13112	-13.8	-32.72	5400	1.58E-01	2.90E-03	473.9
	0.26	1.07E-03	13112	-13.8	-32.33	5400	1.54E-01	2.71E-03	427.1

	0.33	1.07E-03	13112	-13.8	-32.23	5400	1.37E-01	2.53E-03	431.3
	0.405	1.07E-03	13112	-13.8	-31.99	5400	1.46E-01	2.75E-03	493.5
	0.48	1.07E-03	13112	-13.8	-31.2	5400	1.43E-01	2.59E-03	388.6
14	0.025	9.30E-04	8195	-15.4	-40.87	3600	5.60E-02	2.24E-03	337.6
	0.065	9.30E-04	8195	-15.4	-40.96	3600	4.73E-02	1.91E-03	384.2
	0.12	9.30E-04	8195	-15.4	-40.56	3600	4.85E-02	2.07E-03	313.1
	0.19	9.30E-04	8195	-15.4	-40.6	3600	5.10E-02	1.70E-03	421.4
	0.26	9.30E-04	8195	-15.4	-40.37	3600	4.98E-02	1.83E-03	365.3
	0.33	9.30E-04	8195	-15.4	-40.24	3600	4.98E-02	1.38E-03	365.3
	0.405	9.30E-04	8195	-15.4	-40.03	3600	4.98E-02	1.65E-03	423.0
	0.48	9.30E-04	8195	-15.4	-39.29	3600	5.23E-02	2.24E-03	309.4
	0.025	9.30E-04	8195	-15.4	-40.87	5400	8.58E-02	2.54E-03	337.6
	0.065	9.30E-04	8195	-15.4	-40.96	5400	8.09E-02	2.30E-03	384.2
	0.12	9.30E-04	8195	-15.4	-40.56	5400	7.59E-02	2.40E-03	313.1
	0.19	9.30E-04	8195	-15.4	-40.6	5400	8.09E-02	2.07E-03	421.4
	0.26	9.30E-04	8195	-15.4	-40.37	5400	8.71E-02	2.15E-03	365.3
	0.33	9.30E-04	8195	-15.4	-40.24	5400	8.58E-02	1.85E-03	365.3
	0.405	9.30E-04	8195	-15.4	-40.03	5400	7.59E-02	2.02E-03	423.0
	0.48	9.30E-04	8195	-15.4	-39.29	5400	7.09E-02	2.67E-03	309.4
	0.025	9.30E-04	8195	-15.4	-40.87	7200	1.49E-01	2.69E-03	337.6
	0.065	9.30E-04	8195	-15.4	-40.96	7200	1.37E-01	2.57E-03	384.2
	0.12	9.30E-04	8195	-15.4	-40.56	7200	1.26E-01	2.68E-03	313.1
	0.19	9.30E-04	8195	-15.4	-40.6	7200	1.23E-01	2.34E-03	421.4
	0.26	9.30E-04	8195	-15.4	-40.37	7200	1.05E-01	2.46E-03	365.3
	0.33	9.30E-04	8195	-15.4	-40.24	7200	1.16E-01	2.24E-03	365.3
	0.405	9.30E-04	8195	-15.4	-40.03	7200	1.01E-01	2.41E-03	423.0
	0.48	9.30E-04	8195	-15.4	-39.29	7200	1.06E-01	2.83E-03	309.4
15	0.025	8.50E-04	13112	-19.8	-23.75	1800	2.49E-02	1.27E-04	138.5
	0.065	8.50E-04	13112	-19.8	-23.97	1800	1.99E-02	1.14E-04	139.9
	0.12	8.50E-04	13112	-19.8	-24.01	1800	1.74E-02	1.27E-04	116.3
	0.19	8.50E-04	13112	-19.8	-24.1	1800	1.74E-02	1.52E-04	144.0
	0.26	8.50E-04	13112	-19.8	-24.11	1800	1.62E-02	1.32E-04	128.8
	0.33	8.50E-04	13112	-19.8	-24.18	1800	1.49E-02	1.21E-04	124.6
	0.405	8.50E-04	13112	-19.8	-24.17	1800	1.49E-02	1.26E-04	135.7
	0.48	8.50E-04	13112	-19.8	-24.1	1800	1.49E-02	1.25E-04	102.5
	0.025	8.50E-04	13112	-19.8	-23.75	3600	3.98E-02	2.54E-04	138.5
	0.065	8.50E-04	13112	-19.8	-23.97	3600	3.23E-02	2.54E-04	139.9
	0.12	8.50E-04	13112	-19.8	-24.01	3600	2.86E-02	2.29E-04	116.3
	0.19	8.50E-04	13112	-19.8	-24.1	3600	2.74E-02	2.54E-04	144.0
	0.26	8.50E-04	13112	-19.8	-24.11	3600	2.74E-02	2.29E-04	128.8
	0.33	8.50E-04	13112	-19.8	-24.18	3600	2.49E-02	2.29E-04	124.6
	0.405	8.50E-04	13112	-19.8	-24.17	3600	2.49E-02	2.54E-04	135.7
	0.48	8.50E-04	13112	-19.8	-24.1	3600	1.99E-02	2.06E-04	102.5
	0.025	8.50E-04	13112	-19.8	-23.75	5400	5.35E-02	3.56E-04	138.5
	0.065	8.50E-04	13112	-19.8	-23.97	5400	4.48E-02	3.30E-04	139.9
	0.12	8.50E-04	13112	-19.8	-24.01	5400	3.73E-02	2.79E-04	116.3
	0.19	8.50E-04	13112	-19.8	-24.1	5400	3.73E-02	3.05E-04	144.0
	0.26	8.50E-04	13112	-19.8	-24.1	5400	3.48E-02	3.43E-04	130.2
	0.33	8.50E-04	13112	-19.8	-24.11	5400	3.48E-02	3.30E-04	134.3
	0.405	8.50E-04	13112	-19.8	-24.18	5400	3.36E-02	3.56E-04	134.3
	0.48	8.50E-04	13112	-19.8	-24.1	5400	3.11E-02	3.14E-04	102.5

16	0.025	6.40E-04	13112	-20	-38.99	1800	6.10E-02	1.07E-03	431.7
	0.065	6.40E-04	13112	-20	-39.06	1800	4.48E-02	1.11E-03	482.5
	0.12	6.40E-04	13112	-20	-38.94	1800	6.59E-02	9.27E-04	380.9
	0.19	6.40E-04	13112	-20	-39.06	1800	3.98E-02	8.64E-04	501.7
	0.26	6.40E-04	13112	-20	-38.78	1800	4.10E-02	8.64E-04	435.9
	0.33	6.40E-04	13112	-20	-38.78	1800	2.99E-02	5.84E-04	431.8
	0.405	6.40E-04	13112	-20	-38.69	1800	2.61E-02	6.35E-04	499.1
	0.48	6.40E-04	13112	-20	-37.88	1800	2.49E-02	4.83E-04	386.8
	0.025	6.40E-04	13112	-20	-38.99	3600	1.13E-01	2.30E-03	431.7
	0.065	6.40E-04	13112	-20	-39.06	3600	1.03E-01	2.12E-03	482.5
	0.12	6.40E-04	13112	-20	-38.94	3600	8.83E-02	1.76E-03	380.9
	0.19	6.40E-04	13112	-20	-39.06	3600	7.71E-02	1.85E-03	501.7
	0.26	6.40E-04	13112	-20	-38.78	3600	7.21E-02	1.63E-03	435.9
	0.33	6.40E-04	13112	-20	-38.78	3600	6.72E-02	1.37E-03	431.8
	0.405	6.40E-04	13112	-20	-38.69	3600	5.85E-02	1.27E-03	499.1
	0.48	6.40E-04	13112	-20	-37.88	3600	5.85E-02	1.30E-03	386.8
	0.025	6.40E-04	13112	-20	-38.99	5400	1.54E-01	2.95E-03	431.7
	0.065	6.40E-04	13112	-20	-39.06	5400	1.39E-01	2.77E-03	482.5
	0.12	6.40E-04	13112	-20	-38.94	5400	1.27E-01	2.45E-03	380.9
	0.19	6.40E-04	13112	-20	-39.06	5400	1.13E-01	2.29E-03	501.7
	0.26	6.40E-04	13112	-20	-38.78	5400	1.11E-01	2.11E-03	435.9
	0.33	6.40E-04	13112	-20	-38.78	5400	9.70E-02	1.80E-03	431.8
	0.405	6.40E-04	13112	-20	-38.69	5400	9.58E-02	1.96E-03	499.1
	0.48	6.40E-04	13112	-20	-37.88	5400	9.98E-02	1.75E-03	386.8
17	0.025	5.50E-04	13112	-20	-38.97	3600	7.34E-02	1.19E-03	467.4
	0.065	5.50E-04	13112	-20	-39.19	3600	6.10E-02	1.32E-03	505.7
	0.12	5.50E-04	13112	-20	-38.88	3600	5.72E-02	9.40E-04	434.5
	0.19	5.50E-04	13112	-20	-39.33	3600	5.60E-02	9.78E-04	522.1
	0.26	5.50E-04	13112	-20	-39.26	3600	4.85E-02	9.40E-04	442.6
	0.33	5.50E-04	13112	-20	-39.29	3600	4.35E-02	8.25E-04	441.2
	0.405	5.50E-04	13112	-20	-39.3	3600	4.35E-02	1.02E-03	491.9
	0.48	5.50E-04	13112	-20	-38.58	3600	3.98E-02	9.91E-04	377.0
	0.025	5.50E-04	13112	-20	-38.97	5400	1.01E-01	1.45E-03	467.4
	0.065	5.50E-04	13112	-20	-39.19	5400	9.58E-02	1.63E-03	505.7
	0.12	5.50E-04	13112	-20	-38.88	5400	8.34E-02	1.30E-03	434.5
	0.19	5.50E-04	13112	-20	-39.33	5400	7.96E-02	1.25E-03	522.1
	0.26	5.50E-04	13112	-20	-39.26	5400	7.59E-02	1.26E-03	442.6
	0.33	5.50E-04	13112	-20	-39.29	5400	7.21E-02	1.12E-03	441.2
	0.405	5.50E-04	13112	-20	-39.3	5400	6.22E-02	1.30E-03	491.9
	0.48	5.50E-04	13112	-20	-38.58	5400	6.59E-02	1.19E-03	377.0
	0.025	5.50E-04	13112	-20	-38.97	7200	1.38E-01	1.60E-03	467.4
	0.065	5.50E-04	13112	-20	-39.19	7200	1.17E-01	1.68E-03	505.7
	0.12	5.50E-04	13112	-20	-38.88	7200	1.07E-01	1.55E-03	434.5
	0.19	5.50E-04	13112	-20	-39.33	7200	1.02E-01	1.36E-03	522.1
	0.26	5.50E-04	13112	-20	-39.26	7200	9.83E-02	1.41E-03	442.6
	0.33	5.50E-04	13112	-20	-39.29	7200	9.45E-02	1.18E-03	441.2
	0.405	5.50E-04	13112	-20	-39.3	7200	8.96E-02	1.42E-03	491.9
	0.48	5.50E-04	13112	-20	-38.58	7200	6.84E-02	1.56E-03	377.0
18	0.025	4.90E-04	8195	-21.8	-40.42	3600	3.98E-02	8.18E-04	313.1
	0.065	4.90E-04	8195	-21.8	-40.65	3600	3.36E-02	7.92E-04	330.9
	0.12	4.90E-04	8195	-21.8	-40.47	3600	3.23E-02	6.68E-04	256.9

	0.19	4.90E-04	8195	-21.8	-40.57	3600	3.36E-02	6.35E-04	362.4
	0.26	4.90E-04	8195	-21.8	-40.35	3600	3.11E-02	9.65E-04	311.8
	0.33	4.90E-04	8195	-21.8	-40.27	3600	3.23E-02	4.45E-04	307.7
	0.405	4.90E-04	8195	-21.8	-40.28	3600	3.11E-02	8.64E-04	347.5
	0.48	4.90E-04	8195	-21.8	-39.63	3600	3.23E-02	4.14E-04	247.5
	0.025	4.90E-04	8195	-21.8	-40.42	5400	6.10E-02	1.22E-03	313.1
	0.065	4.90E-04	8195	-21.8	-40.65	5400	5.35E-02	1.19E-03	330.9
	0.12	4.90E-04	8195	-21.8	-40.47	5400	4.98E-02	1.04E-03	256.9
	0.19	4.90E-04	8195	-21.8	-40.57	5400	5.23E-02	9.91E-04	362.4
	0.26	4.90E-04	8195	-21.8	-40.35	5400	5.10E-02	1.14E-03	311.8
	0.33	4.90E-04	8195	-21.8	-40.27	5400	5.10E-02	9.02E-04	307.7
	0.405	4.90E-04	8195	-21.8	-40.28	5400	4.48E-02	1.04E-03	347.5
	0.48	4.90E-04	8195	-21.8	-39.63	5400	4.60E-02	9.35E-04	247.5
	0.025	4.90E-04	8195	-21.8	-40.42	7200	9.83E-02	1.72E-03	313.1
	0.065	4.90E-04	8195	-21.8	-40.65	7200	9.33E-02	1.52E-03	330.9
	0.12	4.90E-04	8195	-21.8	-40.47	7200	8.21E-02	1.33E-03	256.9
	0.19	4.90E-04	8195	-21.8	-40.57	7200	7.59E-02	1.02E-03	362.4
	0.26	4.90E-04	8195	-21.8	-40.35	7200	6.72E-02	1.35E-03	311.8
	0.33	4.90E-04	8195	-21.8	-40.27	7200	6.47E-02	1.02E-03	307.7
	0.405	4.90E-04	8195	-21.8	-40.28	7200	6.22E-02	1.44E-03	347.5
	0.48	4.90E-04	8195	-21.8	-39.63	7200	5.97E-02	1.43E-03	247.5
19	0.025	3.80E-04	13112	-24.3	-39.28	3600	4.98E-02	7.11E-04	402.8
	0.065	3.80E-04	13112	-24.3	-39.58	3600	3.98E-02	6.99E-04	430.1
	0.12	3.80E-04	13112	-24.3	-39.62	3600	3.61E-02	5.26E-04	323.0
	0.19	3.80E-04	13112	-24.3	-39.85	3600	3.23E-02	4.32E-04	436.8
	0.26	3.80E-04	13112	-24.3	-39.85	3600	2.86E-02	3.30E-04	360.0
	0.33	3.80E-04	13112	-24.3	-39.92	3600	2.86E-02	3.72E-04	357.2
	0.405	3.80E-04	13112	-24.3	-39.94	3600	2.74E-02	4.83E-04	394.2
	0.48	3.80E-04	13112	-24.3	-39.18	3600	2.74E-02	3.30E-04	279.2
	0.025	3.80E-04	13112	-24.3	-39.28	5400	7.21E-02	1.04E-03	402.8
	0.065	3.80E-04	13112	-24.3	-39.58	5400	6.34E-02	1.03E-03	430.1
	0.12	3.80E-04	13112	-24.3	-39.62	5400	5.60E-02	6.86E-04	323.0
	0.19	3.80E-04	13112	-24.3	-39.85	5400	4.98E-02	6.99E-04	436.8
	0.26	3.80E-04	13112	-24.3	-39.85	5400	4.73E-02	5.97E-04	360.0
	0.33	3.80E-04	13112	-24.3	-39.92	5400	4.48E-02	4.75E-04	357.2
	0.405	3.80E-04	13112	-24.3	-39.94	5400	4.10E-02	6.86E-04	394.2
	0.48	3.80E-04	13112	-24.3	-39.18	5400	3.98E-02	4.70E-04	279.2
	0.025	3.80E-04	13112	-24.3	-39.28	7200	1.02E-01	1.07E-03	402.8
	0.065	3.80E-04	13112	-24.3	-39.58	7200	8.58E-02	1.16E-03	430.1
	0.12	3.80E-04	13112	-24.3	-39.62	7200	7.46E-02	9.65E-04	323.0
	0.19	3.80E-04	13112	-24.3	-39.85	7200	7.21E-02	8.51E-04	436.8
	0.26	3.80E-04	13112	-24.3	-39.85	7200	6.35E-02	9.65E-04	360.0
	0.33	3.80E-04	13112	-24.3	-39.92	7200	6.35E-02	8.02E-04	357.2
	0.405	3.80E-04	13112	-24.3	-39.94	7200	5.97E-02	7.37E-04	394.2
	0.48	3.80E-04	13112	-24.3	-39.18	7200	5.72E-02	6.48E-04	279.2
20	0.025	4.10E-04	13112	-23.4	-39.29	7200	1.27E-01	1.91E-03	346.5
	0.065	4.10E-04	13112	-23.4	-39.55	7200	1.11E-01	1.93E-03	372.5
	0.12	4.10E-04	13112	-23.4	-39.46	7200	1.03E-01	1.59E-03	279.1
	0.19	4.10E-04	13112	-23.4	-39.68	7200	8.96E-02	1.52E-03	375.1
	0.26	4.10E-04	13112	-23.4	-39.33	7200	7.96E-02	1.42E-03	338.2
	0.33	4.10E-04	13112	-23.4	-39.25	7200	7.59E-02	1.17E-03	336.9

0.405	4.10E-04	13112	-23.4	-39.04	7200	7.09E-02	1.45E-03	385.0
0.48	4.10E-04	13112	-23.4	-38.11	7200	6.94E-02	1.36E-03	274.0
0.025	4.10E-04	13112	-23.4	-39.29	14400	2.38E-01	2.54E-03	346.5
0.065	4.10E-04	13112	-23.4	-39.55	14400	1.94E-01	2.46E-03	372.5
0.12	4.10E-04	13112	-23.4	-39.46	14400	1.77E-01	2.29E-03	279.1
0.19	4.10E-04	13112	-23.4	-39.68	14400	1.67E-01	2.13E-03	375.1
0.26	4.10E-04	13112	-23.4	-39.33	14400	1.63E-01	2.07E-03	338.2
0.33	4.10E-04	13112	-23.4	-39.25	14400	1.46E-01	1.82E-03	336.9
0.405	4.10E-04	13112	-23.4	-39.04	14400	1.38E-01	1.96E-03	385.0
0.48	4.10E-04	13112	-23.4	-38.11	14400	1.34E-01	1.80E-03	274.0
0.025	4.10E-04	13112	-23.4	-39.29	21600	3.10E-01	3.11E-03	346.5
0.065	4.10E-04	13112	-23.4	-39.55	21600	2.80E-01	3.30E-03	372.5
0.12	4.10E-04	13112	-23.4	-39.46	21000	2.59E-01	3.01E-03	279.1
0.19	4.10E-04	13112	-23.4	-39.68	21600	2.43E-01	2.72E-03	375.1
0.26	4.10E-04	13112	-23.4	-39.33	21600	2.25E-01	2.60E-03	338.2
0.33	4.10E-04	13112	-23.4	-39.25	21600	2.21E-01	2.30E-03	336.9
0.405	4.10E-04	13112	-23.4	-39.04	21600	2.04E-01	2.60E-03	385.0
0.48	4.10E-04	13112	-23.4	-38.11	21600	2.02E-01	2.41E-03	274.0

APPENDIX E

COMPARISONS BETWEEN SIMULATION RESULTS AND EXPERIMENTAL DATA FOR FROST GROWTH ON FINS

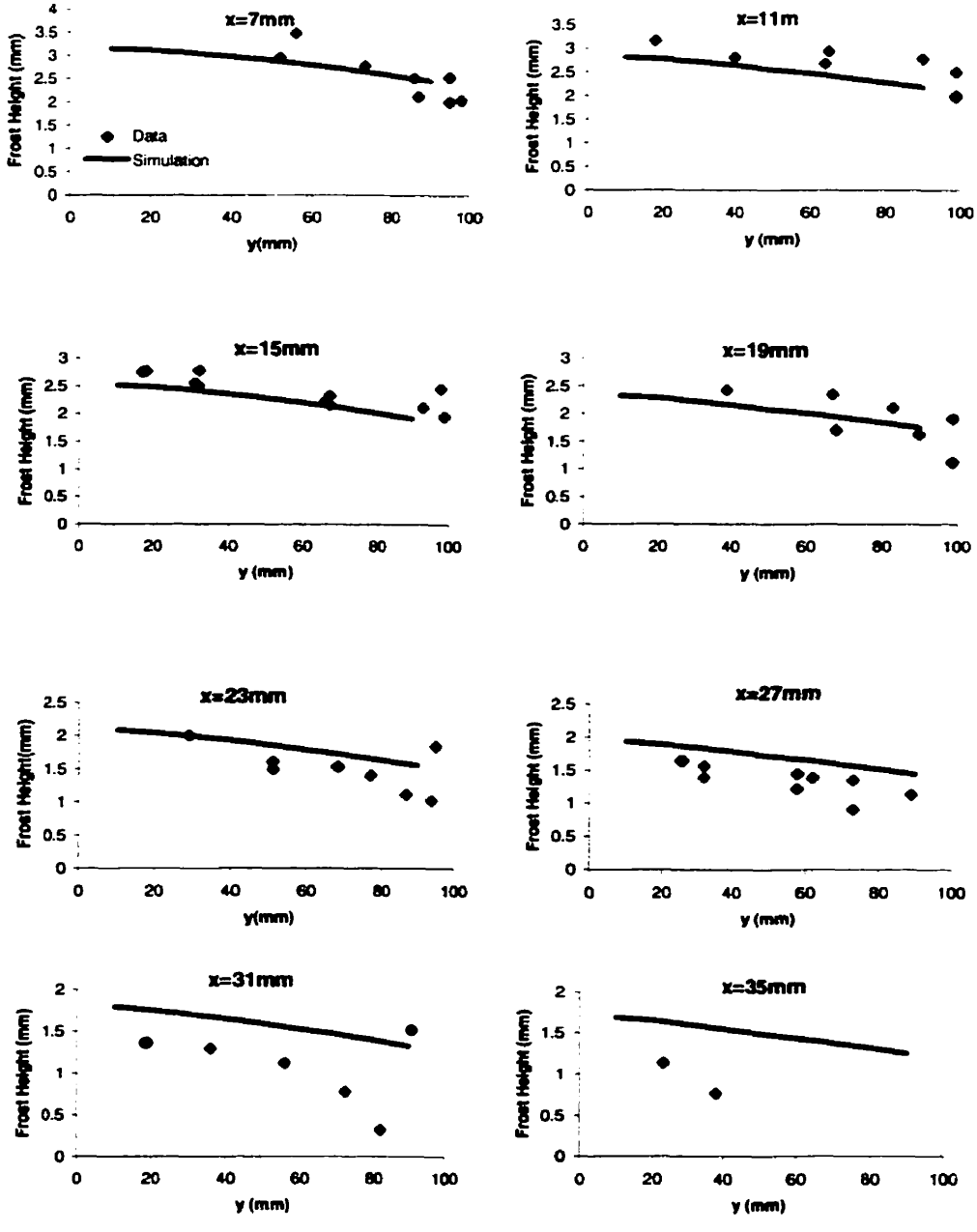

Figure E1 Comparison of simulated and experimental data for Case 1 (T_a = -15.0°C, T_b = -35.0°C, V_{in} = 4.4m/s, W_0 = 9.7x10^{-4}, t = 240min)

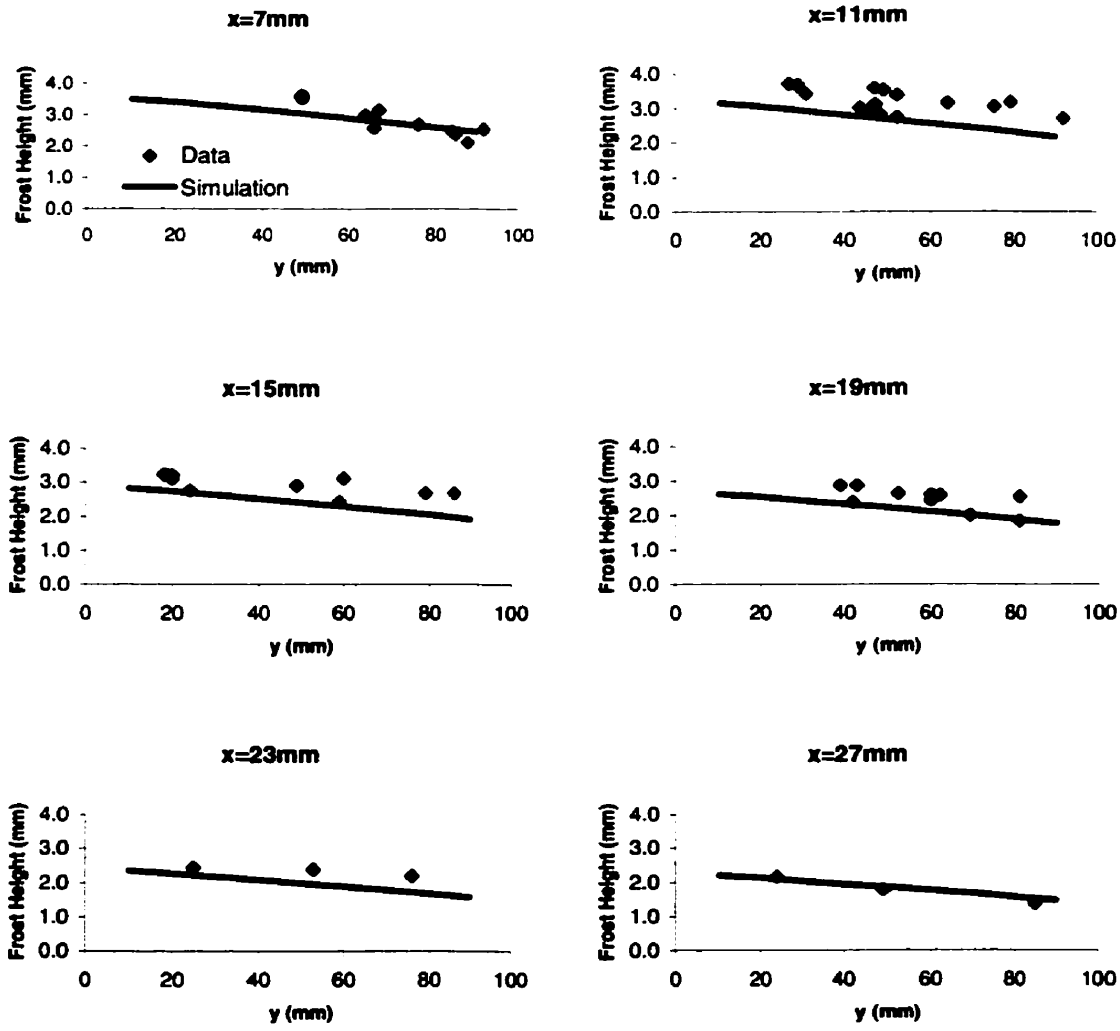

Figure E2 Comparison of simulated and experimental data for Case 2 (T_a = -16.0°C, T_b = -38.0°C, V_{in} = 4.2 m/s, W_0=9.3x10^{-4}, t = 220 min)

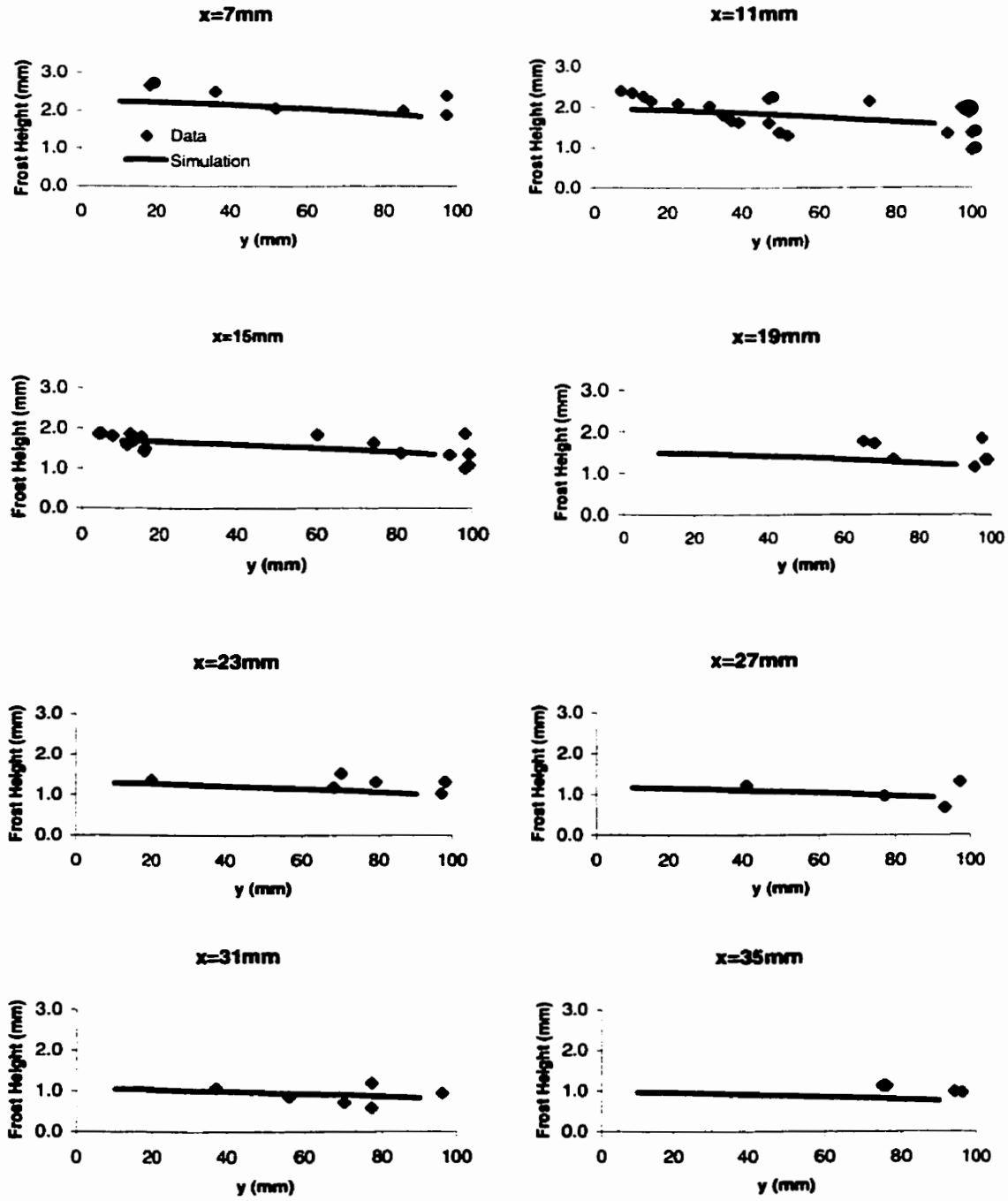

Figure E3 Comparison of simulated and experimental data for Case 3 (T_a = -18.2°C, T_b = -31.0°C, V_{in} = 5.8 m/s, W_0=7.3x10^{-4}, t = 270 Min)

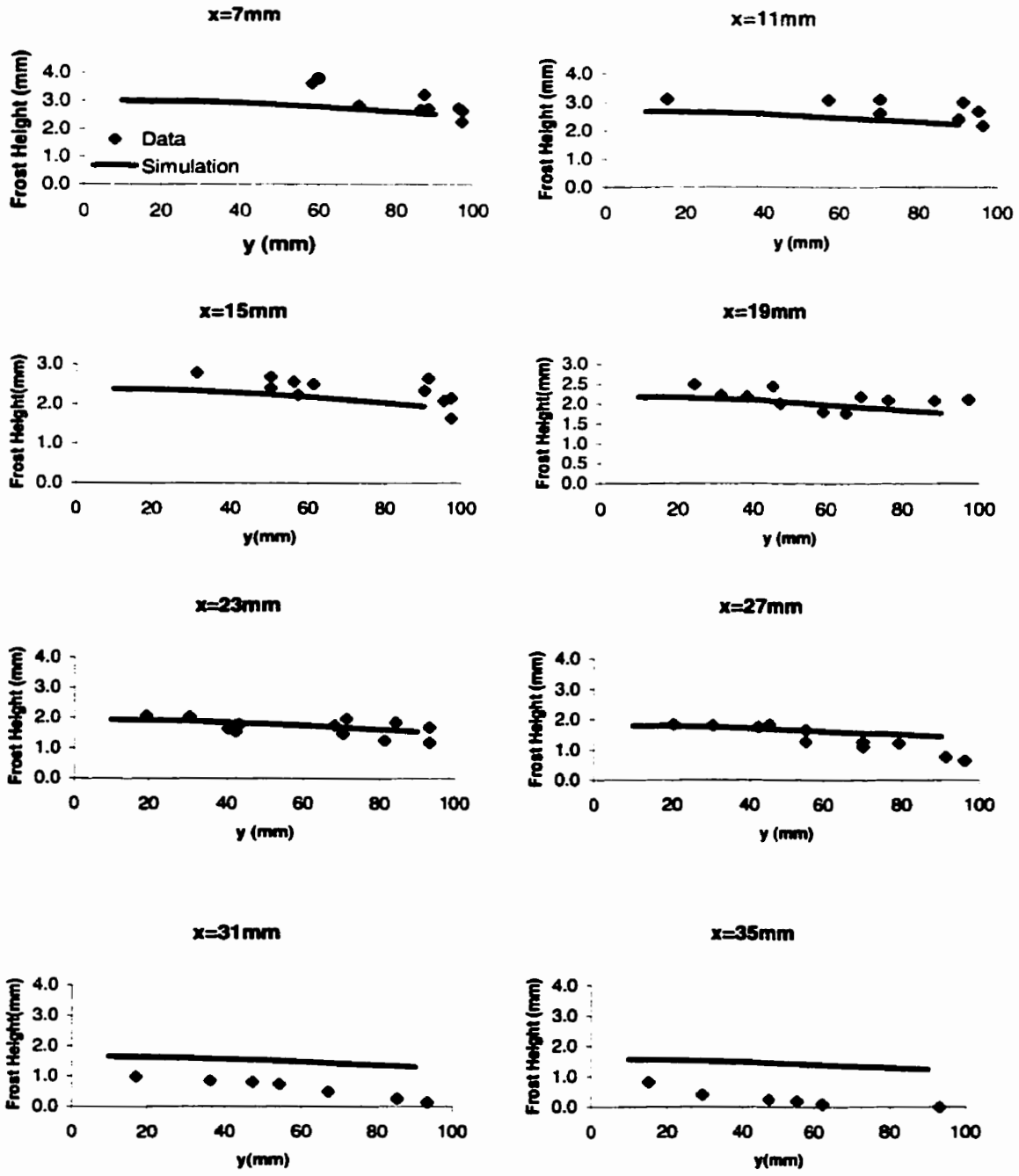

Figure E4 Comparison of simulated and experimental data for Case 4.
(T_a = -13.5°C, T_b = -31.5°C, V_{in} = 5.1 m/s, W_0=11.2x10^{-4}, t = 225 min)

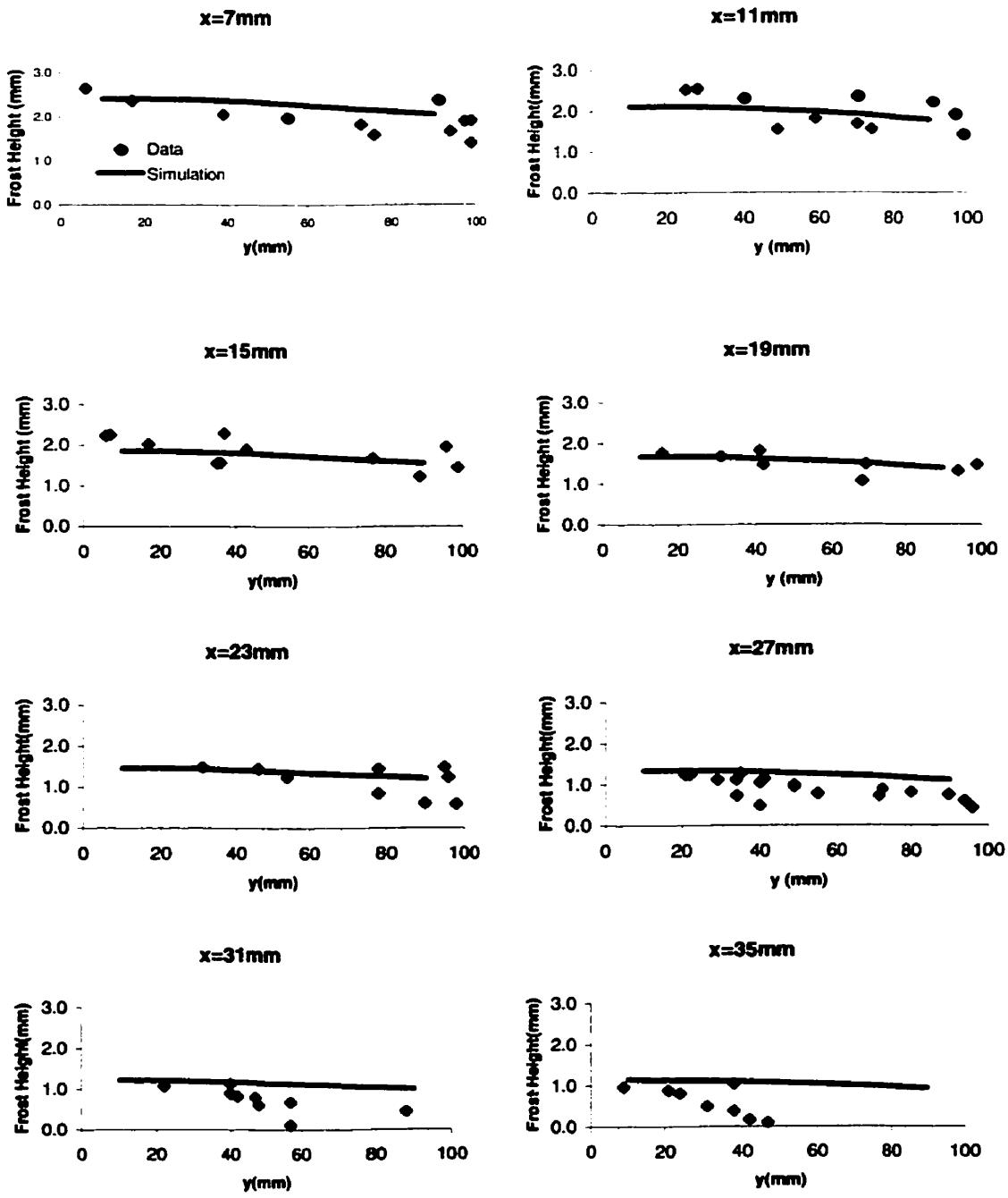

Figure E5 Comparison of simulated and experimental data for Case 5
(T_a = -20.8°C, T_b = -39.0°C, V_{in} = 5.3 m/s, $W_0 = 6.1 \times 10^{-4}$, t = 210 min)

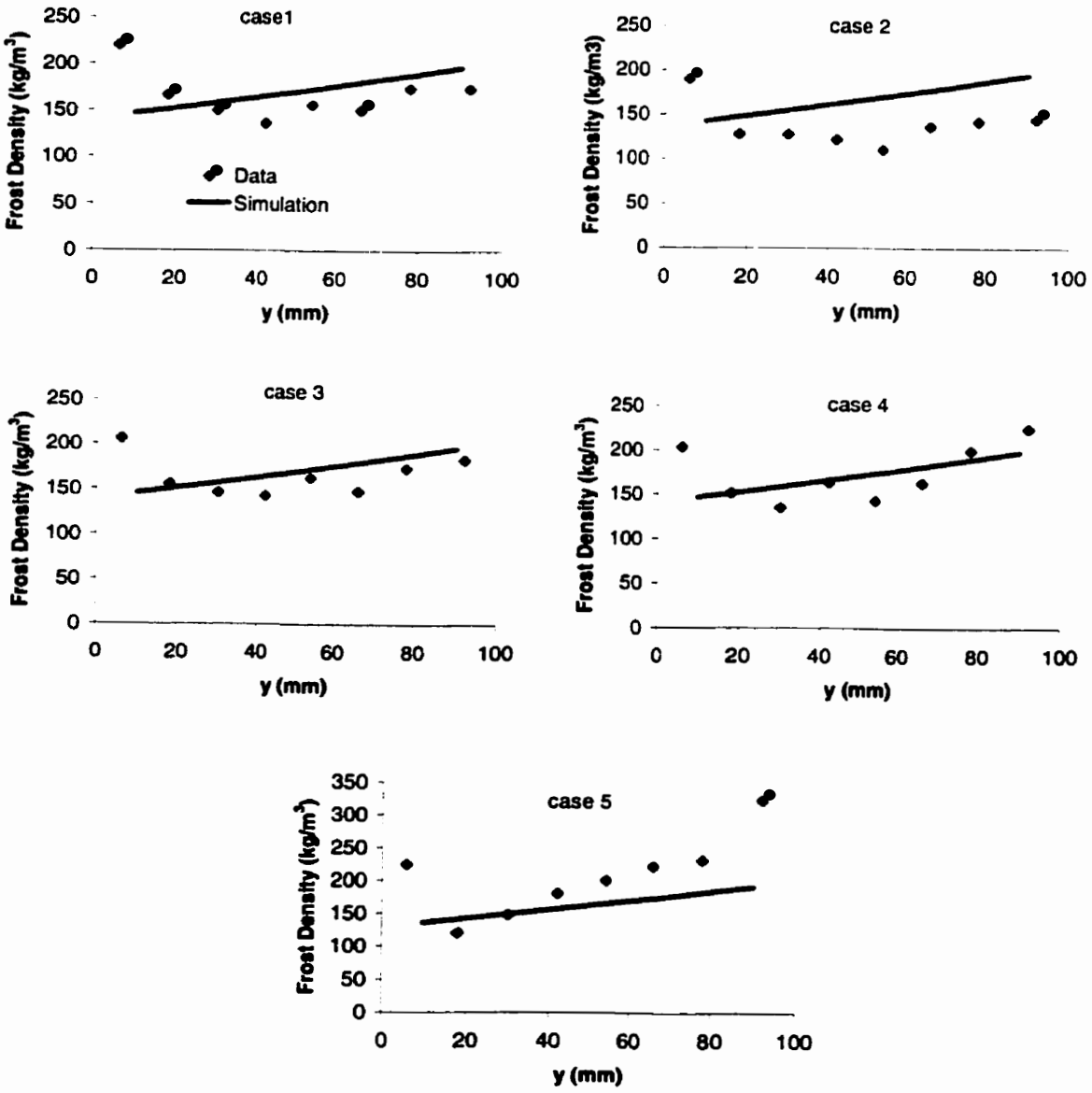

Figure E6 Comparisions for frost density profile between simulations and data

APPENDIX F

SENSITIVITY STUDY RESULTS FOR THE FROST GROWTH ON FINS

Table F1 Parameters used in the sensitivity study

Original Case	Sensitivity Study
Air Flow Temperature T_a=-15°C	T_a=-30°C
Cold Plate Temperature T_b=-35°C	T_b=-50°C
Flow Velocity Before Entering the Fined Section V_{in}=4.4 m/s	V_{in}=6.6m/s
Initial Condition of Volume Fraction of Ice on Fin Surface $\varepsilon_0(x,y)=0.01+0.1x/h_{fin}+0.1y/l_{fin}$	$\varepsilon_0(x,y)=0.5*(0.01+0.12x/h_{fin}+0.1y/l_{fin})$ $\varepsilon_0(x,y)=0.1$
Effective Thermal Conductivity of Frost k_{eff}	k_{eff}=1.2*Original k_{eff}=0.8*Original
Fin Spacing t_{fin}=9.2mm	t_{fin}=7.7mm

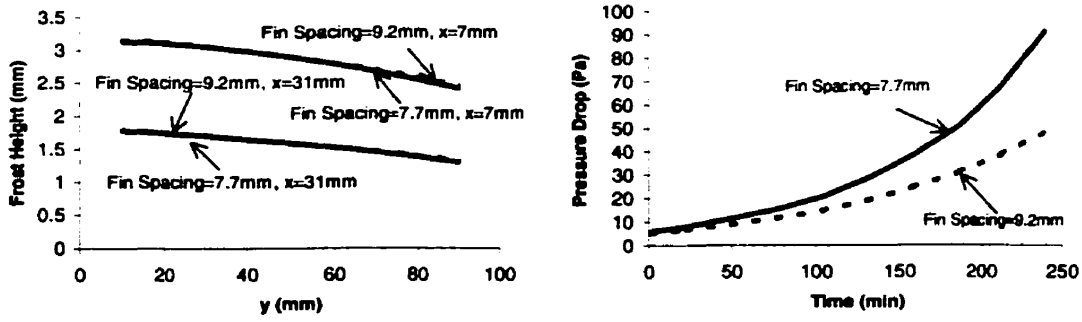

(a) (b)

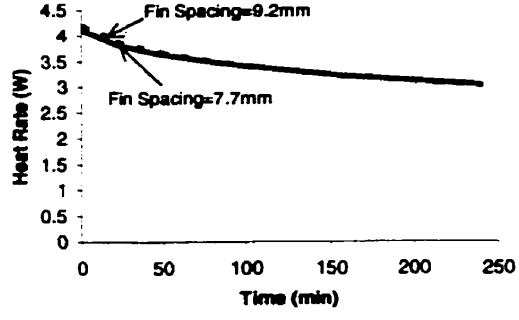

(c)

Figure F1 Sensitivity study for the fin spacing, t_{fin}, a) Frost height at 240min, b) Transient pressure drop, c) Transient heat rate through each fin

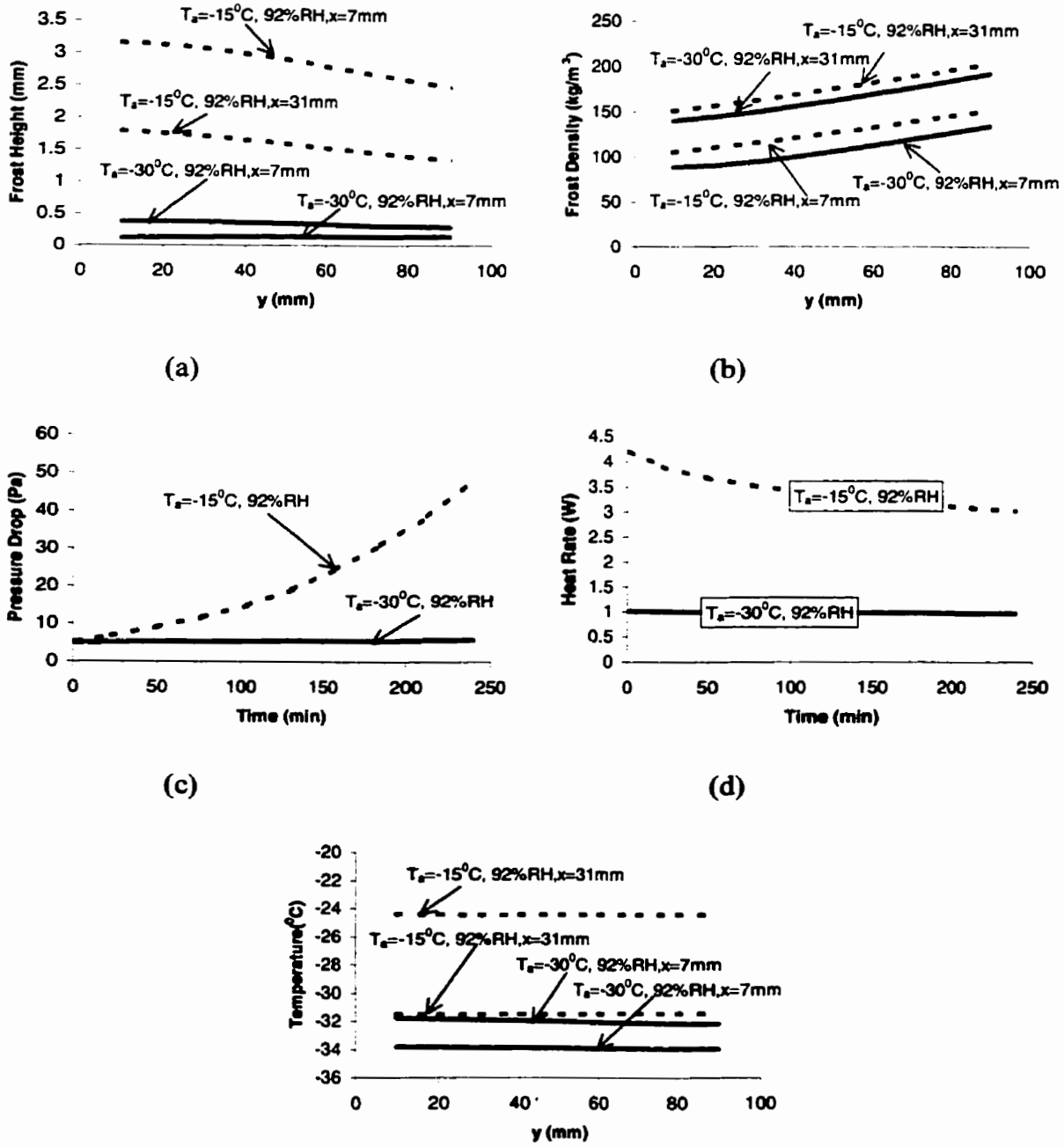

Figure F2 Sensitivity study for the air flow temperature, T_a a) Frost height at 240min, b) Frost density at 240min, c) Transient pressure drop, d) Transient heat rate through each fin, e) Temperature profile on the fin at 240min

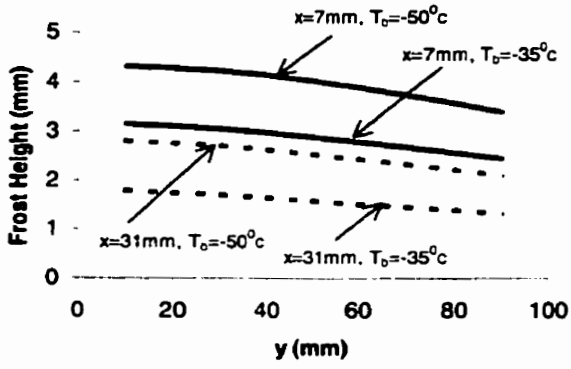

(a)

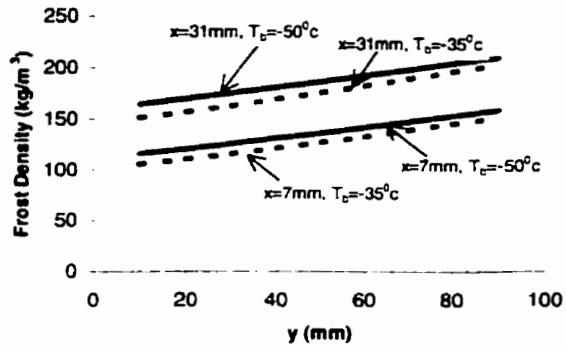

(b)

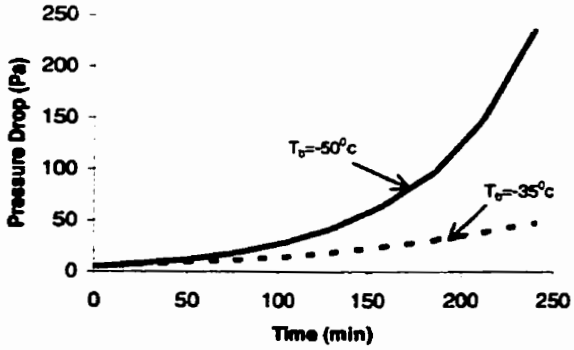

(b)

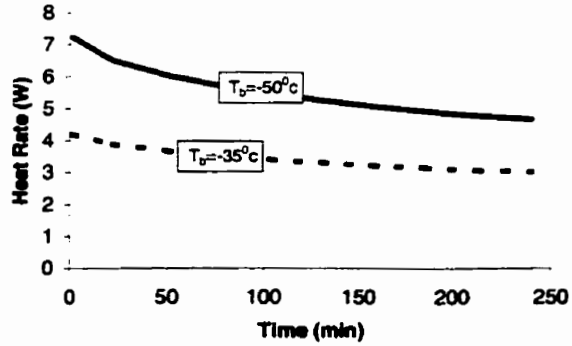

(d)

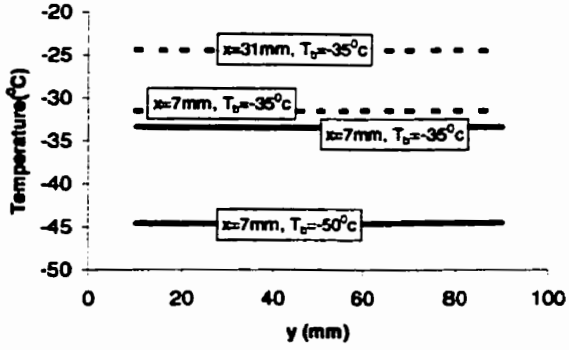

(e)

Figure F3 Sensitivity study for the fin base temperature, T_b a) Frost height at 240min, b) Frost density at 240min, c) Transient pressure drop, d) Transient heat rate through each fin, e) Temperature profile on the fin at 240min

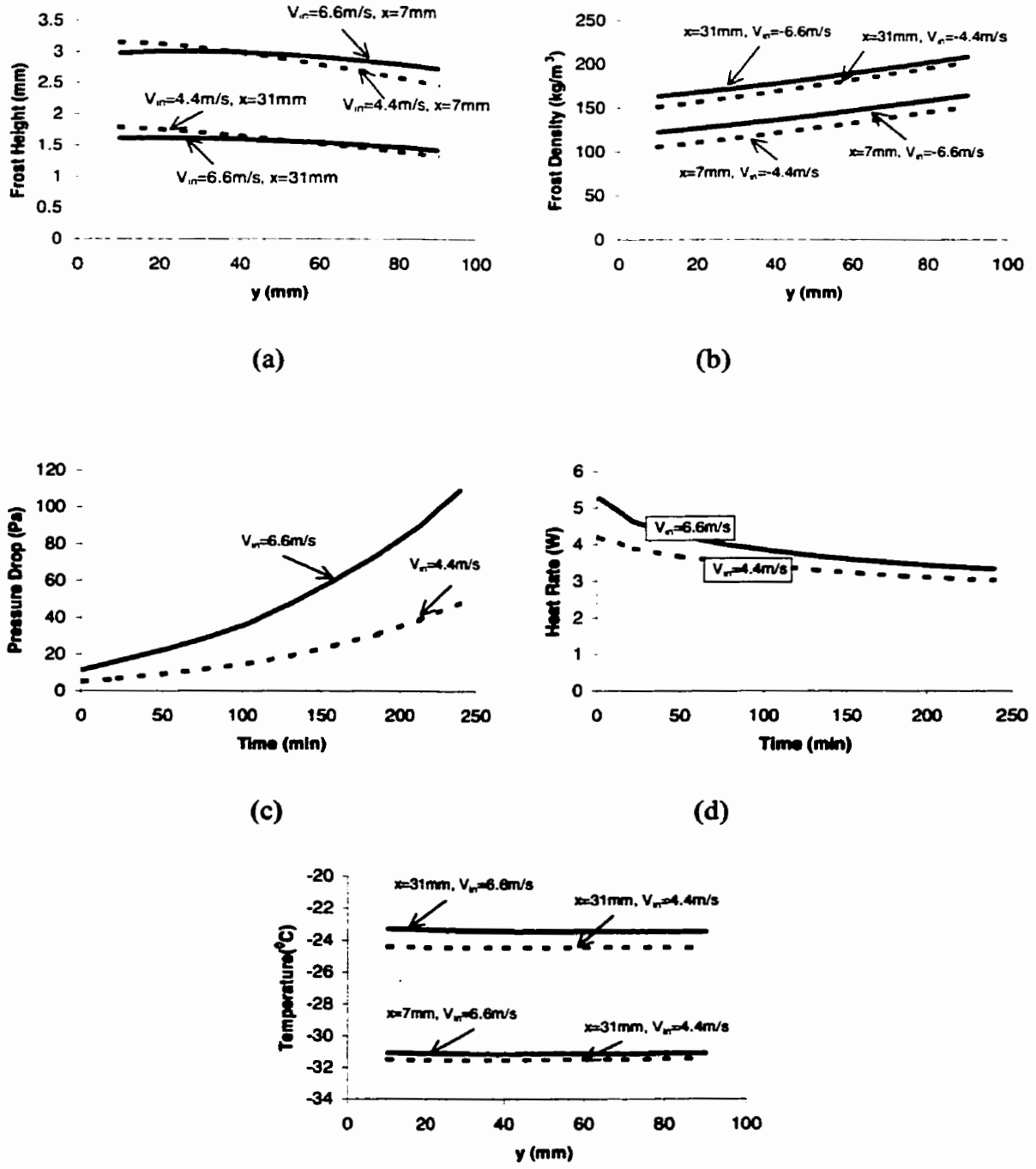

Figure F4 Sensitivity study for the air flow velocity entering fined section, V_{in} a) Frost height at 240min, b) Frost density at 240min, c) Transient pressure drop, d) Transient heat rate through each fin, e) Temperature profile on the fin at 240min

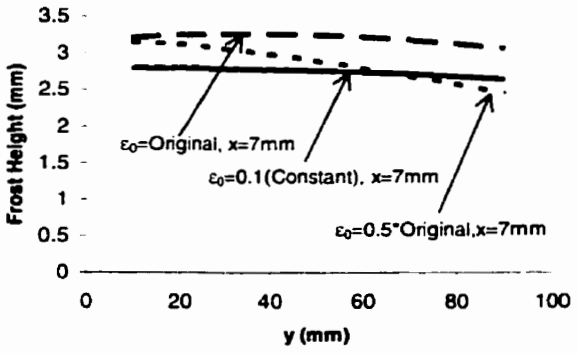

(a)

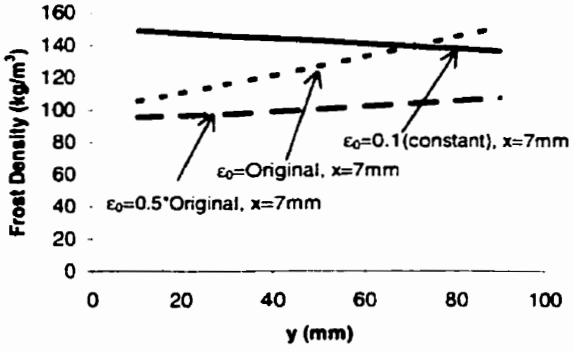

(b)

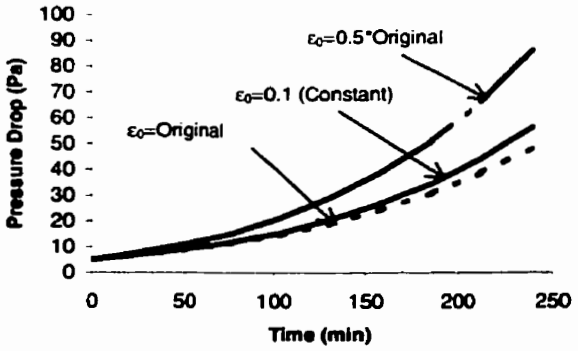

(b)

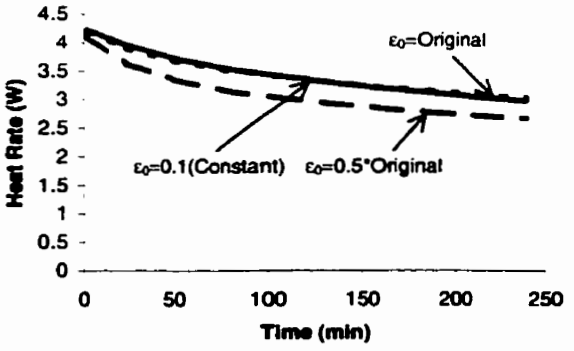

(d)

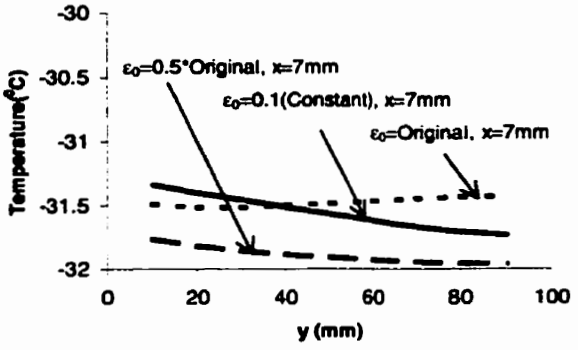

(e)

Figure F5 Sensitivity study for the initial condition of volume fraction of ice on fin surface, $\varepsilon_0(x,y)$ a) Frost height at 240min, b) Frost density at 240min, c) Transient pressure drop, d) Transient heat rate through each fin, e)Temperature profile on the fin at 240 min

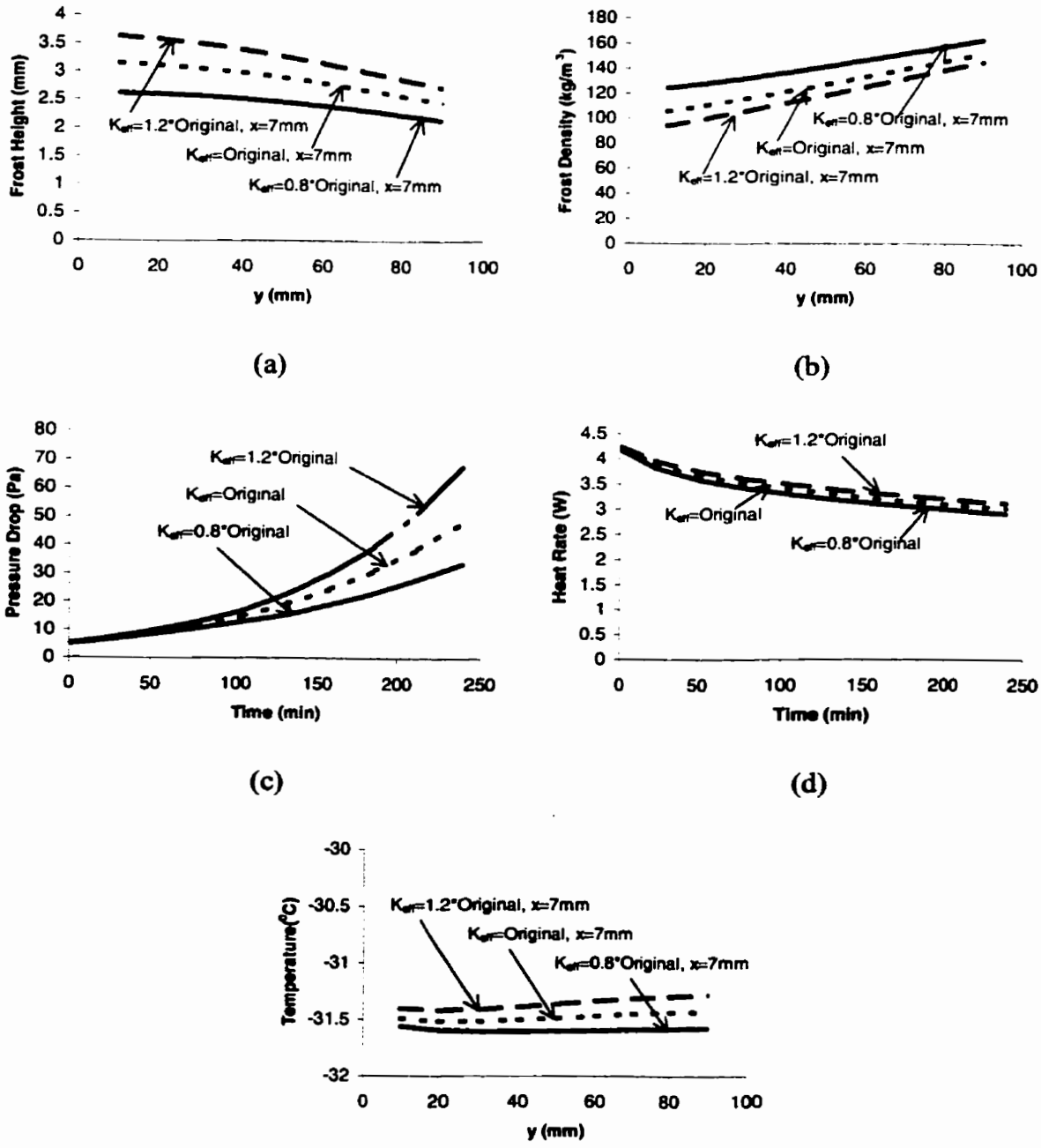

Figure F6 Sensitivity study for the effective thermal conductivity of frost, k_{eff} a) Frost height at 240min, b) Frost density at 240min, c) Transient pressure drop, d) Transient heat rate through each fin, e) Temperature profile on the fin at 240 min